Characterisation of small molecules inhibiting AKAP-PKA interactions

Dissertation

to obtain the academic degree

Doctor rerum naturalium (Dr. rer. nat.)

submitted to the Department of Biology, Chemistry and Pharmacy

of the Freie Universität Berlin

by

Frank Christian

born in Kirchen (Sieg), Germany

Berlin, March 2009

This work was accomplished between
September 2005 and February 2009
at the Leibniz-Institute of Molecular Pharmacology (FMP)
under the supervision of PD Dr. Enno Klußmann.

Dissertation submitted on 5 March 2009.

Date of disputation: 8 July 2009.

1st Reviewer: PD Dr. Enno Klußmann
2nd Reviewer: Prof. Dr. Volker Haucke

Selbstständigkeitserklärung

Hiermit erkläre ich, dass ich die vorliegende Arbeit selbstständig und nur unter Verwendung der angegebenen Literatur und Hilfsmittel angefertigt habe.
Des Weiteren versichere ich, dass die vorliegende Arbeit nie Gegenstand eines früheren Promotionsverfahrens war. Die dem Verfahren zugrunde liegende Promotionsordnung ist mir bekannt.

Berlin, den 5. März 2009

Frank Christian

Contents

Abbreviations **7**

1 Introduction **10**
1.1 Cyclic adenosine monophosphate (cAMP) signalling 10
1.2 cAMP-dependent protein kinase (PKA) 11
1.2.1 Specificity in cAMP-dependent signalling pathways 12
1.3 A-kinase anchoring proteins (AKAPs) and their interaction with PKA. 13
1.4 AKAP18 15
1.5 AKAP18δ and the translocation of AQP2 in renal principal cells 17
1.6 AKAPs in the regulation of cardiac excitation-contraction coupling 20
1.7 Targeting protein-protein interactions with small molecules 22
1.8 Compartmentalised cAMP-dependent signalling as target 24
1.8.1 AKAP-derived anchoring disruptor peptides 25
1.8.2 Applications for small molecule inhibitors of AKAP-PKA interactions 27
1.9 Objective 28

2 Material and Methods **29**
2.1 Material 29
2.1.1 Buffers 29
2.1.2 Chemicals and compounds 32
2.1.3 Antibodies 32
2.1.4 Peptides 33
2.1.5 Proteins 33
2.1.6 Bacterial hosts 34
2.1.7 Animals 34
2.1.8 Equipment 34
2.2 Methods 35
2.2.1 Enzyme-linked immunosorbent assay (ELISA) to detect AKAP-PKA interactions 35
2.2.2 Synthesis of focussed libraries derived from FMP-API-1 and -2 . 36
2.2.3 Preparation and culture of IMCD cells 36
2.2.4 Treatment of IMCD cells with small molecules and AVP 36
2.2.5 AQP2 immunofluorescence staining 37
2.2.6 Trypan blue staining 37
2.2.7 Laser scanning confocal microscopy 37
2.2.8 Preparation and culture of neonatal rat cardiac myocytes 38
2.2.9 Preparation of cell lysates 38
2.2.10 cAMP-agarose pulldown 38
2.2.11 Analysis of RII complex formation 39
2.2.12 Western blotting 39
2.2.13 Patch-clamp measurements of L-type Ca^{2+}-channel currents 40
2.2.14 Surface plasmon resonance measurements 40
2.2.15 Saturation transfer difference nuclear magnetic resonance (STD-NMR) 42
2.2.16 ^{15}N-HSQC-NMR 42
2.2.17 Peptide SPOT array synthesis 43
2.2.18 RII overlay 43
2.2.19 Quantitative cAMP assay 44

2.2.20 PKA activity assay 44
2.2.21 Phosphatase activity assay 45
2.2.22 Fluorescence anisotropy assay 45
2.2.23 Fluorescence anisotropy-based high throughput screening 47

3 Results 49
3.1 High throughput ELISA screening of a small molecule library yielded new AKAP-PKA inhibitors 49
3.2 Reordered compounds showed the same inhibitory effect 49
3.3 Application of the compounds to cell models reveals cell-type specific influence on cAMP signalling pathways 52
3.3.1 FMP-API-2 interferes with the aquaporin 2-shuttle in renal inner medullary collecting duct cells 52
3.3.2 Inhibition of the AQP2 shuttle by FMP-API-2 is reversible 55
3.3.3 Application of FMP-API-2 did not affect cell integrity 57
3.3.4 Synthesis and ELISA analysis of FMP-API-2 derivatives 57
3.3.5 cAMP pulldown experiments from compound-treated IMCD cells 59
3.3.6 FMP-API-1 decreased the interaction of PKA with AKAPs in cAMP pulldown experiments from cardiac myocytes 60
3.3.7 β-adrenoceptor-induced increases in L-type Ca^{2+}-channel currents are prevented by FMP-API-1, but not by FMP-API-2 61
3.4 SPR measurements confirmed the inhibiton of AKAP-PKA interactions by FMP-API-1 63
3.5 FMP-API-1 interacts directly and reversibly with regulatory RII subunits of PKA 64
3.6 The D/D domain of RIIα is not the molecular target of FMP-API-1 66
3.7 SPR measurements confirmed the allosteric binding mode of FMP-API-1 67
3.8 ELISA and peptide SPOT arrays point to additional AKAP-PKA interaction sites outside the D/D domain 68
3.9 FMP-API-1 causes oligomerisation of RII subunits 72
3.10 FMP-API-1 increases PKA-activation, cAMP levels, and PKA substrate phosphorylation 74
3.11 A structural derivative of FMP-API-1 displays higher activity at lower concentrations 79
3.12 DTT seems to influence the binding of compounds to RIIα 81
3.13 Search for new chemophores for the inhibition of AKAP-PKA interactions 83
3.14 High throughput screening of a small molecule library with a fluorescence anisotropy-based assay 87

4 Discussion 93
4.1 FMP-API-1 binds allosterically to RII, inhibits AKAP-PKA interactions and activates PKA 93
4.1.1 Binding sites of the small molecules in PKA regulatory subunits 94
4.1.2 Conformational changes in RII subunits induced by cAMP-binding 97
4.1.3 Crosslinking of regulatory subunits 97
4.1.4 The allosteric binding mode of FMP-API-1 and its influence on AKAP binding to RII 98

4.1.5 The focussed library derived from FMP-API-1 permits first structure-activity-relationship conclusions 99
4.1.6 Characteristics of AKAP-PKA interaction surfaces and small molecules 99
4.2 The identified compounds are active in cell-based assays 100
4.2.1 Interference with compartmentalised cAMP signalling in cardiac myocytes 100
4.2.2 The possible influence of FMP-API-1 on cAMP signalling in failing hearts 102
4.2.3 Inhibition of the AQP2 shuttle in IMCD cells 103
4.2.4 Applications for small molecule AQP2 shuttle inhibitors 104
4.3 Fluorescence anisotropy is a quick, solution-based method to characterise AKAP-PKA interactions 105

5 Summary 107

6 Zusammenfassung 108

Bibliography 109

Publications 119

Appendix A 120

Appendix B 123

Appendix C 124

Acknowledgments 174

Abbreviations

8-AHA	8-(6-aminohexylamino-)
Å	angström
AC	adenylyl cyclase
ADH	antidiuretic hormone
AKAP	A kinase anchoring protein
AMP	adenosine-5’-monophosphate
AMPA	a-amino-3-hydroxy-5-methyl-4-isoxazolepropionic acid
API	AKAP-PKA inhibitor
AQP2	aquaporin-2
ATP	adenosine-5’-triphosphate
AVP	arginine-vasopressin
β-AR	β-adrenergic receptor
BSA	bovine serum albumin
CaM	calmodulin
cAMP	cyclic adenosine-3’,5’-monophosphate
CNB	cyclic nucleotide binding (domain)
CNG	cyclic nucleotide-gated
CRE	cAMP-responsive element
CREB	CRE-binding protein
dbcAMP	dibutyryl cAMP
D/D	docking- and dimerisation domain
DMEM	Dulbecco’s modified eagle medium
DMSO	dimethyl sulphoxide
DNA	deoxyribonucleic acid
DTT	dithiothreitol
EDTA	ethylenediamine tetra-acetic acid
EGTA	ethylene glycol tetra-acetic acid
ELISA	enzyme-linked immunosor-bent assay
EnaC	epithelial Na^+-channel
Epac	exchange protein activated by cAMP
EtOH	ethanol
FA	fluorescence anisotropy
FCS	fetal calf serum
FL	full length
Fmoc	fluoren-9-ylmethoxycarbonyl
FMP	Leibniz-Institut für Molekulare Pharmakologie
FRET	fluorescence resonance energy transfer
Gas	a-Untereinheit des trimeren G-Proteins Gs
GDP	guanosine-5’-diphosphate
GEF	guanine-nucleotide exchange factor
GluR	glutamate receptor channel
GPCR	G protein coupled receptor
G-protein	guanine nucleotide binding protein
G-protein	GTP-binding protein
GSH	glutathione
GST	glutathione-S-transferase
GTP	guanosine-5’-triphosphate
HDM	human double-minute
HEPES	N-2-hydroxyethylpiperazine-N’-2-ethanesulphonic acid

HPLC	high performance liquid chromatography
HSQC	heteronuclear single quantum coherence
HUGO	human genome organisation
IBMX	3-isobutyl-1-methylxanthine
IC_{50}	concentration of half-maximal inhibition
IL	interleukin
IMCD	inner medullary collecting duct
iNOS	inducible nitric oxide synthase
Iso	isoproterenol
KCNQ	voltage-gated potassium channel
Kd	equilibrium dissociation constant
kDa	kilo-Dalton
LB	lysogeny broth
LC-MS	liquid chromatography-mass spectrometry
logP	logarithmic partition coefficient
LSM	laser scanning microscope
MALDI	matrix-assisted laser desorption/ionisation
MAP-Kinase	mitogen-activated protein kinase
MDM2	mouse double minute-2 ubi-quitin ligase
MS	mass spectrometry
NMR	nuclear magnetic resonance
NO	nitric oxide
OD600	optical density at 600 nm
PAGE	polyacrylamide gel electrophoresis
PBS	phosphate buffered saline
PDE	phosphodiesterase
PGE	prostaglandin E
PKA	cAMP-dependent protein kinase
PKC	Ca2+-dependent protein kinase
PLB	phospholamban
PMSF	phenylmethylsulphonyl fluoride
POD	horseradish peroxidase
pPLB	phospho-phospholamban
PP	protein phosphatase
PrKX	X chromosome-coding protein kinase
PVDF	polyvinylidene fluoride
R	regulatory PKA subunit
RDU	relative density units
RIIa	regulatory PKA subunit type IIa
RLU	relative light units
RNA	ribonucleic acid
RNA_i	RNA interference
rpm	revolutions per minute
RT	room temperature
RU	resonance units
RyR	ryanodine receptor
SA	streptavidine
SAR	structure-activity relationship
SDS	sodium dodecylssulfate
SEM	standard error of the mean
SERCA	sarco/endoplasmic reticulum Ca^{2+}-ATPase

SPR	surface plasmon resonance
SR	sarcoplasmic reticulum
STD	saturation transfer difference
STI	soy bean trypsin inhibitor
TAE	tris/acetate/EDTA buffer
TBS	tris buffered saline
TBST	TBS with Tween 20
TE	tris/EDTA buffer
TNF	tumor necrosis factor
TOF	time of flight
Tris	tris(hydroxymethyl)-aminomethane
UV	ultraviolet
V2R	vasopressin V2 receptor

1 Introduction

1.1 Cyclic adenosine monophosphate (cAMP) signalling

The capability of receiving signals from the environment and reacting specifically to them is of fundamental importance for both function and survival of cells. Generally, receptors on the cell surface detect the signals specifically and initiate a cellular response by passing the signal into signalling pathways.

Corresponding to the plethora of possible environmental conditions, huge numbers of extracellular signals and cell surface receptors exist. However, this multiplicity of extracellular signalling molecules is processed by only a very limited number of intracellular signalling routes. One main signalling route in the cell is the cyclic adenosine monophosphate (cAMP) dependent pathway. It is mainly activated by the binding of an extracellular signalling molecule to a G protein-coupled, heptahelical transmembrane receptor. An example is the hormone adrenalin binding to β-adrenergic receptors, which is one of the best studied cAMP signalling pathways.

The so activated receptor passes the signal to a heterotrimeric, guanosine triphosphate-binding protein (GTP-binding or G-Protein), which subsequently exchanges bound guanosine diphosphate (GDP) for GTP and thereby becomes activated[146]. Activation causes dissociation of the trimer into an α- and a dimer consisting of β- and γ-subunits. Both subunits are membrane bound through acylations and modulate downstream effector activities.

G proteins possess an intrinsic GTPase activity to hydrolyse the bound GTP, leading to inactivation and reassociation of the subunits. Thus, the G proteins function as molecular switches. There are at least 20 different Gα subunits that can be divided into four main families: $G_{\alpha s}$, $G_{\alpha i}$, G_q and $G_{12/13}$, and the subunits of all of them may activate or inhibit different effectors. $G_{\alpha s}$ activates adenylyl cyclase (AC), $G_{\alpha i}$ inhibits AC, G_q stimulates phospholipase C, and $G_{12/13}$ activates Src and c-Jun N-terminal kinase (JNK)[144].

Adenylyl cyclase, a membrane-bound enzyme, is stimulated by $G_{\alpha s}$ and catalyses the transformation of adenosine triphosphate (ATP) into the second messenger cAMP[145]. cAMP is freely diffusible and activates various effectors (Fig. 1.1). Among them are cyclic nucleotide-gated (CNG) cation channels,

opening in response to cAMP-binding, and a family of guanine nucleotide exchange factors (GEF), the so-called Epac (exchange proteins activated by cAMP). The binding of cAMP to Epac leads to a conformational change, exposing and activating the GEF domain. cAMP-bound Epac activates the small monomeric GTPases Rap-1 and Rap-2, which suppress the activity of another GTPase, Ras[9]. Ras is engaged in mitogen-activated protein kinase (MAPK) pathways, which are triggered by a number of proliferation- and differentiation-inducing signals, e.g. by cytokines.

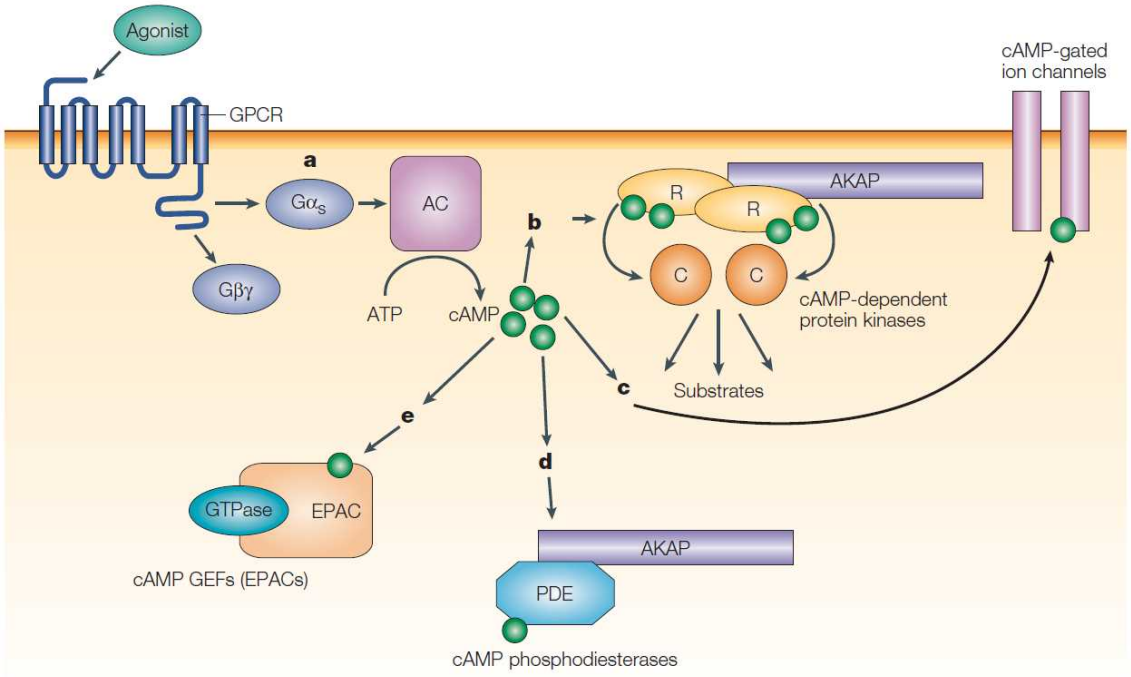

Fig. 1.1: cAMP signalling pathways. Binding of agonists to G-protein coupled receptors (GPCR) leads to activation and dissociation of heterotrimeric G-proteins. $G_{\alpha s}$ (a) subunits activate adneylyl cyclase (AC) to produce cAMP. cAMP has three main effectors in cells: cAMP-dependent protein kinase (PKA; b) consisting of regulatory (R) and catalytic (C) subunits, cAMP-gated ion channels (c) and exchange proteins activated by cAMP (Epac; e). cAMP is degraded by phosphodiesterases (PDE; d). Adapted from [158].

In addition, cAMP may influence gene expression through the transcription factor cAMP-responsive element binding (CREB) protein. CREB binds to cAMP-responsive elements (CRE) of the DNA activating transcription[104].

1.2 cAMP-dependent protein kinase (PKA)

The best characterised effector of cAMP is cAMP-dependent protein kinase (PKA). In its inactive state, the kinase exists as a heterotetramer, consisting of a

dimer of regulatory (R) and two catalytic (C) subunits, each bound to an R subunit. In this bound state, the catalytic subunits are inactive. Upon a rise in cAMP concentration, each R subunit binds two molecules of cAMP. By the conformational change induced by cAMP-binding, the catalytic subunits are released (Fig. 1.2). They phosphorylate serine- and threonine-residues on target proteins in close proximity, thereby regulating their function. Consensus sequences direct the recognition of the target proteins[149].

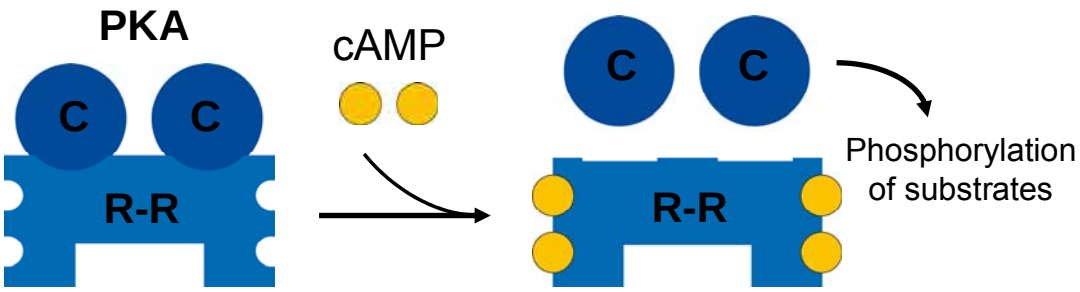

Fig. 1.2: Activation of PKA through cAMP. Two molecules cAMP bind to each the of the regulatory (R) subunits, which leads to a conformational change releasing the catalytic (C) subunits.

Since many different extracellular stimuli converge in the cAMP-PKA pathway, and since PKA is an enzyme with a broad substrate specificity, the question arises, how the numerous different stimuli may elicit different specific cellular responses.

1.2.1 Specificity in cAMP-dependent signalling pathways

One contribution to specificity in the cAMP-PKA pathway is made by the cell type-specific expression of the different isoforms of R- and C-subunits (RIα, RIβ, RIIα, RIIβ and Cα, Cβ, Cγ, PrKX, respectively), that may assemble to PKA isoforms with different cAMP affinities leading to different activation thresholds[138]. Generally, the RI subunits show a higher cAMP-binding affinity than RII subunits. R subunits may form homo- as well as hetero-dimers, offering several possibilities for combination all with finely tunable affinities.

In addition, spatial aspects play an important role for the signalling pathway's specificity: cAMP is produced by the AC close to the G protein coupled receptor, and the free diffusion in the cytosol is limited by phosphodiesterases (PDE), representing the only means of cells to hydrolyse cAMP to adenosine monophosphate (AMP; Fig. 1.1). In this way, cAMP concentration gradients are es-

tablished within cells, and only PKA tetramers present in certain locally confined cAMP-containing microdomains are activated in consequence of an extracellular stimulus[162].

The localisation of PKA itself is realised by A-kinase anchoring proteins (AKAPs), which bind PKA and anchor it in close proximity to its substrates.

1.3 A-kinase anchoring proteins (AKAPs) and their interaction with PKA

AKAPs are a protein family currently comprising around 50 proteins lacking sequence homology, but sharing similar functions (Fig. 1.3)[81,149,158].

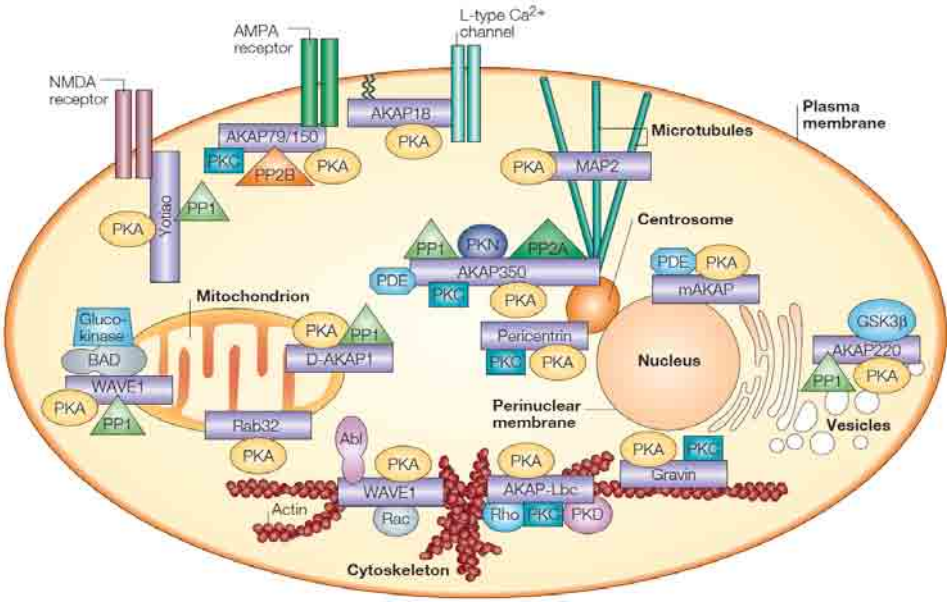

Fig. 1.3: AKAPs compartmentalise cAMP signalling by tethering PKA to subcellular compartments, for example to the plasma membrane, cytoskeleton, vesicles, mitochondria and nucleus. For instance, AKAP18α is located to the plasma membrane and interacts with the L-type Ca^{2+}-channel *via* a leucine-zipper motif. Besides with PKA, AKAPs may interact with a multitude of other signalling molecules, including other protein kinases, protein phosphatases and phosphodiesterases. For a more detailed description, refer to [158].

The hallmark of AKAPs is the presence of the binding domain for regulatory PKA subunits[102], also termed RII-binding domain. This conserved motif forms an amphipathic α-helix consisting of 14 to 18 amino acids, whose hydrophobic side chains interact with a hydrophobic pocket of PKA[17,112,114] (Fig. 1.4). The

hydrophobic pocket is formed by the N-termini of dimerised R-subunits. They arrange in an antiparallel fashion, whereupon a four helix bundle emerges out of two helix-turn-helix motifs. The details were shown in structures solved by both NMR and X-ray analyses[42,112,114]. Further details regarding the direct interaction between the RII-binding domain of AKAPs and the D/D domain of regulatory PKA subunits are reviewed in section 1.8 “Compartmentalised cAMP-dependent signalling as target”.

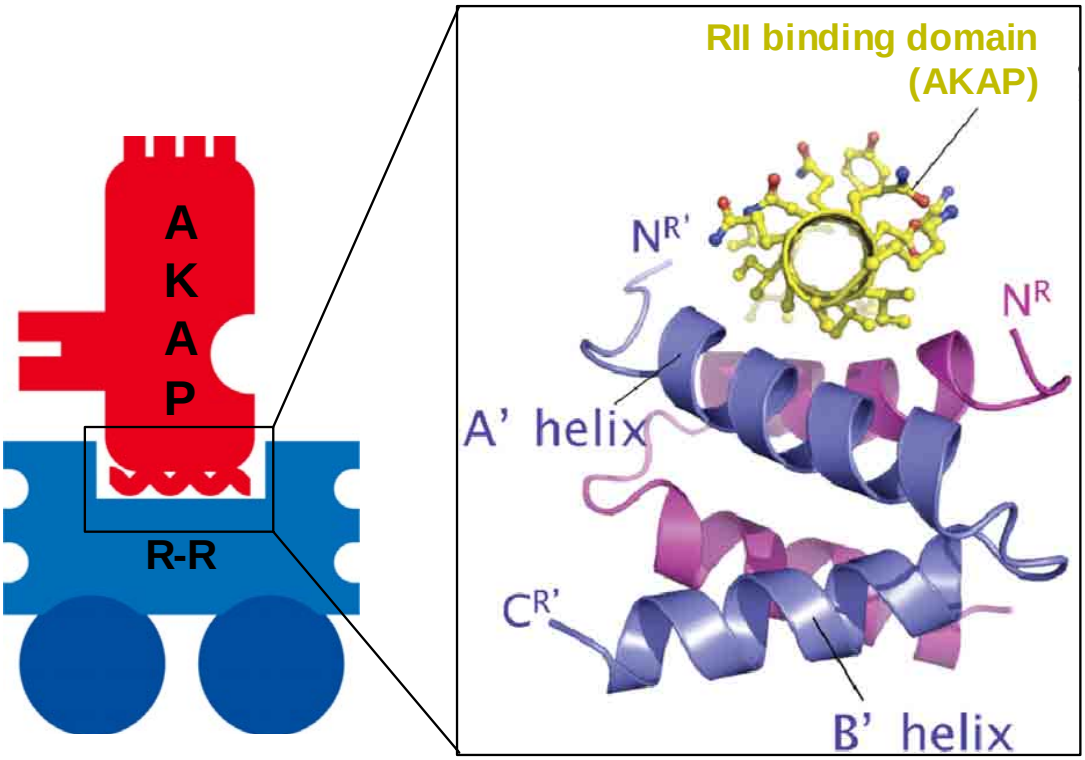

Fig. 1.4: The molecular basis of PKA anchoring. Scheme of an AKAP interacting with an R-subunit dimer (left panel). The docking and dimerisation (D/D) domains, located at the N-termini of the R subunits, form a shallow hydrophobic groove. The RII-binding domain of an AKAP forms an amphipathic α-helix whose hydrophobic side chains interact with the hydrophobic groove of the D/D-domain dimer.

The N-terminal parts of the RI- and RII-subunits have different sequences, leading to different AKAP binding specifities[48,54]. Most AKAPs bind RII subunits with a K_d in the nanomolar range, dividable into low- and high-affinity AKAPs: While AKAP18, AKAP-Lbc/Ht31, AKAP79 and AKAP95 with K_d-values between 1 and 50 nM are assigned high-affinity AKAPs[2,16,54], Gravin and the AKAPs belonging to the Ezrin/Radixin/Moesin protein family are low-affinity AKAPs with K_d-values in the micromolar range[32]. In addition, some dual-specificity AKAPs binding both

types of R subunits exist (D-AKAPs)[57,117]. As RI-specific AKAPs so far only $AKAP_{CE}$ (from *Caenorhabditis elegans*), AKAP82, PAP7 (peripheral-type benzodiazepine receptor (PBR) associated protein 7) and hAKAP220 are known[149]. The interaction of RIα, RIβ and RIIβ subunits with AKAPs appears to be static. In contrast, the binding of RIIα subunits to AKAPs seems to be regulated in some cases. So far, two phosphorylation sites influencing the AKAP-interaction in RIIα are known: Thr54 may be phosphorylated by cyclin-dependent kinase CDK-1[80]. This phosphorylation is proposed to alter the subcellular localisation of RIIα by modulating its binding to AKAP95. The whole process is involved in remodeling chromatin during mitosis. In addition, autophosphorylation of Ser99 within the inhibitory region of RIIα (see below for details) not only led to increased activation through cAMP-induced dissociation of the PKA holoenzyme[34], but also increased the interaction with (among other AKAPs) AKAP18α[90,163].

A further characteristic domain of AKAPs is the so-called targeting domain, anchoring each AKAP to a certain subcellular compartment.

Besides PKA and subcellular compartments, AKAPs may bind further signalling molecules involved in cAMP/PKA signalling including phosphodiesterases and protein phosphatases[139]. The latter reverse phosphorylation reactions and may thereby terminate the effect of a stimulus. Furthermore, AKAPs may bind other protein kinases. For instance, AKAP79/150 binds Ca^{2+}-dependent protein kinase, thus integrating Ca^{2+}- and cAMP signalling. By these means, AKAPs provide a scaffold close to the substrate, to which all proteins required for initiation and termination of a signal can be recruited. The basically freely diffusible signal emanating from the AC is thus locally and temporally focussed to the AKAP-anchored PKA, leading to one specific substrate phosphorylation.

1.4 AKAP18

AKAP18 comprises four splice variants (α-δ). AKAP18α was first described as a membrane-associated, 15 to 18 kDa-large protein (hence also described as AKAP15), tethering PKA to the basolateral plasma membrane of epithelial cells, and in skeletal muscle cells directly to L-type Ca^{2+}-channels in the plasma membrane[46]. In the latter case, AKAP18α interacts directly with the C-terminus of the Ca^{2+}-channels[59].

The protein consists of 81 amino acids, contains a canonical RII-binding domain and N-terminal myristoyl- and palmitoyl-lipid anchors, tethering the AKAP-PKA complex to the plasma membrane[39,45]. The interaction between AKAP18 and the Ca^{2+}-channel is mediated by a leucin zipper-like motif in the C-terminal domain of the channels' α_1-subunits. Thus, PKA is positioned close to Ser1928 to enable its specific phosphorylation[59,61]. Upon β-adrenergic stimulation, the phosphorylation increases the open probability of the channel, leading to increased influx of calcium ions into the cytosol and ultimately to increased contractility of myocytes.

Another function of AKAP18α was described recently[6]: it regulates the epithelial Na^+-channel (ENaC) *via* a PKA-independent mechanism. In its native, membrane-anchored form, it decreased ENaC activity, while a mutant form lacking the membrane targeting domain and thus located in the cytoplasm decreased the Na^+-mediated feedback inhibition of ENaC through direct interaction with PKC, which is involved in this process.

Further studies showed that four splice variants arise from the AKAP18 gene, hence the above mentioned AKAP18 protein was renamed to AKAP18α (or AKAP7 (according to the HUGO gene nomenclature committee), AKAP15). The other splice variants are AKAP18β, -γ and -δ (Fig. 1.5).

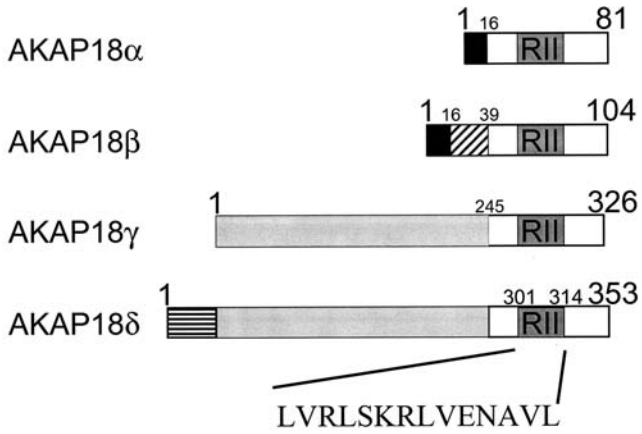

Fig. 1.5: AKAP18 isoforms. Numbers indicate the amino acid position in the proteins. The membrane binding domains of AKAP18α and -β are indicated in black. The RII-binding domains are identical between the isoforms. Adapted from [52].

AKAP18β consists of 104 amino acids and contains the same membrane-targeting domain as the α-variant. Additional 23 amino acids located between

residues 16 and 39 direct the protein to the apical plasma membrane in polarised epithelial cells[151]. The function of AKAP18β remains to be defined.
In contrast to most AKAPs, the 326 amino acid-long AKAP18γ is also localised in soluble cell fractions[151]. In mouse oocytes, it localises RI subunits of PKA to the nucleus, suggesting an involvement in the regulation of transcription[13].
AKAP18δ contains 353 amino acids. The amino acid sequence of its RII-binding domain is identical with those of the splice variants α-γ. AKAP18δ is to 76 % homologous to AKAP18γ (Fig. 1.5). AKAP18δ was discovered in a search for AKAPs that are involved in the translocation of the water channel protein aquaporin-2 (AQP2) from intracellular vesicles to the apical plasma membrane of renal collecting duct principal cells (Fig. 1.6). It was shown that AKAP18δ colocalises with AQP2 on the intracellular vesicles[52,141] and is likely to participate in the regulation of the phosphorylation of AQP2 by PKA.
Recently, a structure of the central domain of AKAP18δ, termed AKAP18δCD, was solved by X-ray structural analysis, representing the first solved structure of a fragment of an AKAP so far (although lacking the RII-binding domain). The central domain is structurally homologous to 2H phosphoesterase domains and binds adenosine monophosphate (AMP)[43].
AKAP18δ was also shown to be involved in the regulation of Ca^{2+} re-uptake into the sarcoplasmic reticulum (SR) of cardiac myocytes[87,88] (see section 1.6).

1.5 AKAP18δ and the translocation of AQP2 in renal principal cells

A major task of principal cells lining renal collecting ducts is the fine-tuning of body water homeostasis by controlling water reabsorption. To accomplish this, they express water-permeable channel proteins, the aquaporins (AQP)[72]. While AQP3 and AQP4 are constitutively expressed in the basolateral plasma membrane, the localisation of AQP2 is subject to regulation by AVP[109,152]. AVP adjusts the amount of AQP2 in the plasma membrane by triggering the redistribution of AQP2 from intracellular storage vesicles into the apical plasma membrane (Fig. 1.6). Through this, the osmotic water permeability of the plasma membrane is increased, and water is reabsorbed from the primary urine[115].

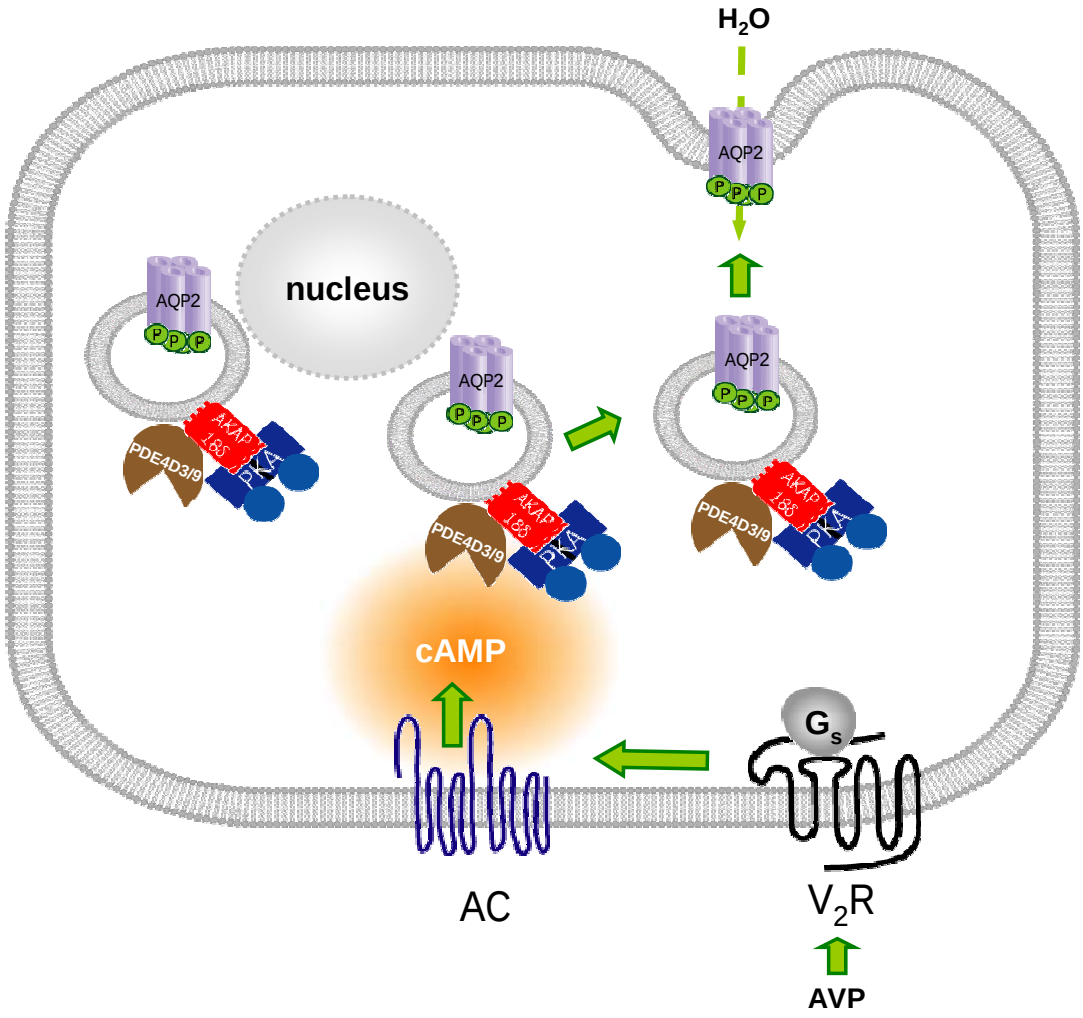

Fig. 1.6: The vasopressin (AVP)-triggered redistribution of AQP2 from intracellular vesicles into the plasma membrane depends on the anchoring of PKA (most probably by AKAP18δ). Activation of the vasopressin V2 receptor (V2R) in the basolateral plasma membrane of renal principal cells by binding of AVP leads to increased intracellular cAMP levels activating perinuclear PKA. AKAP18δ tethers PKA to AQP2-containing vesicles and thereby presumably facilitates the phosphorylation of AQP2, which triggers the AQP2 translocation to the plasma membrane and thus water reabsorption from primary urine. PDE4D3/9 located on the AQP2 containing vesicles decreases local concentrations of cAMP, thereby limiting local PKA activity. Adapted from [147].

Synthesis of the hormone AVP and its secretion into the bloodstream are controlled by osmoreceptors in the hypothalamus, which constantly monitor the osmolarity of the bloodstream. When the osmolarity increases, for instance after reduced liquid uptake, AVP is synthesised and secreted into the bloodstream. This permits adaptation to the changing water demand of the organism. Defects of this mechanism, caused for instance by mutations of the vasopressin V2 re-

ceptor (V2R) or AQP2 genes, lead to nephrogenic diabetes insipidus (NDI), a disease characterised by a massive production of hypoosmotic urine[8].

The translocation of AQP2 is initiated by AVP-stimulation of the V2R, which activates adenylyl cyclase. This is followed by an increase of cAMP[73,109,152]. The AVP-induced raise in cAMP activates PKA, which in turn phosphorylates AQP2. This phosphorylation triggers the translocation of the AQP2-bearing vesicles to the plasma membrane[40,79]. Inhibition of PKA by H-89 or disruption of its interaction with AKAPs by the AKAP-Lbc-derived anchoring-disruptor peptide Ht31 or the AKAP18δ-derived peptide AKAP18δ-L314E abolishes the AVP-induced redistribution of AQP2 in cellular models such as rat inner medullary collecting duct (IMCD) cells[74,147]. In addition, H-89 inhibits an AVP-induced increase in water permeability in rabbit cortical collecting ducts by 90% suggesting that PKA is the principal cAMP effector in this system[140].

Several lines of evidence indicate that cAMP signalling in renal principal cells is compartmentalised[7,63,64,64,98,141,147]. In IMCD cells, forskolin, a direct activator of adenylyl cyclase, increases cAMP levels and PKA activity twofold higher than AVP, while both agents induce the AQP2 translocation to a similar extent. AVP induces perinuclear PKA activation, while forskolin leads to PKA activation throughout the cell, indicating that activation of a pool of PKA in a defined region of the cells has a similar effect on the localisation of AQP2 as activation of PKA throughout the cell[141]. Moreover, displacement of PKA from AKAPs with the PKA anchoring disruptor peptide Ht31 prevents the AVP-induced AQP2 redistribution, indicating that compartmentalisation of PKA is achieved by AKAPs ([74]; Fig. 6b). AKAP18δ is likely to be involved in this process. Besides other AKAPs, it tethers PKA to AQP2-bearing vesicles, thereby presumably facilitating AQP2 phosphorylation[52,64,141].

Local degradation of cAMP by PDEs also participates in controlling the insertion of AQP2 into the plasma membrane[141]. The PDE4 family members are the most abundant ones in renal principal cells[31]. All PDEs are sensitive to inhibition by 3-isobutyl-1-methylxanthine (IBMX), while only the PDE4 family is selectively inhibited by rolipram. In IMCD cells, neither IBMX nor rolipram affect basal cAMP levels but both enhance cAMP generation in response to AVP or forskolin. IBMX increases AVP- or forskolin-induced cAMP raises fivefold each, and rolipram two-threefold each. Together with rolipram, forskolin leads to a fivefold

higher cAMP level than the combination of rolipram and AVP. Despite the different effects of IBMX and rolipram on the AVP-induced accumulation of cAMP, both PDE inhibitors enhance the AVP-induced AQP2 translocation by approximately 20%. The data indicate that PDE4 family members play a major role in the AQP2 redistribution[141].

Of the nine splice variants of PDE4D[120], PDE4D3 and/or PDE4D9 (PDE4D3/9) are located on AQP2-bearing vesicles (Fig. 1.6). Vesicular PDE4D was suggested to prevent activation of vesicular PKA in resting principal cells and thus inappropriate translocation of AQP2, presumably by local hydrolysis of cAMP[141]. The activities of all long isoforms of PDE4A-D are increased by PKA phosphorylation. PDE4D3 is PKA-phosphorylated at serine 54[55,135]. AVP causes the accumulation of both AQP2 and of phosphorylated PDE4D3/9 at the plasma membrane of IMCD cells. The phosphorylation accelerates local hydrolysis of cAMP, thereby lowering PKA activity in close proximity to AQP2. This limits further AQP2 phosphorylation and integration into the plasma membrane[141].

PDE4D and AKAP18δ interact directly, and both proteins reside on the same intracellular vesicles as AQP2 and PKA, suggesting that a local signal transduction module comprising AKAP18δ-anchored PDE4D3/9 and PKA plays a crucial role in the regulation of the phosphorylation of AQP2, and thereby of its cellular localisation[7,98,141] (Fig. 1.6).

1.6 AKAPs in the regulation of cardiac excitation-contraction coupling

Contractility of the heart is subject to regulatory mechanisms providing the possibility to react to changing environmental requirements, e.g. to stress or exertion. An example is the β-adrenoceptor-mediated increase in contractility[33], which relies on PKA-dependent mechanisms and their compartmentalisaton by AKAPs within cardiac myocytes (Fig. 1.7). Stimulation of β_1-adrenoceptors by agonists like norepinephrine leads to activation of the G_S/adenylyl cyclase-system to produce cAMP. AKAP18α tethers PKA to L-type Ca^{2+}-channels in the plasma membrane (see above)[39,45]. After β-adrenergic stimulation, the rise of the cAMP level causes activation of PKA which in turn phosphorylates the channel, thereby increasing its open probability.

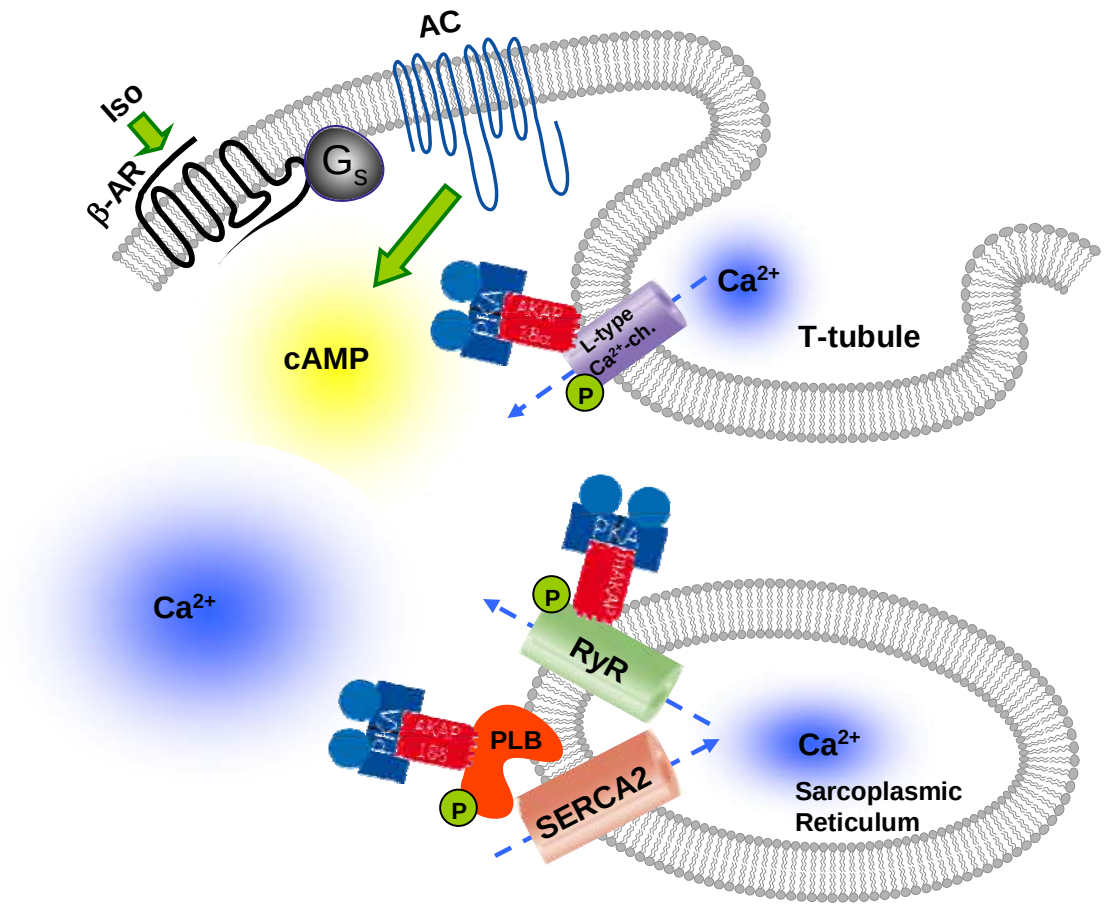

Fig. 1.7: The β-adrenergic regulation of cardiac myocyte contractility depends on AKAPs. Activation of the β-adrenoceptor (β-AR) through agonists, e.g. isoproterenol (Iso), leads to increased cAMP synthesis by adenylyl cyclase (AC). In compartments with increased cAMP concentration PKA is activated. AKAP18α tethers PKA to the L-type Ca^{2+}-channel in the plasma membrane. Phosphorylation increases its open probability, resulting in increased influx of Ca^{2+} into the cytosol. Consequently, the Ca^{2+}-activated Ca^{2+}-release channel ryanodine receptor (RyR) releases more Ca^{2+} from the intracellular Ca^{2+}-store, the sarcoplasmic reticulum, into the cytosol. Its open probability is increased upon phosphorylation through PKA, which is bound to it *via* mAKAP. After contraction, Ca^{2+} is pumped back into the sarcoplasmic reticulum by the sarcoplasmic reticulum ATPase, SERCA2. Phospholamban (PLB) inhibits SERCA2 under basal conditions, but upon phosphorylation through PKA, which is tethered through AKAP18δ, PLB dissociates from SERCA2, increasing its activity. Collectively, the contractility is increased.

In addition, mAKAP targets PKA to the ryanodine-receptor, a Ca^{2+}-induced Ca^{2+}-release channel located in the membrane of the sarcoplasmic reticulum (SR), the intracellular Ca^{2+}-store[68,69,94]. Upon activation of mAKAP-bound PKA and phosphorylation of the channel, its open probability is increased and Ca^{2+} entry into the cytosol is enhanced. Ca^{2+} binds to the myofilament protein tro-

ponin C, thereby increasing the contraction of the myocyte. Contraction is followed by relaxation of the cardiac myocytes. For this, Ca^{2+} is removed from the cytosol. An important mechanism is pumping Ca^{2+} back into the SR by SR Ca^{2+}-ATPase (SERCA2), which resides in the SR membrane. Under basal conditions, its activity is inhibited by interaction with the small regulatory protein phospholamban. After β-adrenergic stimulation, phospholamban is PKA-phosphorylated and dissociates, which increases SERCA2 activity. AKAP18δ interacts with phospholamban and facilitates its PKA phosphorylation[87]. Collectively, these events lead to an increase in cardiac myocyte contractility.

This and the previous example of AKAP18δ-mediated cAMP signalling represent possible disease-relevant processes important to study not only in cells, but also in live animals. To this end, small molecules targeting the AKAP-PKA interaction would be important tools.

1.7 Targeting protein-protein interactions with small molecules

There are numerous examples of successful interference with protein-protein interactions by peptides derived from one of the binding partners[136]. Such peptides mimic the interaction domain of the protein they are derived from and thus inhibit the interaction competitively. Among the successful examples for targeting protein-protein interactions with peptides are the peptides derived from the RII-binding domains of AKAPs (see below).

However, there are a number of disadvantages associated with peptides:

- sometimes expensive, difficult synthesis
- for cellular studies fusions to stearate or poly-Arg sequences are required[12,36], but cellular uptake is difficult to monitor and the final intracellular concentration is difficult to determine[53]
- in case of expression of genetically encoded peptides in cultured cells it can be difficult to control the expression quantitatively
- limited stability
- peptides are subject to proteolytic degradation in the gastrointestinal system and thus need to be administered parenterally for pharmaceutical purposes
- immunogenic effects are possible

Nevertheless, because of some characteristics of protein interaction surfaces, peptides are traditionally thought to be advantageous over small molecules to inhibit protein-protein interactions. The contact surfaces of protein-protein interactions (approx. 1500-3000 Å^2) are large compared to those involved in protein-small molecule interactions (approx. 300-1000 Å^2). The surfaces are generally flat and lack the pocket-like structures present on protein-small ligand interaction surfaces[56,155], at least when the surfaces are considered static, as is sometimes misleadingly suggested by solved protein structures (see below). Furthermore, protein-protein interaction surfaces do not have natural small molecule binding partners as do many enzymes and receptors (e.g., GPCRs), hence the search for a non-peptidic ligand cannot be started from a natural ligand.

On the other hand, there was a number of successes reported, e.g. interleukin 2 (IL2)-IL2-receptor inhibitors and human double minute 2 (HDM2)-p53 inhibitors, underlining that small-molecule-mediated inhibition of protein-protein interactions is possible[3,4,155].

One central feature of a protein-interaction interface is a certain confined area most important to establish the interaction, termed the hotspot [23,106]. It usually consists of a limited number of amino acid residues contributing most of the binding free energy to the interaction. Peptides derived from one binding partner and selected for inhibition of a protein-protein interaction often bind to the hotspot and compete with the native protein ligand[85,137,159].

Small molecules are kinetically advantageous over larger inhibitors like peptides or antibodies, because they may intercalate into protein interaction interfaces and enhance the dissociation of the interacting proteins. This theory is supported by NMR studies showing that protein-protein interfaces can be wobbly[148]. Larger molecules like peptides or antibodies would not be able to intercalate into such interfaces, because they require the preceding dissociation of the partners to bind to the target. This is demonstrated by the example of tumor necrosis factor (TNF), in which a small molecular inhibitor penetrates into TNF trimers and accelerates the dissociation of a monomer, rendering the complex inactive. In the presence of the compound the dissociation was 600 times faster compared to the normal dissocation rate. Consequently, the whole process was not rate-limited by the off-rate of a TNF monomer[50].

Another possibility for a small molecule to target a large protein interaction surface is *via* an allosteric mode of action. In this case, the small molecule binds at a site distant from the interaction surface, and induces conformational changes ultimately leading to modification of the interaction surface causing inhibition. For example, there is a small molecule binding to inducible nitric oxide synthase (iNOS), blocking dimerisation and hence NO synthesis by allosterically disrupting the protein-protein interaction[97].

1.8 Compartmentalised cAMP-dependent signalling as target

Interference with AKAP-mediated PKA anchoring is required to elucidate the function of the compartmentalisation of cAMP signalling[63]. So far, mainly AKAP-derived synthetic peptides (anchoring disruptor peptides)[2,66], but also gene knockout animal models[58,108,111,116], RNA_i approaches[87,89,157] and genetically encoded peptides[2,35,63,130] have been used to interfere with compartmentalised cAMP signalling in cells, suggesting that inhibition of PKA anchoring is a suitable concept to analyse this signalling pathway[63].

The possible points of action for agents interfering with compartmentalisation of cAMP signalling include

- the interaction between AKAPs and PKA-R-subunits (i.e., RII-binding domain and D/D domain)
- the binding of AKAPs or interacting molecules to regulatory subunits by an allosteric mechanism
- the interaction between AKAPs and the subcellular compartment the PKA is anchored to (i.e. AKAP targeting domain and subcellular compartment)
- the interaction between AKAPs and other signal transduction proteins bound to them, e.g. phosphodiesterases
- the dimerisation of regulatory subunits
- the interaction between catalytic and regulatory PKA subunits, influencing PKA activity

In case of gene knockout models or RNA_i–mediated knockdown of AKAPs all interactions mediated by the targeted AKAP are abolished, while peptides specifically disrupt the targeted interaction. However, with anchoring disruptor peptides, all AKAP-R subunit-interactions are non-selectively disrupted, but they

allow for testing experimentally which physiological effects are caused by the abolishment of PKA compartmentalisation by AKAPs.

1.8.1 AKAP-derived anchoring disruptor peptides

All AKAP-PKA anchoring disruptor peptides are derived from the RII-binding domain of AKAPs. They mimick the amphipathic helix required to interact competitively with the D/D domain of regulatory subunits of PKA[17,18,113,153]. The first introduced and so far most frequently used anchoring disruptor peptide is Ht31, consisting of 22 amino acids and derived from the RII-binding domain of AKAP-Lbc[16,17,29].

Using bioinformatic methods and peptide array screenings, a stronger binding peptide called $AKAP_{IS}$ (*in silico*) was generated[2]. Starting from a consensus RII-binding site calculated from various AKAPs, amino acids were exchanged systematically and the peptides were spot-synthesised onto cellulose membranes for binding experiments to determine the peptide with the highest affinity. This peptide is a 17-mer and is able to form additional hydrophobic interactions with the RII subunit through modified positions of two amino acid side chains, and it can form an additional salt bridge, stabilising its conformation.

Inhibitory peptides of similar high affinity have been derived from the RII-binding domain of AKAP18δ. For this, each amino acid of a 25-mer peptide representing the RII-binding domain was individually replaced by all other biogenous amino acids[64]. Through this, a peptide with similar binding affinity, but better solubility as the wildtype sequence was identified. Starting from the obtained peptides, further amino acid substitutions were conducted, based on a structural model of the peptide docked into the hydrophobic pocket of RII. However, a further increase in affinity was not achievable. The peptide AKAP18δ-L314E showed the highest affinity for binding RII subunits (K_d = 0.7 nM) in combination with better solubility compared to the wildtype peptide AKAP18δ-wt (K_d = 0.4 nM). While hydrophobic amino acid side chains of the amphipathic helix form the backbone of the interaction, charged residues and residues introducing hydrogen bonds are present in the AKAP18δ- and $AKAP_{IS}$-RIIα interactions[42,63], increasing the binding affinity.

The N-terminal α-helix of each R subunit is formed by the N-terminal 5 amino acids, with Ile3 and Ile5 playing a pivotal role in the binding of AKAPs[47]. The α-

helix following downstream (until amino acid 30) facilitates the dimerisation (the lower helices in Fig. 1.4)[132]. Beside the amino acids forming the helices, further amino acids of the N-terminus contribute to the interaction with AKAPs by forming salt bridges and hydrogen bonds[64].

The AKAP18δ-derived peptides AKAP18δ-wt and -L314E and Ht31 (Figs. 3.1A, 3.11, 3.18, 3.20, 3.21 and 3.23) were used in this work. It is known that Ht31 inhibits interactions of AKAPs with both regulatory RI and RII subunits[2,16]. However, for the AKAP18δ-derived peptides no studies regarding the RI-interaction were performed, but it is known that AKAP18γ targets RI to the nucleus, indicating interaction of the AKAP18-RII-binding domain with both RI and RII[13].

Recently, newly designed peptides were described to preferentially inhibit interactions of AKAPs with either RI (RI anchoring disruptor, RIAD[14,15]) or RII (super-$AKAP_{IS}$[42]). But also for these improved peptides, there is no specificity for a single AKAP-PKA interaction, although the amino acid sequence similarity among the RII-binding domains of the various AKAPs is below 30 %.

An approach that may lead to higher specificity in targeting of compartmentalised cAMP signalling is the disruption of AKAP targeting to subcellular compartments because the targeting domains are specific for each AKAP, or of the interaction with other signalling proteins (Fig. 1.3). The identity of the targeting domain of many AKAPs is unknown. Therefore, there are only few examples where this approach has been successfully applied.

- The interaction between AKAP18α and the L-type calcium channel in the plasma membrane of myocytes is mediated *via* a leucine zipper motif on AKAP18α, which may be mimicked and competitively disrupted by a peptide[59,60], inhibiting the PKA-mediated potentiation of L-type Ca^{2+}-channel activity in muscle cells.
- Phospholamban resides in the membrane of the sarcoplasmic reticulum (SR) membrane, and upon PKA-dependent phosphorylation, it dissociates from SERCA2, leading to increased calcium reuptake into the SR (see section 1.6 and Fig. 1.7). A peptide derived from the AKAP18δ-interaction domain of phospholamban disturbed the striated distribution pattern of AKAP18δ in neonatal rat cardiac myocytes, indicating inhibition of the interaction between the proteins[87].

- A peptide derived from a leucine zipper motif in the voltage gated potassium-channel, KCNQ1, which binds the AKAP Yotiao was shown to prevent coimmunoprecipitation of Yotiao, PKA and protein phosphatase 1 with KCNQ1[93].
- AKAP79 binds PKA, Ca^{2+}-dependent protein kinase (PKC) and protein phosphatase 2B (PP2B) at the postsynaptic membrane of excitatory synapses. Peptides derived from the AKAP79-region that binds PP2B compete with PP2B binding and attenuate PP2B-dependent down-regulation of glutamate receptor channel (GluR1) currents[25].

Although the above mentioned inhibitory peptides are highly selective tools with high binding affinity for their targets, they also have some disadvantages, as outlined in section 1.7.

1.8.2 Applications for small molecule inhibitors of AKAP-PKA interactions

Since AKAPs bring specificity about many cellular processes by establishing disease-relevant protein-protein interactions, and are sometimes expressed tissue-specifically, they could be an attractive target for new drugs.

This is underlined by a recent study showing that a certain variant of the AKAP Yotiao (AKAP9) is associated with increased breast cancer risk[37] and another study presenting AKAP82 (AKAP4) as a novel tumour-associated antigen for multiple myeloma[21].

Disease-relevant processes involving compartmentalised cAMP signalling in general include insulin secretion from pancreatic β-cells, fat metabolism in adipocytes, modulation of immune responses and control of brain functions[81,147,149,158]. Diseases caused by the malfunction of these cAMP-dependent processes include hypertension, diabetes mellitus, obesity and neurological disorders such as schizophrenia.

During the development of new pharmaceuticals (Fig. 1.8), potential targets need to be identified and validated. To validate the inhibition of disease-relevant protein-protein interactions, for instance between AKAPs and PKA, as a drug target, tools are needed to effectively disrupt the interaction in cell culture and animal models, for which the use of well characterised and specific small molecules would be of great value. Small molecules exert their effects in the moment

of application to their target cells, because they diffuse through the membrane. Thus, they reach their target faster than peptides, which are larger and may (in the case of poly-Arg fusions) rely on active transport mechanisms for cellular uptake. The peptide-inherent drawbacks could be bypassed through the use of small organic molecules as inhibitors of the AKAP-PKA interaction. The application area for such substances is in the first instance the same as for the peptidic inhibitors: as a tool for the further elucidation of AKAP and PKA functions. However, they might also represent lead structures for the development of a new class of drugs.

1.9 Objective

An important effector of the ubiquitous second messenger cyclic adenosine monophospate (cAMP) is cAMP-dependent protein kinase (PKA). PKA activity is confined to subcellular compartments through anchoring by A-kinase anchoring proteins (AKAPs). Investigations of the physiological relevance of compartmentalised signalling in cells and animal models is hampered by a lack of tools. As novel tools, small molecule inhibitors of AKAP-PKA interactions have recently been discovered in a high-throughput screening. The aim of this work was to validate and characterise the effects of the small molecules, and to identify their molecular targets.

2 Material and Methods

2.1 Material

2.1.1 Buffers

Buffers were prepared as 10x stock solution and diluted with *Aqua bidest.* prior to use, if not stated otherwise.

- **Laemmli SDS-PAGE sample buffer (4x)**
  15 ml glycerol
  7.5 ml SDS (20% stock)
  25 ml tris (0.625 M stock)
  1% (w/v) bromphenol blue
  adjusted to pH 6.8, ad 50 ml with *Aqua bidest.*
  30 µl dithiothreitol (DTT, 1 M), added per 1 ml prior to use.
  Final concentration was obtained by dilution with sample.

- **Laemmli SDS-PAGE running buffer**
  30 g Tris (0.5 M)
  144 g glycine (0.19 M)
  10 g sodium dodecylsulfate (SDS, 35 mM)
  ad 1 l with *Aqua bidest.*

- **Blotting buffer (10x)**
  58.2 g Tris (480 mM)
  29.3 g glycine (390 mM)
  0.375 % SDS (13 mM)
  ad 1 l with *Aqua bidest.*

- **Blotting buffer (1x)**
  100 ml 10x blotting buffer
  200 ml methanol
  ad 1 l with *Aqua bidest.*

- **Blocking buffer**
  5 % (w/v) skim milk powder
  ad 500 ml with TBS-T

- **Phosphate-buffered saline (PBS, 10x)**
  80 g NaCl (274 mM)
  2 g KCl (27 mM)
  2 g KH_2PO_4 (15 mM)
  11.5 g Na_2HPO_4 (81 mM)
  adjusted to pH 7.4, ad 1 l with *Aqua bidest.*, autoclaved

- **Tris-buffered saline with Tween-20 (TBS-T, 10x)**
  6 g Tris (10 mM)
  44 g NaCl (150 mM)
  adjust to pH 7.4
  5 ml Tween-20
  ad 1 l with *Aqua bidest.*

- **Standard Lysis Buffer**
  1.14 g KH_2PO_4 (10 mM)
  21.92 g NaCl (150 mM)
  adjusted to pH 7.4
  1.46 g EDTA (5 mM)
  1.90 g EGTA (5 mM)
  1 % (v/v) Triton X-100
  0.2 % (w/v) Na-deoxycholate
  1 % (w/v) Igepal CA-630 (NP-40)
  3.20 µg/ml soybean trypsin inhibitor (STI)
  2.00 µg/ml aprotinin
  0.12 µg/ml benzamidine (1 mM)
  0.88 µg/ml PMSF (0.5 mM)
  ad 500 ml with *Aqua bidest.*

- **NMR phosphate buffer**
  28.48 g Na_2HPO_4 (40 mM) ad 4 l with *Aqua bidest.* and
  12.48 g NaH_2PO_4 (40 mM) ad 1 l with *Aqua bidest.*
  were prepared separately and combined 4:1 to adjust pH 7.4
  final volume doubled with *Aqua bidest.*

- **Separating gel buffer**
  37.8 g Tris (0.625 M)
  adjusted to pH 6.8
  ad 500 ml with *Aqua bidest.*, autoclaved

- **Stacking gel buffer**
  45.41 g Tris (0.75 M)
  adjusted to pH 8.8, ad 500 ml with
  ad 500 ml with *Aqua bidest.*, autoclaved

- **Ponceau S staining solution**
  0.125 g Ponceau S
  1.5 ml acetic acid
  ad 50 ml H_2O

- **Lysogeny broth (LB)-medium**
  50 g Pepton
  25 g NaCl (17 mM)
  25 g Yeast Extract
  adjusted to pH 7.5, ad 5 l with
  ad 500 ml with *Aqua bidest.*, autoclaved
  for dishes: additionally 15 g/l agar-agar

- **M9 salt solution (10x)**
  64 g Na_2HPO_4
  20 g KH_2PO_4
  5 g NaCl
  adjusted to pH 7.2, ad 1 l with *Aqua bidest.*, autoclaved

- **Trace elements solution**
  2.5 g EDTA
  in 400 ml *Aqua bidest.*
  250 mg $FeSO_4$
  25 mg $ZnCl_2$
  5 mg $CuSO_4$
  adjusted to pH 7.6, ad 500 ml with *Aqua bidest.*, autoclaved

- **M9 minimal medium (1x, for ^{15}N-labelling of proteins)**
  all solutions autoclaved (A) or sterile filtrated (S) and combined under sterile conditions
  800 ml Aqua bidest (A)
  10 ml Trace elements sol. (A)
  1 ml 1 M $MgSO_4$ (A)
  0.3 ml 1 M $CaCl_2$ (A)
  100 ml M9 solution 10x (A)
  20 ml 20 % glucose (A)
  1.5 ml 1 mg/ml Thiamin (F)
  15 ml 0.1 mg/ml Biotin (F)
  2 ml 250 mg/ml ^{15}N-NH_4Cl (A)

2.1.2 Chemicals and compounds

Standard chemicals were obtained from Carl Roth (Karlsruhe, Germany) or Sigma-Aldrich (Taufkirchen, Germany) if not stated otherwise.
FMP-API-1 to -7 were ordered from ChemBridge (San Diego, CA, USA) and ChemDiv (San Diego, CA, USA).
FMP-API-1 was additionally ordered from Akos (Steinen, Germany).
FMP-API-1 derivatives 1025, 1026, 1027, 1028 and 1030 were synthesised by Dmitry Kashin and Dr. Hans-Gottfried Genieser at Biolog (Bremen, Germany).
FMP-API-2 and its derivatives SM61, SM65 and SM66 were synthesised by Sina Meyer in the Medicinal Chemistry group of Prof. Dr. Jörg Rademann, FMP (Berlin, Germany).

2.1.3 Antibodies

Primary antibodies

AQP2 antiserum H27, as described previously[74]
A18δ4, as described previously[52]
AKAP150, Upstate (Lake Placid, NY, USA)
$PKA_{RII\alpha}$, BD Biosciences
$PKA_{RII\beta}$, BD Biosciences
PKA R2, Abcam
Phospho-phospholamban, Upstate (Lake Placid, NY, USA)
Calsequestrin, GeneTex (San Antonio, TX, USA)

Secondary antibodies

Peroxidase-conjugated goat anti-rabbit $(F(ab')_2$ fragments), Dianova (Hamburg, Germany)
Peroxidase-conjugated rabbit anti-mouse $(F(ab')_2$ fragments), Dianova (Hamburg, Germany)
Cy3-conjugated goat anti-rabbit IgG Jackson ImmunoResearch Laboratories (Newmarket, UK)

2.1.4 Peptides

The AKAP-PKA disrupting peptides
Ht31 (DLIEEAASRIVDAVIEQVKAAGAY),
AKAP18δ-wt (PEDAELVRLSKRLVENAVLKAVQQY),
AKAP18δ-L314E (PEDAELVRLSKRLVENAVEKAVQQY),
AKAP18δ-L314E-D298A (PEAAELVRLSKRLVENAVEKAVQQY),
the negative control peptides
Ht31-P (DLIEEAASRPVDAVPEQVKAAGAY),
AKAP18δ-PP (PEDAELVRLSKRLPENAPLKAVQQY)
and N-terminally stearate-, fluorescein- or biotin-coupled versions of the peptides were synthesised by the Peptide Synthesis group (Dr. Michael Beyermann, FMP). Peptides were purified to > 90%, provided lyophilised and dissolved in DMSO to obtain a 10 mM stock solution. Further dilutions (as indicated in the Figs.) were prepared in buffer.

2.1.5 Proteins

Purified recombinant, cAMP-free regulatory subunits of PKA (human RIIα: 1.0 mg/ml, rat RIIβ: 0.2 and 0.75 mg/ml) were a kind gift of Prof. Dr. F. Herberg (University of Kassel, Germany).
RIIα deletion mutants (Fig. 2.1) were constructed and purified by Dr. Sabine Friedl and Anita Neumann. RIIα(1-87) was constructed by Michael Zenn (University of Kassel, Germany).

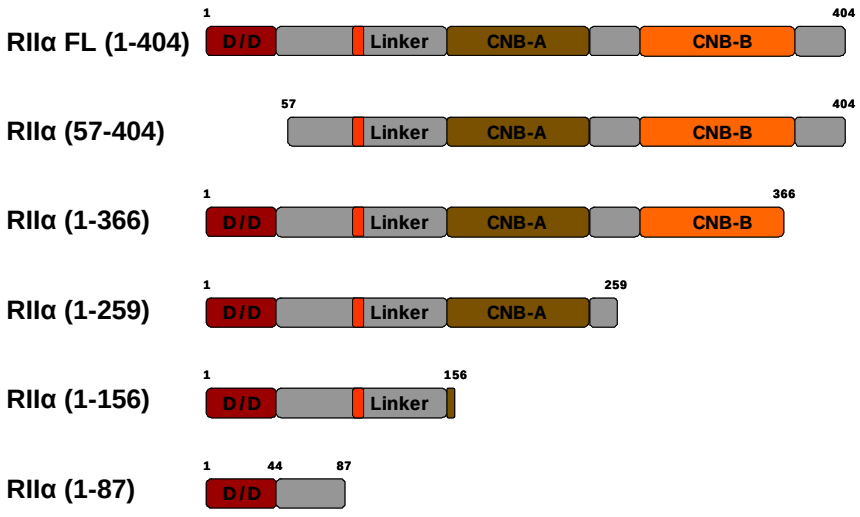

Fig. 2.1: RIIα deletion constructs used in this work. FL, full length. D/D, docking and dimerisation domain. CNB, cyclic nucleotide binding domain.

Catalytic subunits of PKA were obtained in a concentration of 1.66 mg/ml from Promega (Mannheim, Germany).

2.1.6 Bacterial hosts

The *Escherichia coli* strain BL21 Rosetta (DE3) was used for the expression of recombinant RIIα deletion constructs.

2.1.7 Animals

For the generation of primary cells rats were sacrificed by decapitation (*Rattus norvegicus*, strain: Wistar). Organs were prepared and immediately transferred to sterile, ice cold PBS.

2.1.8 Equipment

SDS-PAGE system SE260 Mighty Small II, Hoefer (Holliston, MA, USA)
Trans-Blot SD electrophoretic transfer cell, Bio-Rad (Munich, Germany)
LumiImager F1, Roche Diagnostics (Mannheim, Germany)
Microplates:

- Chemiluminescence: Lumitrac 600 #781074, 384-well, white, flat bottom, polystyrene, high binding, Greiner Bio-One (Frickenhausen, Germany)
- Fluorescence anisotropy: costar #3676, 384-well, low volume, black, round bottom, polystyrene, NBS, Corning (Schiphol-Rijk, The Netherlands)

Power Washer 384, Tecan (Crailsheim, Germany)
Sciclone ALH3000 Pipetting Workstation, Caliper (Hopkinton, USA)
MicroFill Microplate Dispenser, Biotek (Bad Friedrichshall, Germany)
Automatic 12-channel dispenser pipettes, Eppendorf (Hamburg, Germany)
GeniosPro microplate reader, Tecan (Crailsheim, Germany)
Profinia protein purification system, Bio-Rad (Munich, Germany)
Centrifuges

- Beckmann TLK 100 (Krefeld, Germany)
- Beckmann Optima L70 (Krefeld, Germany)
- Sorvall RC 285 (Bad Homburg, Germany)
- Haereus Biofuge pico (Osterode, Germany)
- Haereus Megafuge 1.0 (Osterode, Germany)

EPC-9 patch clamp amplifier, HEKA Elektronik (Lambrecht, Germany)

510 META (UV, NLO and FCS) inverted confocal laser-scanning microscope, Zeiss (Jena, Germany)

Photometer GeneQuantII, GE Healthcare (Freiburg, Germany)

Rotator Blood tube rotator SB1, Stuart Scientific (Leek, UK)

Scintillator Wallac 1409, Liquid Scintillation Counter, PerkinElmer (Rodgau, Germany)

Thermomixer 5436, Eppendorf (Hamburg, Germany)

Pure-water generator MilliQ plus, Millipore (Schwalbach, Germany)

2.2 Methods

2.2.1 Enzyme-linked immunosorbent assay (ELISA) to detect AKAP-PKA interactions

An ELISA-based assay was established to screen a small molecule fragment library (www.chembionet.info; www.fmp-berlin.de) for potential inhibitors of the AKAP-PKA interaction. White 384-well plates (781074, Lumitrac 600, high protein-binding capacity, Greiner Bio-One, Frickenhausen, Germany) were coated with regulatory RIIα subunits of PKA (25 nM in phosphate-buffered saline (PBS) containing 1 mM benzamidine, 0.5 mM phenylmethanesulfonyl fluoride, 3.2 µg/ml trypsin inhibitor I-S, 1.4 µg/ml aprotinin; 20 µl/well) by incubation for 1 h at 22 °C. Free binding sites were blocked with blocking buffer (PBS containing 0.3 % dried skimmed milk and 0.05 % Tween-20; 1 h, 22°C). The wells were washed three times with washing buffer (PBS containing 0.05% Tween-20), GST–AKAP18δ (10 nM in blocking buffer) was added (2 h, 22°C) in the absence or presence of small molecules, peptides or DMSO (the solvent for peptides and compounds) in the concentrations indicated in the legends to the figures. The samples were washed with washing buffer three times. Binding was detected with rabbit anti-AKAP18δ (A18δ3) and peroxidase-conjugated secondary anti-rabbit antibodies (1 h, 22°C for each antibody). The wells were rinsed with washing buffer, LumiLight Western blotting substrate solution (Roche Diagnostics, Mannheim, Germany) was added, and luminescence intensity was assessed in a microplate reader (GeniosPro, Tecan, Durham, NC, U.S.A.) with 10 ms integration time/well. Curves were fitted based on a one-site-binding or -competition model (depending on experiment), and relative IC_{50} values were

calculated using Prism 4.0 (GraphPad Software, San Diego, CA, USA). The IC_{50} value equals the concentration required of a test substance to obtain half-maximal inhibition of the interaction.

2.2.2 Synthesis of focussed libraries derived from FMP-API-1 and -2

The compounds 1025, 1026, 1027, 1028 and 1030 are part of a focussed library derived from FMP-API-1 (formerly also termed 18882), synthesised by Dmitry Kashin and Dr. Hans-Gottfried Genieser at Biolog Life Science Institute GmbH (Bremen, Germany).

The compounds SM61, SM65 and SM66 are part of a focussed library derived from FMP-API-2 (formerly also termed 990), synthesised by Sina Meyer in the Medicinal Chemistry group of Prof. Dr. Jörg Rademann (FMP)[101].

2.2.3 Preparation and culture of IMCD cells

The primary cultures of inner medullary collecting duct (IMCD) cells were prepared from rat kidneys as described before[91,105,142]. Cells prepared from 2 inner medulla were required per 18 cm^2, and plated onto 21 cm^2 (60 mm) tissue culture dishes for cAMP-agarose-pulldowns. For immunofluorescence staining, cells were plated on cover slips in 21 cm^2 dishes. After culturing the cells for 6 days at 37 °C and 5 % CO_2, the dibutyryl-cAMP-containing medium (required to maintain the AQP2 shuttle) was replaced by fresh medium without dibutyryl-cAMP for 24 h prior to use in the procedures described below.

2.2.4 Treatment of IMCD cells with small molecules and AVP

To test the effect of the small molecules on the AQP2 shuttle, they were added from 25 mM or 100 mM stock solutions in DMSO directly into the cell culture medium to achieve the final concentrations indicated in Figs. 3.2-3.5. For control, only DMSO was added in corresponding amounts. The culture dishes were slightly agitated to obtain a homogenous distribution of the compounds, and incubated at 37 °C at 5 % CO_2 for 15 min. To induce the AQP2 shuttle, cells were stimulated by incubation with 100 nM AVP (added after the incubation with the small molecules) for 15 min at 37 °C and 5 % CO_2.

2.2.5 AQP2 immunofluorescence staining

After treatment with compounds and stimulation with AVP, IMCD cells were washed 2 times with PBS. Fixing solution (100 mM cacodylate, 100 mM saccharose, 10 % paraformaldehyde, 0.2 % NaOH) was applied for 15 min at room temperature (RT). Following two washing steps with PBS, cells were permeabilised for 5 min with 0.1 % Triton X-100 in PBS at RT. After two more washing steps with PBS, the cover slips with the fixed cells were transferred to cover slip racks, and washed once again with PBS to remove residual Triton X-100. Fish skin gelatine (0.15 % in PBS) was applied for 20 min at 37 °C as blocking reagent. The fixed and permeabilised cells were incubated with primary anti-AQP2 antibody (H27, 30 µl of a 1:300 dilution per cover slip) for 45 min at 37 °C. Following three washing steps as above, secondary Cy3-conjugated goat anti-rabbit-IgG (30 µl of a 1:300 dilution per cover slip, Jackson ImmunoResearch, USA) was applied for 45 min at 37 °C. After three final washing steps, cover slips were embedded on glass slides with immu-mount (Thermo-Shandon, Pittsburgh, USA).

2.2.6 Trypan blue staining

For plasma membrane integrity analysis, cells were treated with compounds or DMSO as above, and cover slips with living cells were then transferred into an incubation chamber in the laser scanning microscope. After focussing, 50 µl of a 0.5 % trypan blue solution was added, and images were taken immediately afterwards to avoid membrane damaging by trypan blue. For control, cells were treated with 5 % DMSO. At high concentrations, DMSO disintegrates the cell membrane, allowing trypan blue to enter the cell.

2.2.7 Laser scanning confocal microscopy

Laser scanning confocal microscopy (LSM) was carried out with IMCD cells after immunofluorescence or trypan blue staining on an LSM 510 META (Carl Zeiss, Jena, Germany). The Cy3 fluorophore was excited at 543 nm wavelength, and emission was detected at 560 nm. Trypan blue was excited and detected at the same wavelengths. All confocal images shown in this work are representative images from at least three independent experiments.

To quantify the effects of the small molecules on the AQP2 shuttle, the ratio of intracellular fluorescence *vs.* plasma membrane fluorescence of AQP2 was determined by defining regions of interest around the plasma membrane or the intracellular compartment as described previously[52].

2.2.8 Preparation and culture of neonatal rat cardiac myocytes

The cardiac myocytes from hearts of 1-3 days old sacrificed rats were obtained by isolating the lower left ventricles and digesting them enzymatically with 0.48 mg/ml collagenase type II (Biochrom AG, Berlin, Germany) and 0.6 mg/ml pancreatin. A suspension of the remaining cells in a 4:1 mixture of DMEM and M199 medium supplemented with 10 % horse serum (Invitrogen, Karlsruhe, Germany) and 5 % fetal calf serum (Invitrogen, Karlsruhe, Germany) was incubated for 1 h at RT on tissue culture plates to deplete fibroblasts. The supernatant containing the myocytes was plated onto tissue culture dishes as required for the subsequent experiments (see below) in DMEM/M199 medium containing 10 % horse serum, 5 % fetal calf serum, 200 mM glutamine and 1 % penicillin-streptomycin. After 24 h at 37 °C and 5 % CO_2 the medium was exchanged by DMEM/M199 medium containing 10 % horse serum, 0.5 % fetal calf serum, 200 mM glutamine and 1 % penicillin-streptomycin, and cells were incubated for further 24 h at 37 °C and 5 % CO_2 prior to use.

2.2.9 Preparation of cell lysates

The medium was removed from IMCD cells or cardiac myocytes and the cells were homogenised in lysis buffer (10 mM K_2HPO_4, 150 mM NaCl, 5 mM EDTA, 5 mM EGTA, 1% Triton X-100, 0.25% deoxycholate, 1 mM benzamidine, 0.5 mM phenylmethanesulfonyl fluoride, 3.2 µg/ml trypsin inhibitor I-S, 1.4 µg/ml aprotinin). The lysates were cleared by centrifugation (12,000 g, 4 °C, 10 min), and supernatants used as described below.

2.2.10 cAMP-agarose pulldown

cAMP-agarose pulldowns from cardiac myocytes were carried out by Dr. Márta Szaszák (FMP). Cardiac myocytes were plated onto 100 mm tissue culture dishes at a density of 10^7 cells/dish and cultured for 48 h.

Small molecules were added into the culture medium of cardiac myocytes or IMCD cells for 30 min at 37 °C. After preparation of lysates, 40 µl of a 50 % slur-

ry of cAMP-agarose (8-AHA-cAMP agarose; Biolog, Bremen, Germany) was added per ml lysate in the absence or presence of 50 mM cAMP, and incubated for 3 hours at 4 °C. Proteins bound to cAMP-conjugated agarose were washed four times with lysis buffer and eluted with Laemmli sample buffer at 95 °C. Eluted proteins were analysed by Western blotting (see below).

2.2.11 Analysis of RII complex formation

For analysis of complex formation with recombinant RIIβ, the protein was diluted to 1.2 µM in PBS, and FMP-API-1 was added to final concentrations of 2 or 4 mM (final volume 15 µl). For control DMSO was added (4 %). The solution was incubated at 37 °C for 1 h. 10 µl Laemmli sample buffer containing 1 mM DTT was added.

For analysis of RII complex formation in cardiac myocytes, which were carried out by Dr. Márta Szaszák, cells were plated onto 6-well tissue culture plates at a density of $2 \cdot 10^6$ cells/well. Serum was withdrawn 16 h prior to the experiments which were carried out 2 days after seeding. Small molecules were directly added into the culture medium for the indicated times at 37 °C. The medium was removed and cells were lysed in 100 µl of Laemmli sample buffer containing 1 mM DTT.

2.2.12 Western blotting

Samples were loaded onto 10 %- or 15 %-SDS-PAGE gels and separated at 20 mA per gel for 75 min. After transfer on polyvinylidene fluoride (PVDF) membranes (60 min at 10 V), membranes were stained with ponceau S for 5 min to detect proteins for successful transfer onto the membranes. Free binding sites on the membrane were blocked by incubation with 5 % skim milk solution in TBS-T for 1 h.

The membrane was then incubated for 2 h at room temperature with primary antibody and, after three 5 min washing steps with TBS-T, subsequently for 1 h at room temperature with secondary horseradish peroxidase (POD)-coupled antibody. After three 10 min washing steps with TBS-T the membrane was incubated 5 min in LumiLight Western Blotting substrate solution (Roche). Detection and quantification of luminescence were carried out in the LumiImager F1 (Roche).

2.2.13 Patch-clamp measurements of L-type Ca^{2+}-channel currents

Electrophysiological patch-clamp measurements were carried out in collaboration with Dr. Dorothea Lorenz (FMP). 3-5 days after seeding of neonatal rat cardiac myocytes, whole-cell L-type I_{Ca} (Ca^{2+} current) was recorded as previously described[64] at room temperature. For a comparison of different cell current densities, I_{Ca}/C_m was calculated. Cardiac myocytes were perfused with small molecules (100 µM each, DMSO content 0.1 %) or DMSO (0.1 %) *via* the patch pipette. The influence of small molecules on the isoproterenol stimulation of L-type Ca^{2+}-channels was measured 11 min after patch rupture. Isoproterenol was applied through an application pipette (QMM Ala Scientific Instruments, New York, USA) positioned near the cell. The direct channel activator Bay K8644 was added directly into the measurement buffer (where indicated). For statistical analysis (Student's t-test) isoproterenol-evoked I_{Ca}/C_m was expressed as a fraction of unstimulated I_{Ca}/C_m.

2.2.14 Surface plasmon resonance measurements

Surface plasmon resonance (SPR) measurements were carried out in collaboration with Dr. Bastian Zimmermann (Biaffin, Kassel, Germany). A Biacore 3000 instrument (Biacore/GE Healthcare, Uppsala, Sweden) was used as described to measure AKAP-PKA interactions (Figs. 3.8, 3.18B and 3.19)[51]. In brief, streptavidin (SA) chips (research grade, Biacore/GE Healthcare) were used to capture 100 resonance units (RU) of the N-terminally biotinylated peptide AKAP18δ-L314E, derived from the RII binding domain of AKAP18δ[65]. The subsequent interaction studies were performed in running buffer (10 mM HEPES (pH 7.4), 150 mM NaCl, 0.1 mg/ml BSA and 0.005 % surfactant P20) at 25 °C. Non-specific binding was subtracted on the basis of a blank surface with biotin-saturated streptavidin. 30 nM RIIα or truncated versions thereof (human; cAMP-free) were incubated for 120 min with different concentrations of FMP-API-1 and injected for 180 s with a flow rate of 30 µl/min. After each injection the dissociation phase was monitored for 60 s. The surface was regenerated with two 20 s injections of 0.1 % SDS prior to the next interaction analysis.

A fixed concentration of 30 nM RIIα was incubated with the FMP-API-1 derivatives (6.25 - 200 µM) for 120 min (Fig. 3.18B). The mixture was analysed on an AKAP18δ-L314E surface prepared on an SA-chip as described above (running

buffer: 10 mM HEPES (pH 7.4), 150 mM NaCl, 0.1 mg/ml BSA, 0.2 % DMSO, 0.005 % surfactant P20).

Influence of DTT (Fig. 3.19A and B) was measured as above with 30 nM RIIα incubated with concentrations of 25 - 200 µM FMP-API-1 or 1027 for 120 min in running buffer (20 mM HEPES (pH 7.4), 150 mM NaCl, 50 µM EDTA, 0.005 % surfactant P20, 2 % DMSO, 5 mM DTT where indicated) with or without 5 mM DTT prior to analysis as described above.

To measure the binding of RIIα and truncated versions thereof (Fig. 2.1) to immobilised AKAP18δ-L314E in presence of compound 1027 (Fig. 3.19C), the compound (200 µM) was incubated with 30 nM of the RIIα deletion constructs for 14 h in running buffer (20 mM HEPES pH 7.4, 150 mM NaCl, 50 µM EDTA, 0.005 % surfactant P20, 2 % DMSO) and interaction with AKAP18δ-L314E was analysed as described above. In a second series of experiments, 10 µM cAMP was added during incubation.

To assess the influence of DTT on the effect of 1027 (Fig. 3.19D), 30 nM RIIα was preincubated with 300 µM 1027 for 4 h in running buffer (20 mM HEPES pH 7.4, 150 mM NaCl, 50 µM EDTA, 2 µg/ml BSA, 0.005 % surfactant P20, 3 % DMSO). The sample was split and incubated for 20 hours in buffer either containing 10 mM DTT or no DTT. Binding to AKAP18δ-L314E was monitored as described above.

Direct binding of the compounds to RIIα (Figs. 3.9A and 3.18C) was monitored on a Biacore S51 (Biacore/GE Healthcare, Uppsala, Sweden). 7000 RU of RIIα were covalently immobilised on an S-CM5 chip (research grade, Biacore/GE Healthcare) by standard amine-coupling as described by the manufacturer. Non-specific binding was subtracted using an activated and deactivated (NHS/EDC and ethanolamine) control surface. In running buffer (25 mM Tris pH 7.4, 150 mM NaCl, 50 µM EDTA, 5 % DMSO) 6 – 200 µM compound was injected for 60 s at a flow rate of 30 µl/min. Dissociation was monitored for 60 s. Regeneration of the surface was not necessary due to a fast off-rate.

For solution competition assays of Ht31 and compounds (Figs. 3.11 and 3.18D), 10000 RU of RIIα were immobilised via amine-coupling on an S-CM5 chip for use on the Biacore S51. 100 µM compound, 50 nM Ht31 and a mixture of both components were injected for 60 s in running buffer (25 mM Tris pH 7.4, 150 mM NaCl, 50 µM EDTA, 5 % DMSO, 0.005 % surfactant p20) at a flow rate of

30 µl/min followed by a dissociation phase of 60 s. The figures show an overlay plot of the three individual injections.

2.2.15 Saturation transfer difference nuclear magnetic resonance (STD-NMR)

STD-NMR experiments[99,156] were carried out in collaboration with Dr. Carolyn Vargas and Dr. Peter Schmieder (FMP) on a Bruker DRX600 spectrometer equipped with a Z-axis-gradient 5-mm TXI Cryoprobe at 300 K. Nuclear magnetic resonance (NMR) samples of unlabelled PKA-RIIα, GST-AKAP18δ and Ovalbumin were prepared in 20 mM phosphate buffer (pH 7.4) at 14 µM, 19 µM and 18 µM, respectively, and 1 mM FMP-API-1 in DMSO-d_6 was added to each. The final protein–ligand solutions contained 2 % DMSO-d_6. Saturation transfer difference (STD) NMR experiments were recorded with the carrier frequency set at 0.68 ppm for on-resonance irradiation and about 330 ppm for off-resonance irradiation. A train of 50 Gaussian-shaped pulses at 40 ms was applied, each separated by a 1-ms delay, for a total duration of 2.05 s, to achieve selective protein saturation. Spectra acquisition was done with 32 scans and a relaxation delay of 1.3 s. A $T_{1\rho}$ spin lock pulse of 40 ms was used to suppress the background protein signals. The STD spectrum was obtained from the internal subtraction of the on-resonance from the off-resonance data by phase cycling.

2.2.16 ^{15}N-HSQC-NMR

Isotopically enriched RIIα-D/D domain (GST-RIIα(1-44)) was expressed in the *E. coli* BL21 (DE3) strain. ^{15}N-NH_4Cl was used as sole nitrogen source in M9 minimal medium. The GST-tag was removed during the purification by thrombin cleavage of the glutathione-sepharose-bound fusion protein. The obtained tag-free protein was dialysed overnight at 4 °C against a 20 mM sodium phosphate buffer containing 150 mM NaCl, pH 7.4.

The NMR experiments were carried out by Dr. Mangesh Joshi (FMP). Spectra were recorded on a Bruker 600 MHz Avance spectrometer equipped with a triple channel cryoprobe. The temperature was set to 30 °C in all experiments. ^{1}H,^{15}N-correlation experiments were recorded using a standard HSQC pulse program employing WATERGATE for solvent suppression. For small molecule binding studies, the typical protein concentration was in the order of 0.2 mM. The concentration of the small molecule FMP-API-1 was increased stepwise

from 0 to 2 mM. Each step was followed by recording of a new spectrum. The acquisition time in the direct dimension was restricted to 150 ms. A total of 256 increments was recorded in the indirect dimension.

2.2.17 Peptide SPOT array synthesis

Peptide arrays were generated by Angelika Ehrlich (FMP) by automatic SPOT-synthesis on Whatman 50 cellulose membranes by using Fmoc (fluoren-9-ylmethoxycarbonyl) chemistry and the AutoSpot-Robot ASS 222 (Intavis Bio-analytical Instruments AG, Cologne, Germany) as described[38,78,141]. Control spots (approx. 50 nmol of peptide per spot) were excised from the cellulose membrane and analysed by MALDI-TOF (matrix-assisted laser-desorption ionisation-time-of-flight)-MS and HPLC.

2.2.18 RII overlay

RII overlay assay was carried out by Philipp Skroblin (FMP) as described previously[74] using recombinant, ^{32}P-labelled human RIIα. Briefly, membranes were equilibrated in EtOH, washed in PBS and incubated in blocking buffer for a minimum of 2 hours at room temperature. Purified recombinant RIIα subunits (2.5 µg) were radiolabelled by incubation with 2 µl of purified catalytic subunit of PKA (1.66 µg/µl, Promega, Mannheim, Germany) and 0.1 µM γ-^{32}P-ATP (6000 Ci/mmol; GE Healthcare, Munich, Germany) in 500 µl buffer (25 mM KH_2PO_4, 10 mM $MgCl_2$, 10 µM cAMP and 0.5 mM DTT). The final concentration of 10 µM ATP was reached after 10 min by adding 5 µl 1 mM cold ATP. After 50 min 70 µl dextran blue (10 mg/ml) was added and the reaction was stopped by removal of cAMP and the separation of radiolabelled RII subunits using gel filtration (Sephadex G-50, medium; GE Healthcare, Munich, Germany). The dextran blue fraction contains the RII subunits. The total activity of the dextran blue fraction was measured and specific activity was calculated in cpm (counts per minute; Liquid scintillation counter Wallac 1410). The membranes were incubated overnight with radiolabelled RII subunits in blocking buffer, washed with blocking buffer (4 times, 10 min) and twice with PBS. Signals were detected by autoradiography (Phosphoimager Storm 830) and analysed with the ImageQuant software (GE Healthcare, Munich, Germany).

2.2.19 Quantitative cAMP assay

Determination of cAMP concentration was carried out in collaboration with Dr. Jens Furkert (FMP). Cardiac myocytes (see above) were plated onto 24-well tissue culture plates at a density of $6 \cdot 10^5$ cells/well. After 48 h the cells were washed with serum-free medium. 2 h later the cells were washed with 1 ml of stimulation medium (culture medium without serum, supplemented with 10 mM HEPES, 0.5 % BSA, 0.25 mM 3-isobutyl-1-methylxanthine (IBMX)) and incubated for 30 minutes at 37 °C with isoproterenol, PGE_1 or PGE_2 and FMP-API-1 as indicated in Fig. 3.16. The incubation was terminated by aspiration of the medium and lysis of the cells with 750 µl of 0.1 % trifluoroacetic acid, 0.005 % Triton X-100 for 30 min at 4 °C. The cellular cAMP content was determined by radioimmunoassay (RIA) as described previously[44].

2.2.20 PKA activity assay

The PKA activity assay (Promega, Madison, WI, USA) was carried out by Dr. Márta Szaszak (FMP) on cardiac myocytes and by Hendrikje Göttert (FMP) on recombinant proteins. It is based on phosphorylation of a PKA substrate peptide (PepTag A1 peptide). By addition of the phosphate group, the peptide obtains a negative charge compared to a positive one before the reaction, and can thus be separated from the non-phosphorylated peptide by an agarose gel electrophoresis. The peptide substrate is labelled fluorescently, hence detection and semiquantification can be carried out by scanning densitometry of the agarose gel.

The PKA activity assay was conducted according to the manufacturer's protocol. To measure PKA activity in neonatal rat cardiac myocytes, cells were plated onto 6-well tissue culture plates at a density of $2 \cdot 10^6$ cells/well. Myocytes were used 48 h after preparation and serum-starved overnight prior to the experiment. Small molecules were added to the medium as indicated in the legends to the figures. Medium was removed and lysates were prepared. PepTag A1 peptide (56 ng/µl) was incubated with 15 µl of cleared supernatant in PepTag PKA reaction buffer (final volume 25 µl) at 30 °C for 10 min. The reaction was stopped by boiling the samples for 10 min. Phosphorylated and non-phosphorylated PepTag A1 peptides were separated by 0.8 % agarose gel electrophoresis. Images were taken with the Lumi Imager F1 and bands were

analyzed densitometrically. In order to determine the influence of small molecules on purified PKA, recombinant catalytic subunits and RII subunits were used instead of cell lysates as indicated in the legends to the figures.

2.2.21 Phosphatase activity assay

For the determination of phosphatase activities, a calcineurin assay kit (Calcineurin Cellular Assay Kit Plus, Biomol GmbH, Hamburg, Germany) was used. Briefly, it is a microplate assay based on dephosphorylation of an RII phosphopeptide substrate by the phosphatases to be assayed. The produced free phosphate is quantified by addition of malachite green which forms a complex with phosphate ions. For analysis of neonatal rat cardiac myocyte cell lysates, cells seeded in 6-well plates according to section 2.2.8 (2,000,000 cells/well seeded for use on the next day) were treated as indicated in Fig. 3.17C for 30 min. After washing with TBS (3x), cells were detached from the wells with a cell scraper and suspended in 270 µl ice cold lysis buffer. The lysis buffer and all other reagents were used according to the instructions of the kit manufacturer. After 10 min centrifugation at 4 °C and 22,000 g, the assay was conducted according to instructions.
To measure the influence on calcineurin, the kit-included recombinant enzyme was diluted 1:6.25 in lysis buffer, treated with DMSO or FMP-API-1 as indicated in Fig. 3.17C and further analysed like the cell lysates.

2.2.22 Fluorescence anisotropy assay

Fluorescence anisotropy (FA) measures the rotational diffusion of fluorescent dyes excited by linearly polarised light. When light linearly polarised in a defined oscillations plane is used to excite the dyes, only the dyes with their absorption transition vectors aligned parallel to the electric vector of the polarised light are selectively excited. The excited dyes will also emit polarised light. The orientation of the emission oscillations plane depends on how fast the dye tumbles in its solution between the time points of excitation and emission. A small, free, fluorescein-conjugated peptide tumbles quickly, while the same peptide bound to a large protein binding partner tumbles much slower. Hence, fluorescence anisotropy can be used to determine the binding state of a fluorescently labelled peptide (and also other ligands)[19,86]. Because of its advantages – direct and fast measurement of interactions in solution, no need to separate unbound from

bound ligands, low reagent requirements – it was used successfully in a number of interaction studies and high throughput screening approaches[121-124].

Technically, the degree of polarisation is determined from measurements of fluorescence intensities parallel and perpendicular to the linearly polarised excitation light. It is expressed as fluorescence polarisation (P) or fluorescence anisotropy (r):

$$P = \frac{(F_{=} - F_{+})}{(F_{=} + F_{+})} \qquad r = \frac{(F_{=} - F_{+})}{(F_{=} + 2F_{+})}$$

where $F_{=}$ = fluorescence intensity parallel to the excitation plane

F_{+} = fluorescence intensity perpendicular to the excitation plane

In order to exploit fluorescence anisotropy to measure AKAP-PKA interactions, fluorescein-conjugated versions of the AKAP-PKA disruptor peptides AKAP18δ-wt, AKAP18δ-L314E and AKAP18δ -L314E-D298A were used, and their binding to RIIα was determined.

Generally, TBS buffer containing 0.1 % Tween-20 (TBS-T) and 1 mM DTT was used (FA buffer). The detergent Tween-20 was added to reduce non-specific interactions, which might cause unspecifically increased FA values. Black 384-well microplates with round bottoms and low volume (Corning #3676) were used to avoid well-to-well crosstalk and reflections. Additionally, the plates had NBS (non-binding surface) properties to avoid binding of proteins or peptides to the wells. The final assay volume was 10 µl/well.

For the binding experiment (Fig. 3.20A), 3 µl FA buffer were pipetted into the wells. 4 µl of the fluorescein-labelled peptides (final concentration 10 nM) were added. After centrifugation of the microplate (1 min, 1,000 g), 3 µl RIIα (0.25 – 500 nM) was added. After another centrifugation step and 30 min incubation at 37 °C, FA was measured in a microplate reader.

For competitive inhibition experiments (Figs. 3.20B, 3.21), 3 µl FA buffer containing the competitive peptides AKAP18δ-wt (2.5 pM – 250 µM, Fig. 3.20B), AKAP18δ-L314E (100 pM – 100 µM, Fig. 3.21) or small molecules (250 nM – 2.5 mM, Fig. 3.21) were pipetted into the wells. After centrifugation, 3 µl RIIα (20 nM) was added, and the plate was incubated for 60 min at room temperature. F-AKAP18δ-wt (10 nM, Figs. 3.20B, 3.21A and C) or F-AKAP18δ-L314E-

D298A, Figs. 3.21B and D) was added, the plate centrifuged and again incubated for 30 min at 37 °C. FA was measured in a microplate reader.
For the control reactions (Fig. 3.20B) the peptides and protein were combined as indicated in the figure and as described above.

2.2.23 Fluorescence anisotropy-based high throughput screening

For the fluorescence anisotropy-based high throughput screening, the ChemBioNet screening collection was used. The library (16671 compounds) has been designed after analysis of the World Drug Index (WDI) for privileged substructures or scaffolds (maximum common substructures) by the drug design and modelling group of the FMP (www.fmp-berlin.de, www.chembionet.info). The library is placed on 48 384-well microtiter plates with compounds solubilised at 10 mM concentrations in DMSO (supplied by ChemDiv, San Diego, CA, USA). The last two columns of each plate contain only DMSO for set up of controls on the assay plates.
The following pipetting sequence was planned for the automated screening:

1. All wells of a 384-well microplate (the screening microplate) were filled with 5 µl FA buffer by a dispenser
2. Small molecules or competitive peptides (AKAP18δ-wt or AKAP18δ-PP) were added from their respective reservoir plates (see below) into the sample or control wells of the screening microplate by the pipetting workstation (each 0.4 µl/well; see Table 2.1)
3. F-AKAP18δ-wt was added from its reservoir plate to the screening microplate by the pipetting workstation (3 µl/well)
4. RIIα was added from its reservoir plate to the screening microplate by the pipetting workstation (1.6 µl/well)

To obtain the final concentrations of the reagents as indicated in Table 2.1, the following solutions were prepared.

- 70 ml of an F-AKAP18δ-wt solution (33.3 nM) were prepared in FA buffer.
- For each of the competitive peptides AKAP18δ-wt and AKAP18δ-PP 100 µl of both a 425 nM and a 62.5 µM solution were prepared in FA buffer.

- RIIα was diluted to 125 nM in a total volume of 35 ml, and to 1.5 µM in a total volume of 200 µl.

Table 2.1: Screening microplate layout for the fluorescence anisotropy-based high-throughput screening. F-18δ-wt = F-AKAP18δ-wt, 18δ-wt = AKAP18δ-wt, 18δ-PP = AKAP18δ-PP

	1-22	23	24
A	10 nM F-18δ-wt + 20 nM RIIα + 20 µM compound	10 nM F-18δ-wt + 0 nM RIIα	10 nM F-18δ-wt + 20 nM RIIα
B		10 nM F-18δ-wt + 20 nM RIIα	10 nM F-18δ-wt + 20 nM RIIα + 2.5 µM 18δ-PP
C		10 nM F-18δ-wt + 240 nM RIIα	10 nM F-18δ-wt + 20 nM RIIα + 17 nM 18δ-PP
D		10 nM F-18δ-wt + 20 nM RIIα + 17 nM 18δ-wt	10 nM F-18δ-wt + 20 nM RIIα + 2.5 µM 18δ-wt
E		10 nM F-18δ-wt + 20 nM RIIα + 2.5 µM 18δ-wt	10 nM F-18δ-wt + 20 nM RIIα + 17 nM 18δ-wt
F		10 nM F-18δ-wt + 20 nM RIIα + 17 nM 18δ-PP	10 nM F-18δ-wt + 240 nM RIIα
G		10 nM F-18δ-wt + 20 nM RIIα + 2.5 µM 18δ-PP	10 nM F-18δ-wt + 20 nM RIIα
H		10 nM F-18δ-wt + 20 nM RIIα	10 nM F-18δ-wt + 0 nM RIIα
I			
J			
K			
L			
M			
N			
O			
P			

The fluorescent peptide solution was equally filled into the wells of a 384-deep well-microplate according to Table 2.1, which was then placed in the automatic pipetting workstation. Similarly, the non-fluorescent peptides AKAP18δ-wt and AKAP18δ-PP were pipetted into the respective wells of another deep well-microplate according to Table 2.1 (columns 23 and 24). The RIIα solutions were pipetted into a diamond plate (with a low dead volume to reduce protein requirement) according to Table 2.1, which was also placed in the pipetting workstation.

The small molecules of the ChemBioNet library were prediluted for the screening to reduce unspecific effects and precipitation upon addition to the buffer. From each of the 48 plates, the pipetting workstation transferred 0.5 µl/well compound stock solution (10 mM) to a prepared intermediate plate containing 10 µl FA buffer/well (resulting in a concentration 500 µM). This plate was then placed into the pipetting workstation, and 0.4 µl of each compound were transferred onto the screening microplate (resulting in a final concentration of 20 µM).

After combination of all reagents, the plates were incubated for 15 min at 37 °C and FA was measured in a microplate reader to assess the binding of F-AKAP18δ-wt to RIIα in presence of the compounds or control peptides.

3 Results

3.1 High throughput ELISA screening of a small molecule library yielded new AKAP-PKA inhibitors

This work aimed at the characterisation of small molecules found in a screening approach conducted to identify new AKAP-PKA inhibitors (during the diploma thesis “Identifizierung niedermolekularer Inhibitoren von A-Kinase-Ankerprotein – Proteinkinase A-Interaktionen”[22]).

Major goals of this work were to identify the molecular target of these small molecules and their applicability to study physiological functions of AKAP-PKA interactions. For clarity, the results of the diploma thesis are shortly summarised in the following.

The expression and purification of recombinant AKAP18δ was optimised, and a 384-well microtiter plate-based ELISA was developed to quantify the direct interaction between RIIα subunits of PKA and AKAP18δ in a high throughput manner. The assay was validated with the AKAP-PKA anchoring disruptor peptides Ht31 and AKAP18δ-L314E (Fig. 3.1A).

Then, the FMP20,000 library consisting of 20,064 small molecules (selected for their chemical diversity and fulfilment of Lipinski rules[84] to increase the chance for good bioavailability, and an average molecular weight of 250 g/mol) was screened. Nine compounds were shown to inhibit the RIIα-AKAP18δ interaction concentration-dependently in the ELISA assay with IC_{50} values between 10 and 75 µM[22]. The identities of the compounds were verified by combined liquid chromatography and mass spectrometry (LC-MS) analyses.

3.2 Reordered compounds showed the same inhibitory effect

The LC-MS verification was repeated with restocked compounds obtained from different commercial suppliers in sufficient amounts for further investigations. They were subjected to the ELISA assay to confirm their inhibitory activity on the AKAP18δ-RIIα interaction. For seven of the nine compounds the inhibitory effect was confirmed, and IC_{50} values between 1 and 386 µM were calculated (Fig. 3.1B, Table 3.1). The reduced activity (i.e. higher IC_{50} value) of some compounds (e.g. FMP-API-7) is likely to be caused by differences in purity.

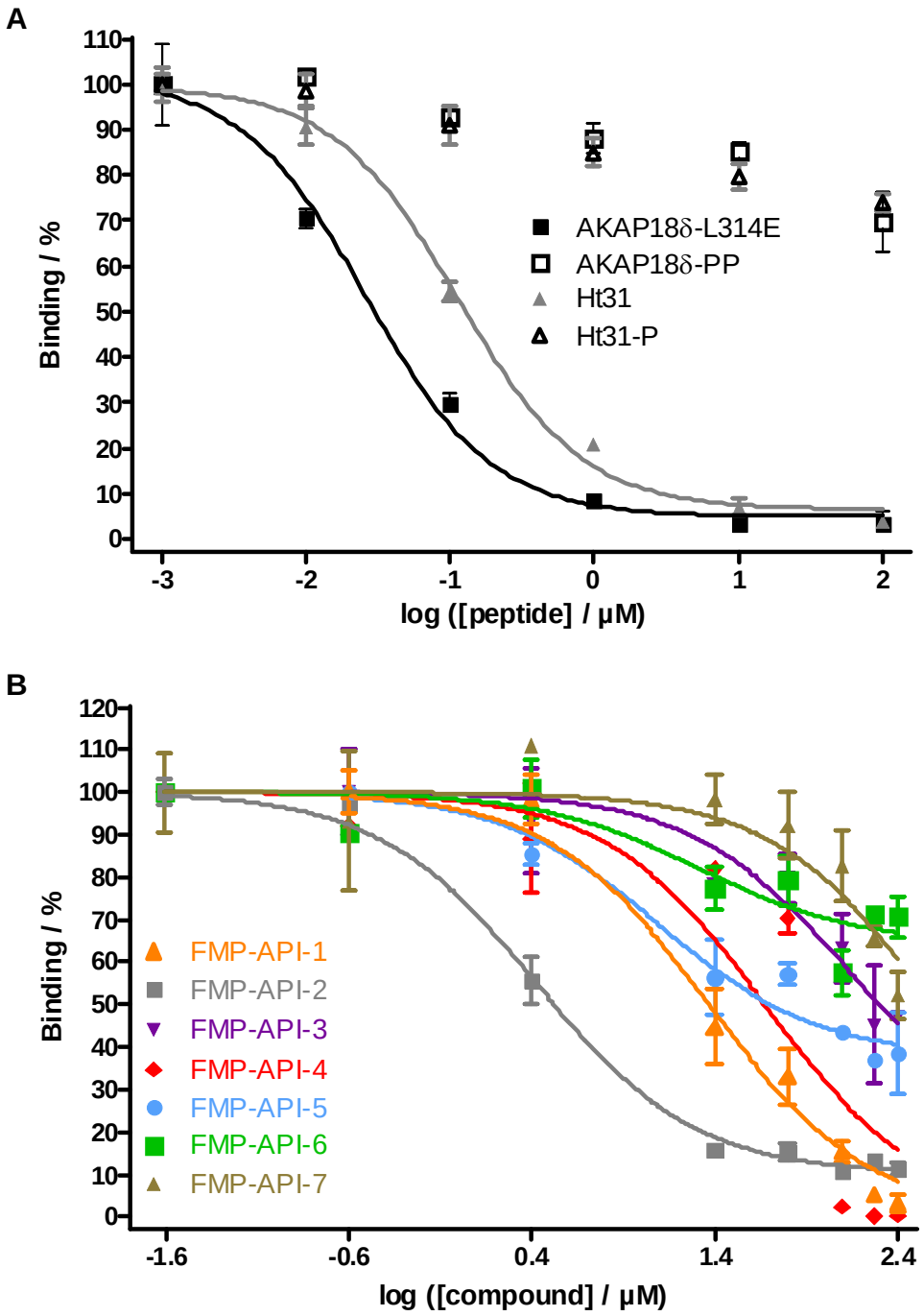

Fig. 3.1: ELISA-based assay to quantify the interaction between AKAP18δ and PKA-RIIα subunits. A. 384-well microplates were coated with RIIα (25 nM). Free binding sites were blocked and GST-AKAP18δ (10 nM) was added in the presence of the indicated AKAP-PKA anchoring disruptor peptides or control peptides. The bound AKAP18δ was detected by incubation with rabbit AKAP18δ-specific and peroxidase-conjugated anti-rabbit secondary antibodies, followed by incubation with a luminol-containing peroxidase substrate solution. Chemiluminescence intensity was measured in a plate reader (n = 3; means ± SEM). Data were normalised to control wells. B. Assay as in panel A; instead of peptides the small molecules identified in the high throughput screening (0.25 – 250 µM) were added as indicated (n = 3; means ± SEM).

Table 3.1: List of small molecules from high througphut screening validated to disrupt AKAP-PKA interactions. Name, name of the small molecules used throughout this work. Compound-ID, identifier used in the FMP20000 compound library. MW, molecular weight in g/mol. logP, calculated partition coefficient. H-Acc., number of H-bond-acceptors in the molecule. H-Don., number of H-bond-donors in the molecule. IC_{50} / µM, inhibitory concentration for 50 % activity in the ELISA assay in µM.

Name	Compound-ID	Structure	Formula	MW / g/mol	logP	H-Acc.	H-Don.	IC_{50} / µM
FMP-API-1	18882	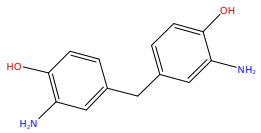	C13H14N2O2	230.26	1.777	2	6	23
FMP-API-2	990	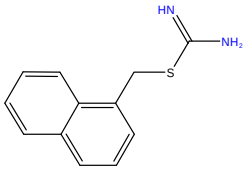	C12H12N2S	216.30	3.440	2	3	1
FMP-API-3	8724	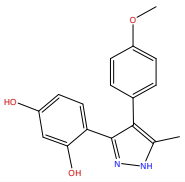	C17H16N2O3	296.32	3.334	4	3	134
FMP-API-4	11546	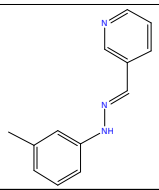	C13H13N3	211.26	2.342	2	1	47
FMP-API-5	14741	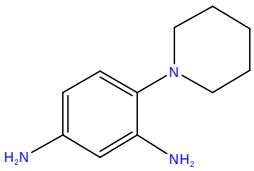	C11H17N3	191.27	1.416	0	4	12
FMP-API-6	14794	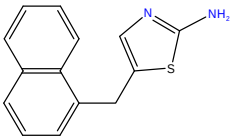	C14H12N2S	240.32	3.164	2	2	20
FMP-API-7	4496	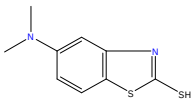	C9H10N2S2	210.32	3.308	3	1	386

The next step was to investigate the effects of the compounds in cell models to study the influence on AKAP-dependent processes in living cells.

3.3 Application of the compounds to cell models reveals cell-type specific influence on cAMP signalling pathways

3.3.1 FMP-API-2 interferes with the aquaporin 2-shuttle in renal inner medullary collecting duct cells

Experimental evidence indicates that the AQP2 shuttle depends on the interaction between AKAPs and PKA[52,75,77,141]. To test for the influence of the compounds on the AQP2 shuttle, inner medullary collecting duct (IMCD) cells were obtained from inner medulla of rat kidneys. IMCD cells maintain aquaporin 2 (AQP2) expression and respond to AVP with the translocation of intracellularly stored aquaporin-2-bearing vesicles into the plasma membrane (AQP2 shuttle; see introduction for details), which may be monitored by immunostaining for AQP2 and immunofluorescence microscopy. The cells were treated with the compounds in the desired concentrations and under conditions described in the legends to the Figs. 3.2-3.5.

Initially, all primary hit compounds were tested in the IMCD cell model by adding them directly into the culture medium for 15 min. The final concentrations tested were higher than the IC_{50} values calculated from the ELISA experiments (Fig. 3.1) to circumvent potential low membrane permeability. However, some of the compounds precipitated upon addition to the culture medium. For these compounds, the concentration was reduced in further experiments to avoid precipitation. The IMCD cells were stimulated with AVP for 15 min to activate the cAMP-dependent signalling cascade leading to translocation of AQP2 into the plasma membrane. The cells were analysed by immunofluorescence staining and microscopy as described in section 2.2.5 and 2.2.7.

As controls, cells were left untreated or were treated with DMSO, the solvent for the compounds. In both untreated and DMSO-treated cells, a mainly cytosolic distribution of AQP2 was observed, with a large proportion in the perinuclear region, as was observed previously[52,141] (Fig. 3.2A, left panel). AVP caused a clear and significant ($p < 0.001$) redistribution of AQP2 to the plasma membrane (Fig. 3.2A, right panel).

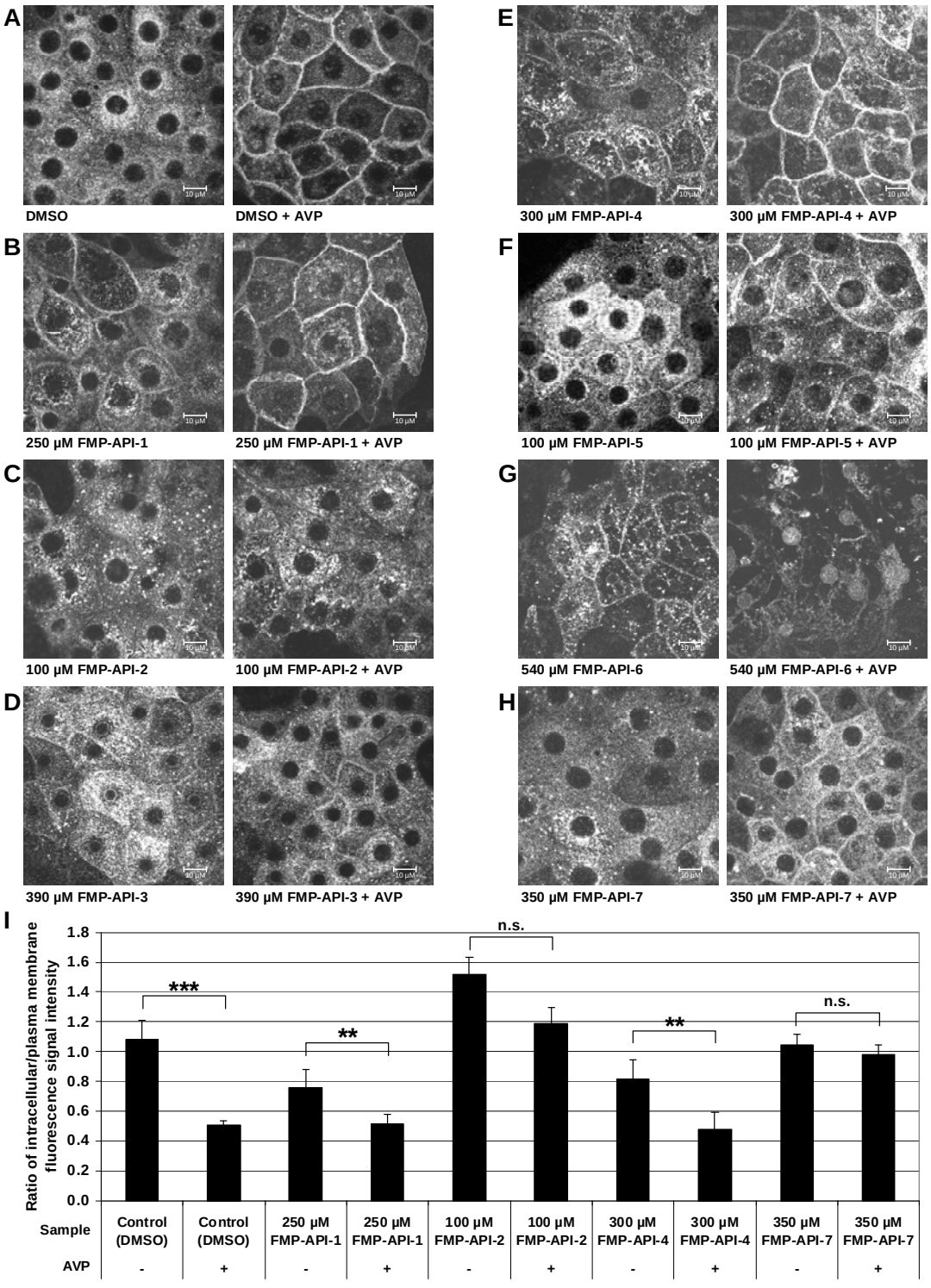

Fig. 3.2: Small molecules identified in the screening (FMP-API-1-7) were tested for effects on the AQP2 shuttle in IMCD cells. IMCD cells were treated for 15 min with the solvent DMSO (A) or small molecules in the indicated concentrations (B-H) in the absence or presence of AVP (+ AVP). Cells were fixed, permeabilised and immunostained with AQP2-specific and Cy3-conjugated secondary antibodies, and analysed by laser scanning confocal microscopy. I. The redistribution of AQP2 to the plasma membrane was quantified by calculating the ratio of intracellular *vs.* plasma membrane fluorescence signal intensity[74] (**, $P < 0.01$; ***, $P < 0.001$; n.s., not significant).

FMP-API-1 displayed no influence on the AQP2 shuttle. Microscopic inspection of the cells suggested that they appeared as control cells (Fig. 3.2B). The subtle membrane staining in the unstimulated cells was also observed in untreated cells in some of the IMCD cell preparations, suggesting no influence of the compound.

For FMP-API-2, the ratio of intracellular/plasma membrane AQP2 fluorescence signal intensity[74] after AVP stimulation was twice as large as in control cells (Fig. 3.2I). The difference determined between unstimulated and AVP-stimulated cells was not significant (Fig. 3.2I), indicating complete inhibition of the AQP2 shuttle by the compound in a concentration of 100 µM (Fig. 3.2C). The compound also significantly ($p < 0.05$) increased the cytosol/membrane ratio by 1.4-fold in the absence of AVP. FMP-API-2 caused the accumulation of AQP2 in vesicle-like structures. For future studies, compartmental markers like GTPases of the Rab family, which are involved in the regulation of endocytosis, could be used in colocalisation studies to assess the identitiy of the AQP2-enriched structures.

Treatment of IMCD cells with FMP-API-3 led to inhibition of the AQP2 shuttle in 80 % of the cells (Fig. 3.2D).

After addition of FMP-API-4 to the cell culture medium crystals formed that dissolved upon agitating the culture dish; furthermore, bright particles were observed outside the cells during microscopic analysis, suggesting incomplete solubility. The AQP2 shuttle was not impaired significantly in FMP-API-4-treated cells (Fig. 3.2E, I), presumably because the compound was not taken up by the cells.

Cells treated with FMP-API-5 resembled the untreated ones, while AVP stimulation led to the formation of bright, dot-shaped structures, and shuttling of AQP2 (Fig. 3.2F).

Upon treatment with FMP-API-6, again dot-shaped bright AQP2-accumulations were formed intracellularly. No membrane translocation of AQP2 was observable in response to AVP. Interestingly, AQP2 accumulated in the nuclei (Fig. 3.2G).

FMP-API-7 inhibited the shuttle, although residual plasma membrane translocation of AQP2 was observable. However, the difference in the ratio of intracellular/plasma membrane AQP2 fluorescence signal intensity between unstimulated

and AVP-stimulated cells was not significant (Fig. 3.2I). Precipitation occurred upon addition of the compound to the medium, but was resolvable by agitation (Fig. 3.2H).

3.3.2 Inhibition of the AQP2 shuttle by FMP-API-2 is reversible

To investigate whether FMP-API-2 modifies its targets covalently, it was tested whether the inhibitory effect on the AQP2 shuttle is reversible. For this purpose IMCD cells were left untreated or were treated for 15 min with FMP-API-2 (Fig. 3.3A, B).

Additionally, compound-treated cells were washed three times with fresh medium and stimulated with AVP to test for reversibility of its effects (Fig. 3.3C). Subsequently, AQP2 was immunostained and its localisation analysed by laser scanning confocal microscopy. Membrane shuttling of AQP2 after a washout of the compound was again significantly inducible with AVP (Fig. 3.3C, D), revealing that the effect of FMP-API-2 was reversible.

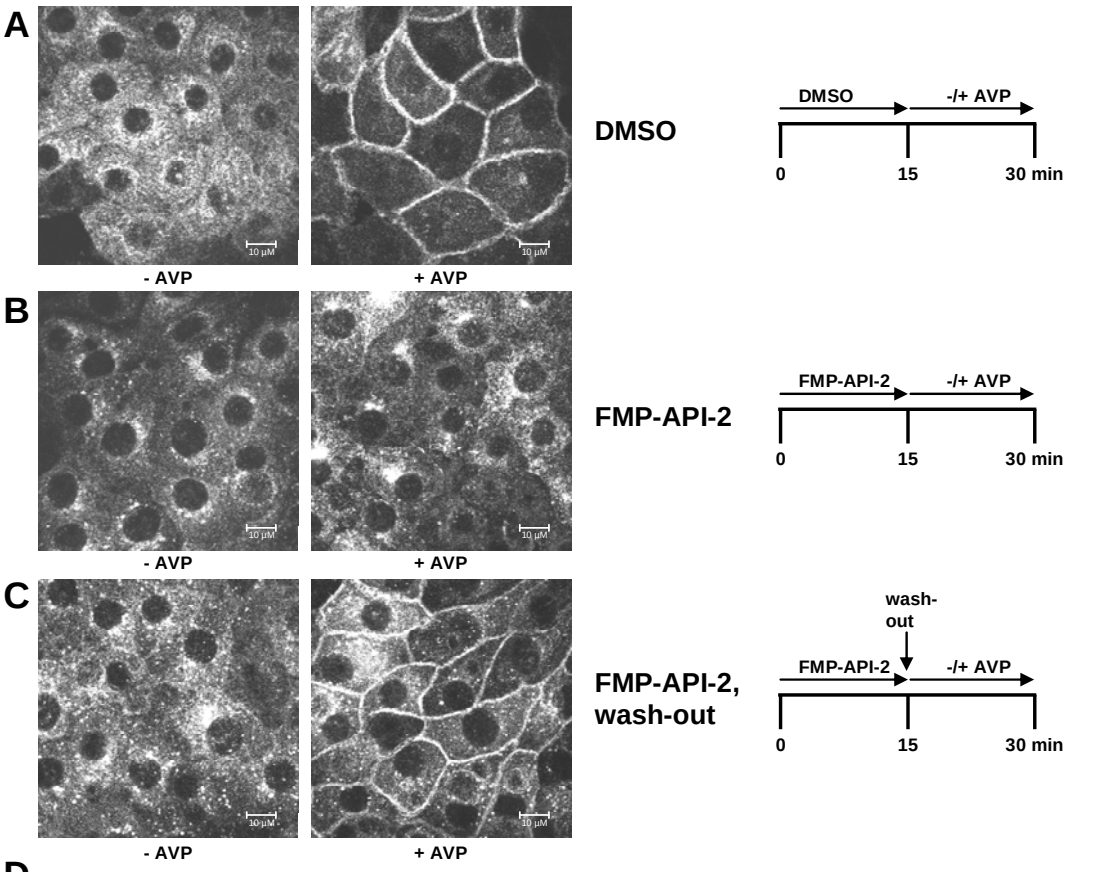

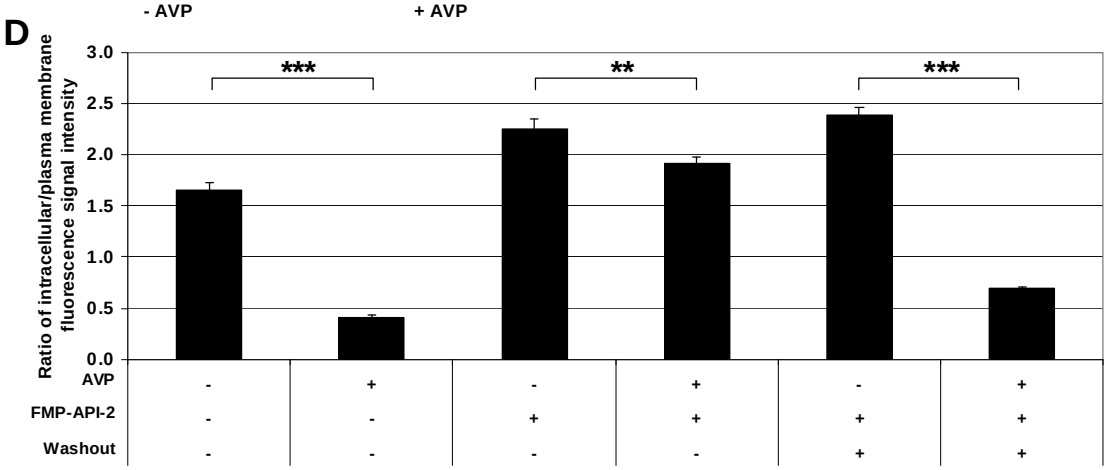

Fig. 3.3: The effect of FMP-API-2 on the AQP2 shuttle in IMCD cells is reversible. A-C. IMCD cells were treated for 15 min with the solvent DMSO (A) or FMP-API-2 (100 µM; B and C). Cells were stimulated with AVP (+ AVP) or left unstimulated (- AVP). After washing the cells with fresh medium to remove the compound the cells were again treated with AVP (C). Cells were fixed, permeabilised and immunostained with AQP2-specific and Cy3-conjugated secondary antibodies, and analysed by laser scanning confocal microscopy. D. The AQP2-shuttle was quantified by determining the ratio of intracellular *vs.* plasma membrane fluorescence signal intensity (**, $P < 0.01$; ***, $P < 0.001$).

3.3.3 Application of FMP-API-2 did not affect cell integrity

As a toxicity test, the influence of FMP-API-2 and DMSO on living IMCD cells was tested. Intact plasma membranes are impermeable for trypan blue. Thus intracellular staining with the dye indicates interference with the integrity of the plasma membranes. Dye-stained cells were observed in the laser scanning confocal microscope at 560 nm.

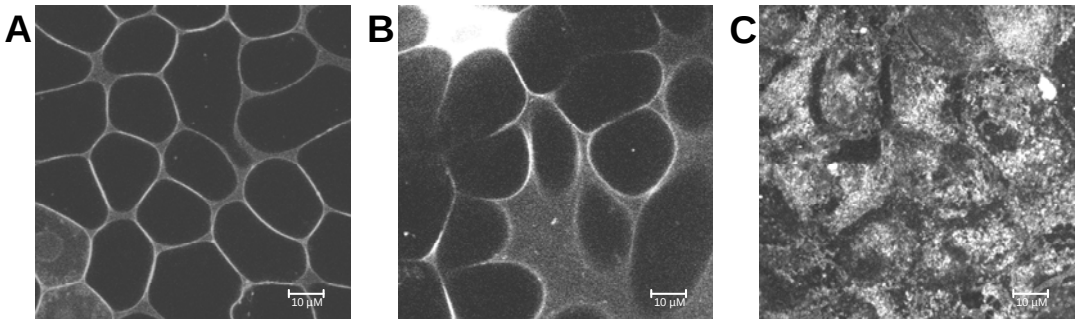

Fig. 3.4: FMP-API-2 does not impair the integrity of IMCD plasma membranes. Living IMCD cells were left untreated (A) or incubated with 100 µM FMP-API-2 (corresponding to a DMSO concentration of 0.1 %; B) for 15 min before adding trypan blue and subsequent analysis by laser scanning confocal microscopy to assess the distribution of the dye. A DMSO concentration of 5 % (C) leads to disintegration of plasma membranes and allows the dye to enter the cytosol.

Upon treatment with 100 µM FMP-API-2, plasma membranes were not damaged as only the membranes were stained by the dye, which was also the case in the untreated control (Fig. 3.4A-B). The final DMSO concentration in these samples was 0.1 %. DMSO only damaged plasma membranes if the concentration was increased to 5 % (Fig. 3.4C). In this case, the dye entered the cells.

3.3.4 Synthesis and ELISA analysis of FMP-API-2 derivatives

After FMP-API-2 inhibited the interaction of AKAP18δ and RIIα in the ELISA and the AQP2 shuttle in IMCD cells, a focussed library of derivatives of FMP-API-2 was synthesised to elucidate the structure-activity relationship (SAR) of this compound. The work was largely carried out by Sina Meyer in her master's thesis "Design, synthesis and evaluation of potential inhibitors for the protein-protein interaction of PKA and AKAP18δ"[76,101]. The newly synthesised compounds were all tested in the ELISA assay.

The compounds SM61 and SM65, which were the most potent inhibitors of the AKAP-PKA interaction with IC_{50} values of 0.1 µM in the ELISA, and the compound SM66 (IC_{50} = 14.8 µM, Table 3.2), which was less potent compared to FMP-API-2, were tested on the IMCD cells for their inhibitory effect on the AQP2 shuttle (Fig. 3.5). The FMP-API-2-derivative SM61 was the most potent one among them, as it inhibited the AQP2 shuttle at a concentration of 25 µM (Fig. 3.5C), which was four times lower than the inhibitory concentration of FMP-API-2 (100 µM; Fig. 3.2C).

Table 3.2: Small molecules derived from FMP-API-2. Displayed are the molecular weight (MW) in g/mol, partition coefficient (logP), number of H-bond-acceptors (H-Acc.), number of H-bond-donors (H-Don.), and IC_{50} value in µM.

Compound	Structure	Formula	MW / g/mol	logP	H-Acc.	H-Don.	IC_{50} / µM
SM61	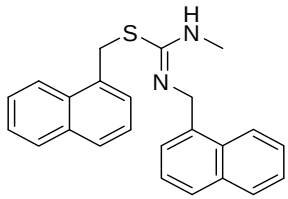	C24H22N2S	370.51	5.89	2	1	0.1
SM65	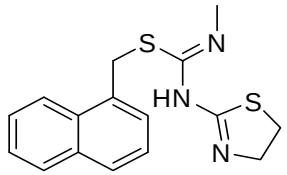	C16H17N3S2	315.46	1.68	3	1	0.1
SM66	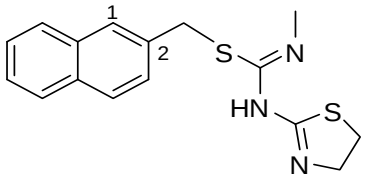	C16H17N3S2	315.46	1.68	3	1	14.8

The compound SM66 did not affect the AQP2 shuttle, which is in line with its much weaker activity in the ELISA. Also other compounds with the 2-methylisothiourea-group in the 2- instead of the 1-position of the naphthalene moiety (see structure of SM66 in Table 3.2) were inactive, rendering the substitution at the 1-position a critical structural feature for activity.

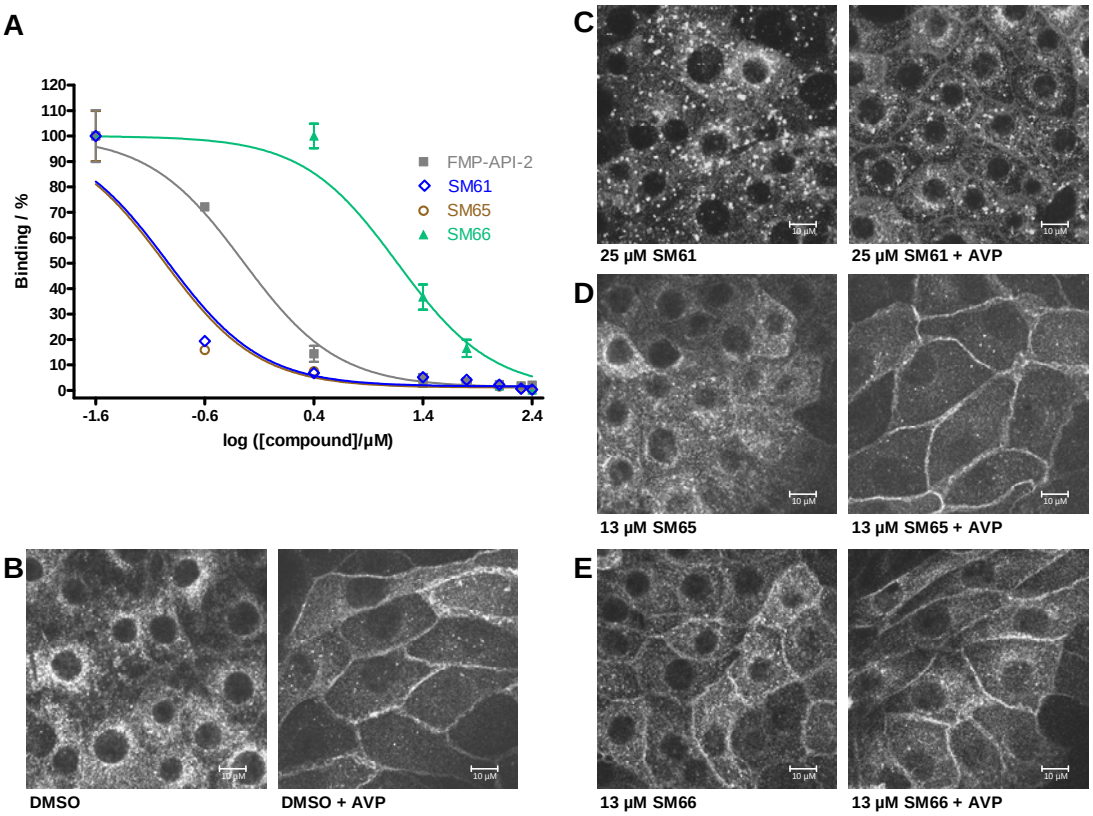

Fig. 3.5: Derivatives of FMP-API-2 inhibit the AKAP18δ-PKA interaction with lower IC_{50} values and inhibit the AQP2 shuttle in IMCD cells at lower concentrations compared to FMP-API-2. A. ELISA assay to measure the inhibition of the interaction between GST-AKAP18δ and RIIα. Serial dilutions of small molecules (0.25 – 250 µM) were added together with 10 nM AKAP18δ to microtiter plates coated with 25 nM RIIα. Following washing steps, AKAP-RII complex formation was detected by incubation with rabbit AKAP18δ-specific- and peroxidase-conjugated anti-rabbit antibodies. After addition of a luminol-containing peroxidase substrate solution, the resulting chemiluminescence intensity was measured in a plate reader. B-E. IMCD cells were treated for 15 min with DMSO (B) or small molecules in the indicated concentrations (C-E). The cells were stimulated with AVP (+ AVP) or left untreated (- AVP), fixed, permeabilised and immunostained with AQP2-specific and Cy3-conjugated secondary antibodies, and analysed by laser scanning confocal microscopy.

3.3.5 cAMP pulldown experiments from compound-treated IMCD cells

Western blot analysis of cAMP pulldowns from cell lysates is a more direct method than analysing immunostained cells, and a much larger number of cells contributes to the result. After incubation of IMCD cells with DMSO (as control) or with the compounds, cAMP-agarose is incubated with lysates of the cells. All cAMP-binding proteins such as the regulatory subunits of PKA bind to the cAMP-agarose and can subsequently be separated from the remaining lysate,

whereby R-subunit interacting proteins such as AKAPs will be coprecipitated. Analysis of such precipitates is conducted by eluting the proteins from the beads with Laemmli sample buffer, separation of the proteins by SDS-PAGE and transfer onto a PVDF membrane. The proteins are analysed either by specific antibodies directed against the proteins of interest, or by RII-overlay. The latter employs radioactively labelled RII subunits of PKA to globally detect AKAPs on the membrane[74].

Although FMP-API-2 and SM65 precipitated less AKAP18δ but surprisingly also less RIIα with cAMP-agarose, the results of cAMP-agarose pulldowns from IMCD cells were generally ambiguous, and the small molecules did not show significant effects in this assay (data not shown). FMP-API-1 had no effect in IMCD cells at all. Possibly, the plasma membranes of IMCD cells are too impermeable for small molecules. This assumption is supported by the fact that toxins (*Clostridium difficile* toxin B and *Clostridium limosum* toxin C3) used to study the influence of the small GTPase Rho on the AQP2 shuttle in IMCD cells had to be used in higher concentrations than published for other cell types. For example, toxin B had to be applied at a concentration of 4 µg/ml to IMCD cells to take effect[77], while for Swiss 3T3 and Caco-3 cells a 200-fold lower concentration was sufficient[41].

Interference with other targets than the tested protein-protein interaction might also be responsible for the observed inhibition of the AQP2 shuttle. This has to be examined in future studies.

3.3.6 FMP-API-1 decreased the interaction of PKA with AKAPs in cAMP pulldown experiments from cardiac myocytes

Similar to the experiments with IMCD cells, cAMP-agarose pulldowns were performed from compound-treated neonatal rat cardiac myocytes (experiments on cardiac myocytes were carried out by Dr. Márta Szaszák, FMP). The cells were treated in the same way and lysed as IMCD cells, followed by detection of cardiac myocyte-relevant AKAPs (see introduction) by Western blotting. Representative blots from the analysis of the eluted cAMP-agarose-beads are shown (Fig. 3.6). While 100 µM FMP-API-1 did not influence the binding of RIIβ to the cAMP-agarose beads, the amounts of coprecipitated AKAP18δ and AKAP150 were reduced. For example, the RII-AKAP18δ interaction was reduced by 60 %

(Fig. 3.6B). These results suggest an inhibition of AKAP-PKA interactions in neonatal rat cardiac myocytes by FMP-API-1.

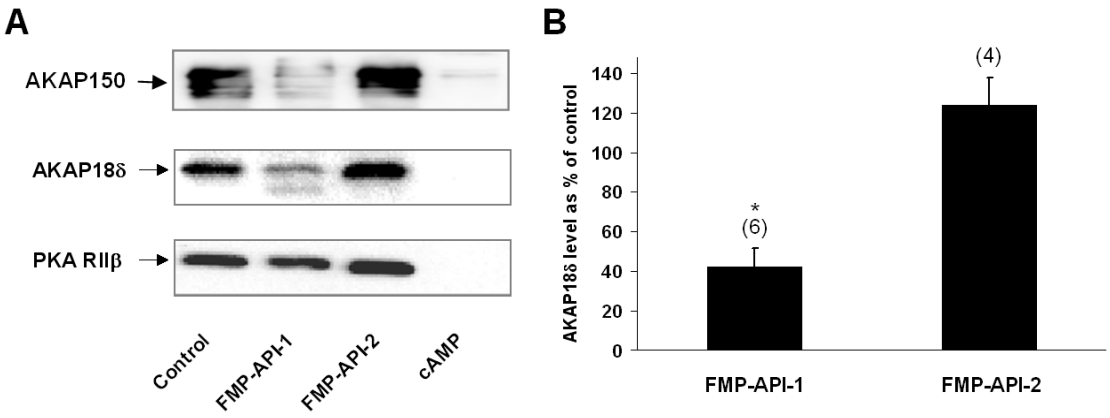

Fig. 3.6: Biochemical analysis of the small molecules' effects on AKAP-PKA interactions in neonatal rat cardiac myocytes. A. Cells were incubated with small molecules (100 µM) or DMSO (control; 1 %) as indicated. Lysates of the treated cells were incubated with 8-AHA-cAMP-agarose to precipitate regulatory PKA subunits and the associated binding partners including AKAPs. Where indicated (cAMP), excessive cAMP (50 mM) was added prior to cAMP-agarose incubations as a negative control. Precipitates were separated by SDS-PAGE and blotted onto PVDF membranes. Blots were subjected to Western blot analysis. AKAP150, AKAP18δ and RIIβ were detected by specific primary and peroxidase-conjugated secondary antibodies. B. Densitometric analysis of the AKAP18δ blot shown in A. Numbers in brackets indicate numbers of experiments; means ± SEM.

3.3.7 β-adrenoceptor-induced increases in L-type Ca^{2+}-channel currents are prevented by FMP-API-1, but not by FMP-API-2

To assess functional implications of the disruption of AKAP-PKA interactions in cardiac myocytes, whole cell patch clamp measurements of L-type Ca^{2+} channel currents were conducted. The channel's open probability is increased by PKA-dependent phosphorylation of serine 1928 in the α_1-subunit as a consequence of β-adrenergic stimulation[61,133]. The resulting increase in cytosolic Ca^{2+} concentration causes an increase in contractility of the cardiac myocytes. The AKAP involved in this process is AKAP18α. It directly interacts with the L-type Ca^{2+}-channel *via* a leucine zipper motif and thereby anchors PKA to the channel[59].

Disruption of the AKAP18α-PKA interaction using anchoring disruptor peptides (Ht31 or AKAP18δ-L314E) prevents the β-adrenergic receptor-mediated Ca^{2+}-

channel current increase[59,60,64]. Additionally, a similar effect was observed with an AKAP18α-derived peptide mimicking the leucine zipper motif region[60].

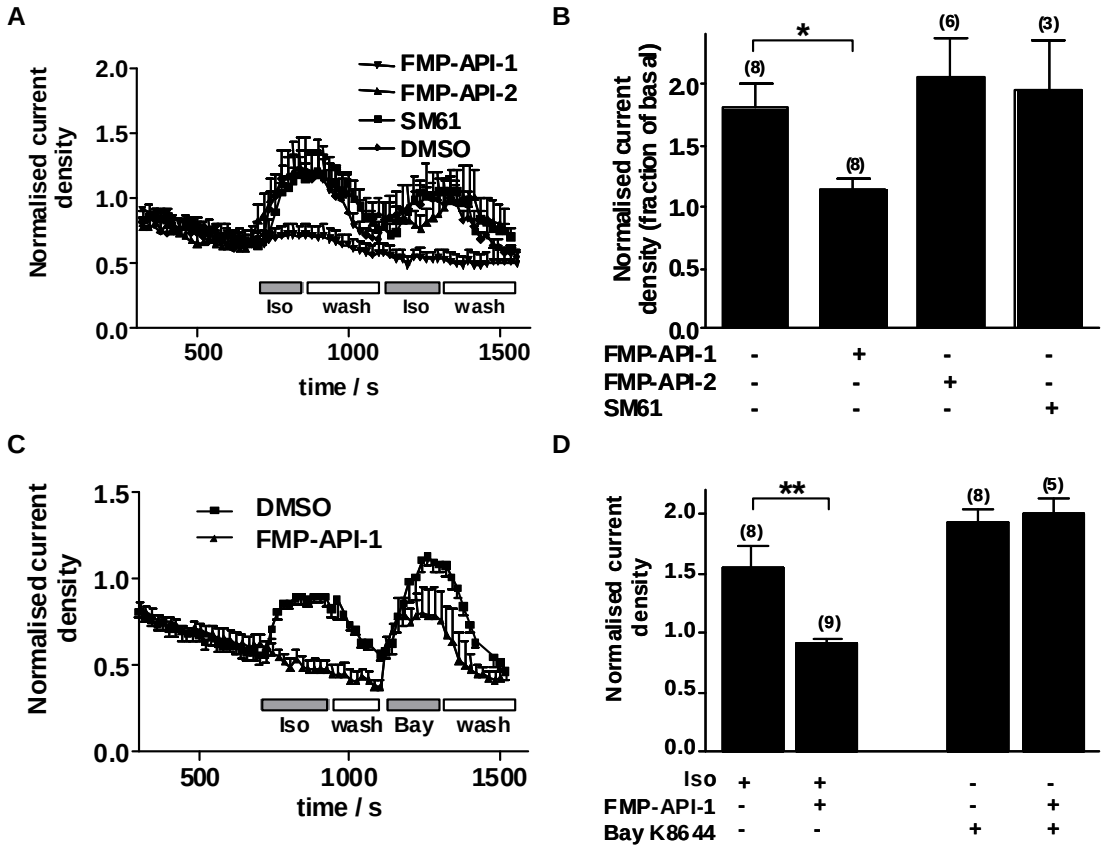

Fig. 3.7: FMP-API-1 impairs β-adrenoreceptor-mediated increases in L-type Ca^{2+}-channel currents in neonatal rat cardiac myocytes. L-type Ca^{2+}-channel currents were measured using the patch-clamp technique. Cells were clamped to -70 mV and repetitively depolarised to a test potential of 0 mV after a 400 ms ramp to -35 mV. The cells were perfused with the small molecules (100 µM each) or DMSO via the patch pipette. Current recordings were started 400 s after establishing whole cell configuration. A, B. Ca^{2+}-currents were induced by isoproterenol-stimulation (Iso; 1 µM) at the indicated times followed by washouts with buffer (wash). Time courses of normalised current densities are shown. B. To test whether FMP-API-1 (200 µM) inhibits the L-type Ca^{2+}-channel activity reversibly, the cells were treated with the channel activator Bay K8644 (Bay; 70 nM) for the indicated time, followed by a washout. C. Summary of individual experiments (numbers in brackets indicate the numbers of experiments; means ± SEM; **, $P < 0.01$; *, $P < 0.05$).

Neonatal rat cardiac myocytes responded to a 100 nM isoproterenol treatment with a 1.5-fold increase in Ca^{2+} currents (Fig. 3.7A, C). The effect was reversible upon replacement of isoproterenol by buffer. When 100 µM FMP-API-1 were perfused into the cells through the patch clamp pipette prior to the isoproterenol

stimulation, the Ca^{2+}-current increase was prevented, suggesting that inhibition of the AKAP18α-PKA interaction is the cause for this effect. The inhibitory effect of FMP-API-1 was similar to the effect of AKAP-PKA anchoring disruptor peptides[64]. FMP-API-2 (100 µM) or its derivative SM61 (100 µM) did not prevent the current increase.

The direct channel activator Bay K8644[126] (70 nM) was added in the presence of FMP-API-1 and evoked a Ca^{2+}-current increase, indicating that FMP-API-1 does not inhibit the L-type Ca^{2+}-channel activity irreversibly (Fig. 3.7B, C).

3.4 SPR measurements confirmed the inhibiton of AKAP-PKA interactions by FMP-API-1

Surface plasmon resonance (SPR) measurements were used previously to determine binding affinities of regulatory PKA subunits to anchoring disruptor peptides[64] and of AKAPs to R subunits[52,54], making it a secondary screening method of choice for the validation of the ELISA results.

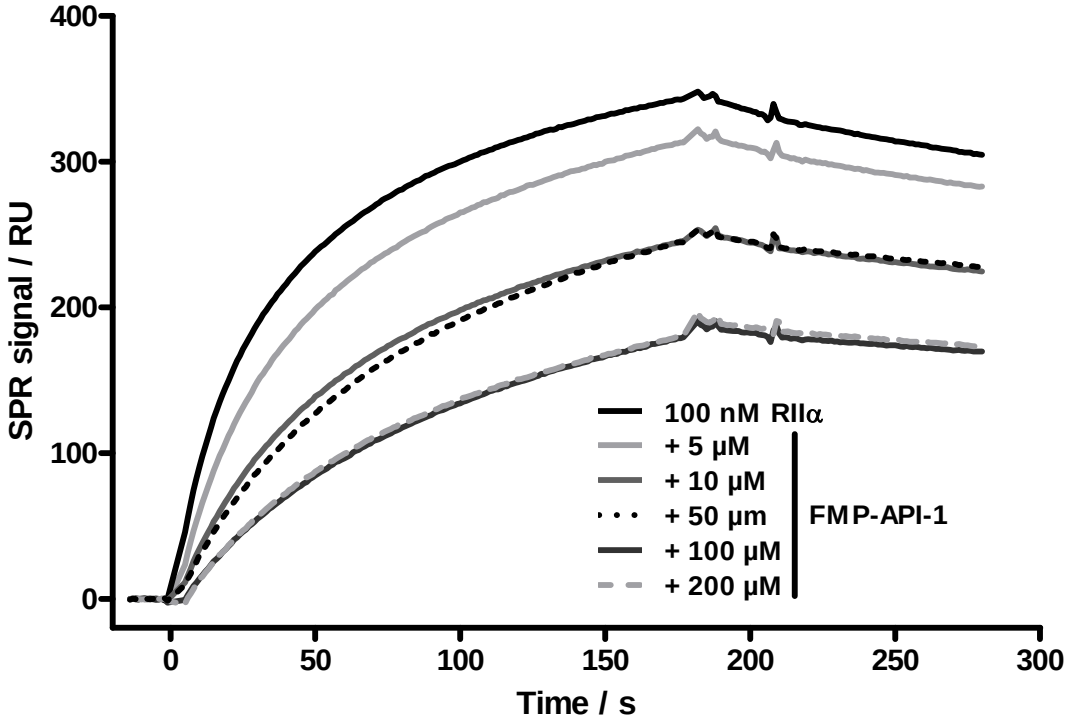

Fig. 3.8: Surface plasmon resonance (SPR) measurements confirm the inhibition of AKAP-PKA interactions by FMP-API-1. Association and dissociation curves of the interaction between RIIα and the peptide AKAP18δ-L314E in absence and presence of the indicated concentrations of the small molecule FMP-API-1. RU, resonance units.

The effects of FMP-API-1 on AKAP-PKA interactions were determined by coupling the biotinylated AKAP18δ-derived peptide AKAP18δ-L314E to a streptavidin-coated sensor chip surface, and incubation with RII solutions in the absence and presence of FMP-API-1 (Fig. 3.8). FMP-API-1 alleviated the association of RIIα with the AKAP-peptide in a concentration-dependent manner. In this assay, the maximum inhibition was 50 %. FMP-API-2, in contrast, showed no inhibitory activity in this experimental setup.

3.5 FMP-API-1 interacts directly and reversibly with regulatory RII subunits of PKA

Next, it was aimed to elucidate the target protein of the compound FMP-API-1, i.e., to clarify whether it binds to either the AKAP or the RII subunit. It is possible to coat SPR-chips covalently with proteins to assess direct binding of ligands to the protein. After amine-coupling of RIIα to dextran-COOH chips, FMP-API-1 was added as analyte in different concentrations to observe direct binding to RIIα (Fig. 3.9A). Binding curves represented by SPR signal intensities were obtained, showing that the compound bound directly and concentration-dependently to RIIα subunits on the chip. The fast binding kinetics observed are typical for small ligands binding to larger proteins[166].

It was not possible to bind AKAP18δ to the SPR chips to provide a *vice versa* experiment. Therefore, saturation transfer difference (STD) nuclear magnetic resonance (NMR) spectroscopy[100] was utilised to detect direct binding of the small molecule ligand to the proteins.

STD-NMR yields signals of compounds only if they are reversibly binding to proteins (see Materials and Methods). A strong signal was only obtained in combination with full length-RIIα, while GST-AKAP18δ and Ovalbumin (as control for a non-related protein not involved in the examined protein-protein interaction) did not yield signals (Fig. 3.9B).

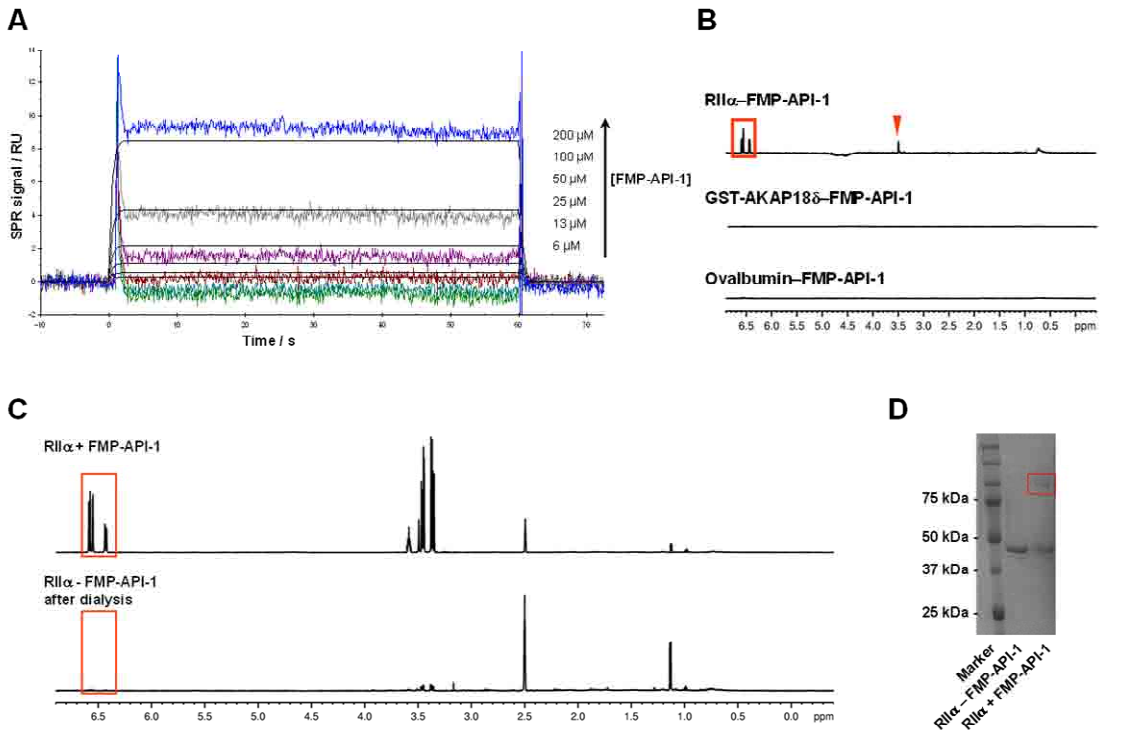

Fig. 3.9: FMP-API-1 binds to RIIα in a direct and reversible fashion. A. The small molecule FMP-API-1 was added in the indicated concentrations to SPR sensor chips covalently coated with RIIα subunits to assess direct binding to the protein. B. Saturation transfer difference (STD) NMR measurements of FMP-API-1 (1 mM) in the presence of either RIIα (14 µM), GST-AKAP18δ (19 µM) or Ovalbumin (18 µM). C. An STD-NMR sample containing RIIα and FMP-API-1 was measured (upper panel), dialysed against phosphate buffer and measured again (lower panel) to assess reversibility of the binding. D. Aliquots of the same STD-NMR samples as in panel C were separated by SDS-PAGE and Coomassie-stained.

In order to further confirm the reversible binding mode, the RIIα STD-NMR sample was subjected to dialysis for removal of reversibly bound compound, and subsequently analysed again by STD-NMR and SDS-PAGE. Fig. 3.9C indicates that the FMP-API-1 signal almost completely disappeared after dialysis, thus confirming the reversibility of the binding. Additionally, the Coomassie-stained SDS-PAGE gel in Fig. 3.9D showed a protein in the size of an RIIα-dimer in the RIIα + FMP-API-1 sample, that was also found in Western blots of FMP-API-1-treated RII (see section 3.9). This was not detectable after dialysis, suggesting that FMP-API-1 caused a reversible RIIα-dimer formation.

3.6 The D/D domain of RIIα is not the molecular target of FMP-API-1

The dimerisation and docking (D/D) domain of RIIα (i.e., RIIα(1-44)) is a putative binding site for FMP-API-1, because it directly interacts with AKAPs. In order to test the RIIα-D/D domain as a target of FMP-API-1, it was expressed and purified in an ^{15}N-labelled version, and heteronuclear single quantum coherence (HSQC) NMR experiments comprising ^{1}H and ^{15}N signals were conducted with a 0.2 mM solution of the protein. These NMR measurements yield signals for all H-N bonds of a protein, with the majority of signals derived from the peptide bonds of the protein backbone. The H and N signals are each plotted on one axis (Fig. 3.10), and the peaks are depicted by contour lines in the spectrum. Each peak represents an H-N bond. The position of each peak (as in 1D-NMR) strongly depends on the chemical environment of the H-N bond, and thus a change in the environment will lead to a shift of the peak in the spectrum.

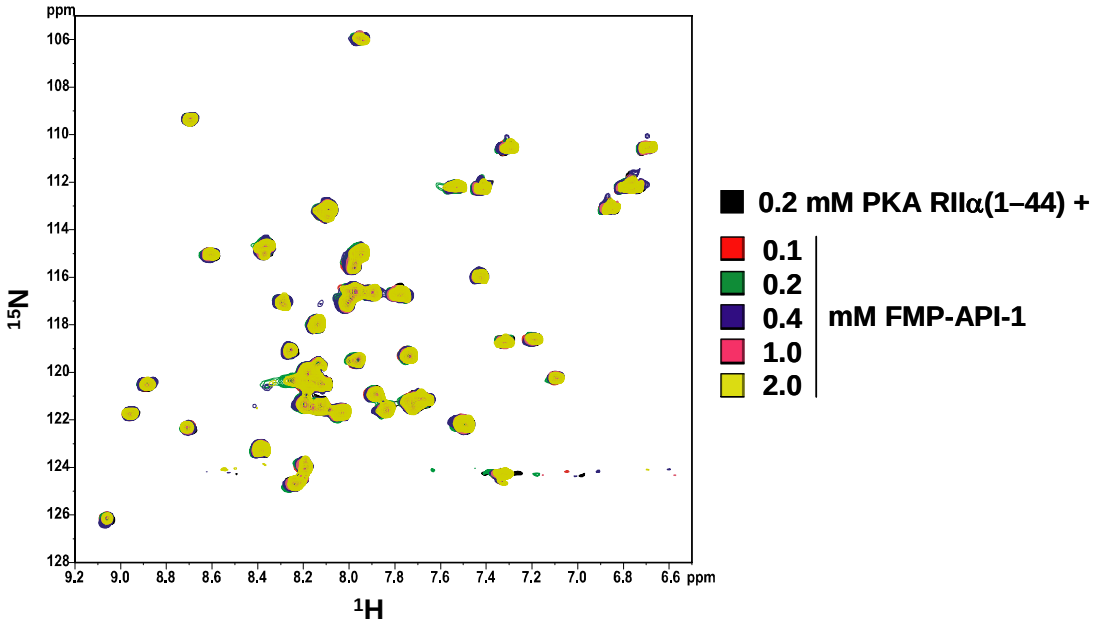

Fig. 3.10: The RIIα docking and dimerisation (D/D) domain – comprising the N-terminal 44 amino acids – is not the binding target of FMP-API-1. The RIIα-D/D domain was purified as ^{15}N-labelled protein (0.2 mM) and subjected to ^{15}N/^{1}H-HSQC-NMR measurements in absence and presence of the indicated concentrations of FMP-API-1. Concentration-dependent peak shifts due to perturbations of the chemical environment of the protein's H-N bonds in response to binding of FMP-API-1 were not observed.

Changes in the chemical environment can be caused e.g. by conformational changes of the protein or by the binding of a peptide or small molecule[154]. Spectra were measured in the presence of FMP-API-1 (0.1, 0.2, 0.4, 1.0 and 2.0 mM). All spectra were overlayed to observe possible peak shifts. However, the combined spectra revealed, that the compound caused no peak shifts, and thus does not bind to the D/D domain of RIIα (Fig. 3.10), indicating that the compound is an allosteric binder.

3.7 SPR measurements confirmed the allosteric binding mode of FMP-API-1

The binding of FMP-API-1 to RIIα outside the D/D-domain suggested that the interaction of FMP-API-1 and the PKA disruptor peptide Ht31 yield additive signals when analysed for their binding to RIIα by SPR (with the same experimental setup as used for Fig. 3.9A). Therefore, peptide and compound were added separately as well as in combination (50 nM Ht31, 100 µM FMP-API-1) to chip-bound RIIα (Fig. 3.11). The binding curve obtained from the combination of peptide and small molecule closely resembled the combined binding curves of the separate treatments as expected for additive effects. This indicates that the inhibitors do not compete for the same binding site on RIIα, but rather have different molecular targets on the same protein to which they may bind simultaneously.

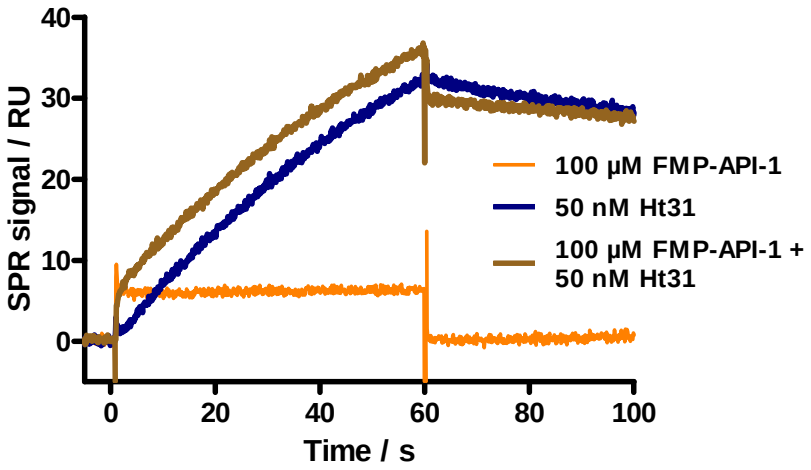

Fig. 3.11: The peptide Ht31 and the small molecule FMP-API-1 bind additively to RIIα. Association and dissociation of FMP-API-1 (100 µM) and Ht31 (50 nM) – either alone or in combination – were measured by SPR using a sensor chip coated with full length RIIα. RU, response units.

3.8 ELISA and peptide SPOT arrays point to additional AKAP-PKA interaction sites outside the D/D domain

Since solved structures of full length AKAPs with regulatory PKA subunits or D/D domains are not available so far, it cannot be excluded that further interaction sites between AKAPs and R subunits exist. In addition, previous observations (e.g. in fluorescence resonance energy transfer (FRET) interaction analyses[52]; see below) pointed to the possibility of additional interaction sites between AKAP18δ and PKA regulatory subunits. Such sites may be interesting targets for small molecules and may lead to substances that interfere potentially with a specific AKAP-PKA interaction, e.g. AKAP18δ and PKA.

In ELISA assays it was found, that RIIα subunits interacting with plate-bound AKAP18δ (and thus in the opposite way compared to the ELISA used for the high throughput screening) could not be detected with the routinely used $PKA_{RIIα}$ antibody (BD) directed against RIIα, which worked reliably when RIIα was directly detected on the plate and AKAP18δ was absent. However, binding of RIIα to AKAP18δ in this assay was detectable with a different anti-RIIα antibody (Abcam PKA R2; Fig. 3.12A).

The antibody epitopes on RIIα were elucidated by the use of peptide SPOT membranes, onto which the complete RIIα protein sequence was spot-synthesised in the form of overlapping 25mer-peptides. The epitopes were found to be located in different parts of the sequence (Fig. 3.12B). The BD $PKA_{RIIα}$ antibody epitope is located between the amino acids 126 and 160 of the RIIα sequence, and the Abcam PKA R2 antibody epitope between amino acids 301 and 340.

In further experiments the spot-synthesised RIIα sequence was overlayed with recombinant GST-AKAP18δ (Fig. 3.13A), revealing potential additional interaction sites of RIIα with AKAP18δ being located outside the D/D-domain/RII-binding domain. The AKAP cannot interact with the D/D-domain of RIIα in this assay because only a D/D-monomer is present on the spot membrane (spots A1-A5), but a dimer is required for AKAP binding. Strikingly, the sequence of spot B11 is contained in both the BD antibody epitope (Fig. 3.12B, upper panel) and an interaction site of RIIα and AKAP18δ (Fig. 3.13A), explaining the failure of the BD antibody in the ELISA assay to detect AKAP18δ-bound RIIα as the interaction blocks its epitope. However, also the epitope for the Abcam antibody

is among the additional interaction sites (E1-E3), but seems not to disturb the detection.

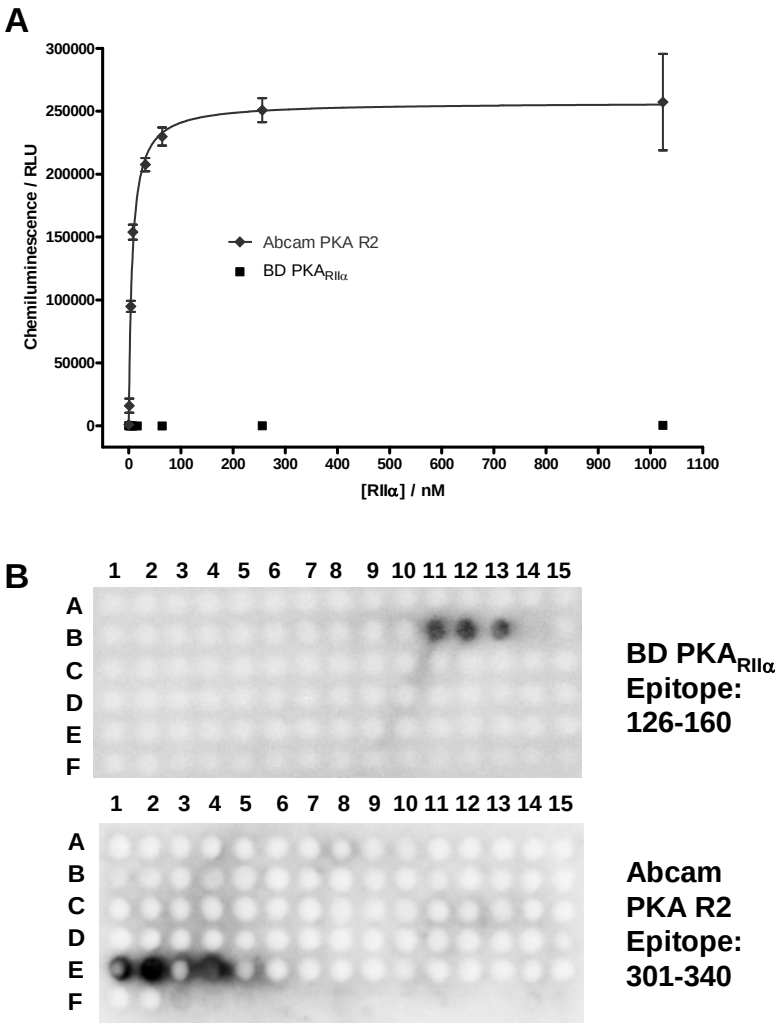

Fig. 3.12: AKAP18δ blocks the epitope of an RIIα-directed antibody, which is located outside the D/D domain. A. Microtiter plates were coated with GST-AKAP18δ (220 nM). Free binding sites were blocked, and RIIα was added in the indicated concentrations. After washing, the binding of RIIα to AKAP18δ was detected by incubation either with mouse BD $PKA_{RIIα}$ antibody and peroxidase-conjugated anti-mouse antibody, or with rabbit Abcam PKA R2 antibody and peroxidase-conjugated anti-rabbit secondary antibody. Luminol-containing peroxidase substrate solution was added, and the chemiluminescence intensity was measured in a plate reader. B. The complete sequence of human RIIα was spot-synthesised as 25-mers with an overlap of five amino acids onto cellulose membranes, and free binding sites were blocked. RIIα was detected with the indicated primary and peroxidase-conjugated secondary antibodies as in panel A. The antibody binding was determined by incubation with a luminol-containing peroxidase substrate solution and detection of luminescence in the LumiImager. For spotted peptide sequences, see Appendix A.

In an inverse assay, the AKAP18δ sequence was spot-synthesised and overlayed with either RIIα or RIIα(57-404) to reveal possible additional interaction sites on AKAP18δ (Fig. 3.13B). Both RIIα and RIIα(57-404) interacted with spots A2-A4 when detected with the Abcam antibody, but not with the BD antibody, thus confirming the blocked epitope theory. A2-A4 represent amino acids 6-40 of AKAP18δ, matching the AKAP18δ-specific N-terminal part of the sequence. However, RIIα seemed unexpectedly not to interact with the RII-binding domain of AKAP18δ (amino acids 301-314, spots D14-E3) when detected by antibodies, but did interact when autoradiography was detected after a ^{32}P-RII overlay (Fig. 3.13C). The radioactive overlay takes advantage of the autophosphorylation mechanism of PKA-RII and is used as the standard assay to identify and detect AKAPs[74]. The autoradiography detection method revealed further possible interaction sites (e.g., spots C11-D3), possibly due to greater sensitivity, but phosphorylated RIIα did not bind to the new possible interaction domain in spots A2-A4. Perhaps this new interaction domain interacts exclusively with non-phosphorylated RIIα.

The additional interaction site could account for a regulation of the AKAP18δ-PKA-RIIα interaction, which was discovered by FRET measurements in CD8 cells transfected with fluorescent versions of AKAP18δ and RIIα[52]. These measurements showed a decrease of the AKAP18δ-RIIα interaction after elevation of cAMP by the direct adenylyl cyclase activator forskolin. An inverse regulatory mechanism for an AKAP18-RIIα interaction is the affinity increase observed after Ser96-phosphorylation of RIIα in cardiac myocytes[90]. However, in this case it is the short splice variant AKAP18α whose affinity is regulated, and this lacks the AKAP18δ-specific N-terminus.

The potential additional interaction sites need to be confirmed by other assays, e.g. ELISA or SPR measurements, and in cells transfected with proteins mutated at the identified sites.

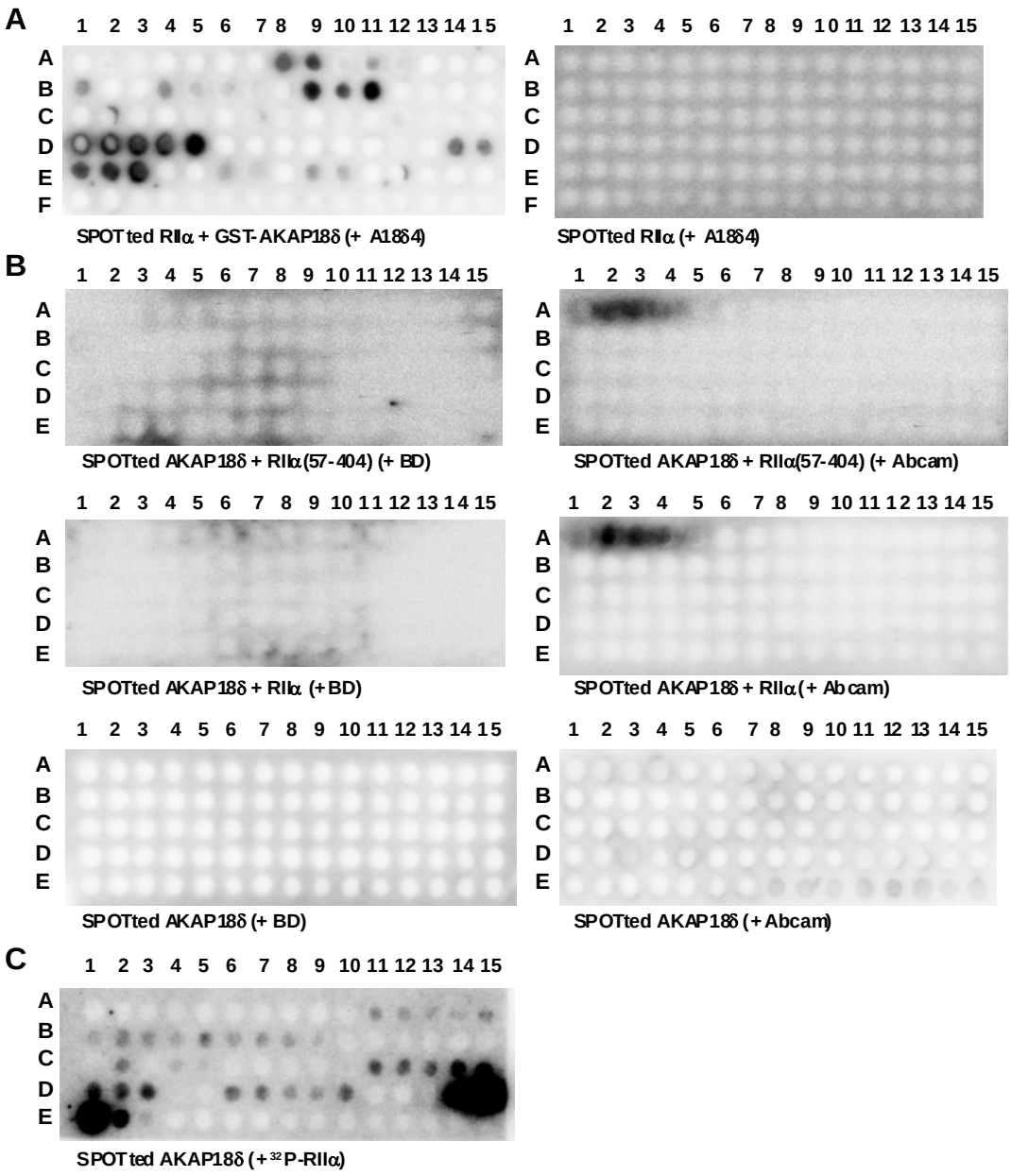

Fig. 3.13: Peptide spot arrays show possible additional interaction sites between AKAP18δ and PKA-RIIα. A. Cellulose membranes with the RIIα sequence spot-synthesised as 25mer peptides with five amino acids overlap were blocked, and incubated with recombinant GST-AKAP18δ (left panel) or left untreated (right panel). Bound AKAP18δ was detected by the AKAP18δ-specific rabbit A18δ4 antibody and peroxidase-conjugated anti-rabbit secondary antibody. B. Cellulose membranes with the AKAP18δ sequence spot-synthesised as 25mer peptides with five amino acids overlap were blocked and incubated with recombinant RIIα(57-404) (upper panels), full length RIIα (middle panels) or left untreated (lower panels). Bound RIIα was detected by the RIIα-specific mouse BD PKARIIα antibody (left panels) or rabbit Abcam PKA R2 antibody (right panels) and peroxidase-conjugated secondary antibodies. C. A cellulose membrane with the AKAP18δ sequence spot-synthesised as 25mer peptides with five amino acids overlap were blocked and incubated with ^{32}P-phosphorylated RIIα-subunits (RII-overlay) and detected by autoradiography. For spotted peptide sequences, see Appendix A.

3.9 FMP-API-1 causes oligomerisation of RII subunits

During the analysis of cAMP pulldown experiments (see above) and cell lysates from cardiac myocytes it was observed, that FMP-API-1 did not only lead to the disruption of AKAP-PKA interactions, but also to the concentration-dependent formation of oligomers or higher molecular weight complexes including RIIβ (Fig. 3.14).

In cAMP-agarose pulldowns from neonatal rat cardiac myocytes treated with 100 or 300 µM FMP-API-1, high molecular weight complexes were found at 150 kDa when the Western blots were detected for AKAP18δ (Fig. 3.14A), and at 250 kDa when detected for RIIβ (Fig 3.14B). When cells were treated with DMSO as control, no high molecular weight complexes were observed, and as expected when excessive cAMP (50 mM) was added to show specificity of cAMP-agarose pulldown, no proteins were detected.

When lysates from FMP-API-1-treated cardiac myocytes were analysed for the presence of RIIβ by Western blotting, high molecular weight complexes appeared with high FMP-API-1 concentrations (larger than 300 µM) at 100 and 150 kDa, but not at 250 kDa (Fig. 3.14C). The lack of 250 kDa complexes when compared to cAMP-agarose pulldowns might be explained by the enrichment of this species above the detection limit by the cAMP-agarose pulldown.

Next, purified recombinant RIIβ subunits (1.2 µM) were incubated with 2000- or 4000-fold molar excess (2 and 4 mM) of the compound (corresponding to the compound:protein ratio in the ELISA) to see whether RII subunits alone are sufficient for the formation of high molecular weight complexes. Indeed, complexes appeared at 100 and 250 kDa (Fig. 3.14D), indicating that they most likely consist exclusively of RIIβ.

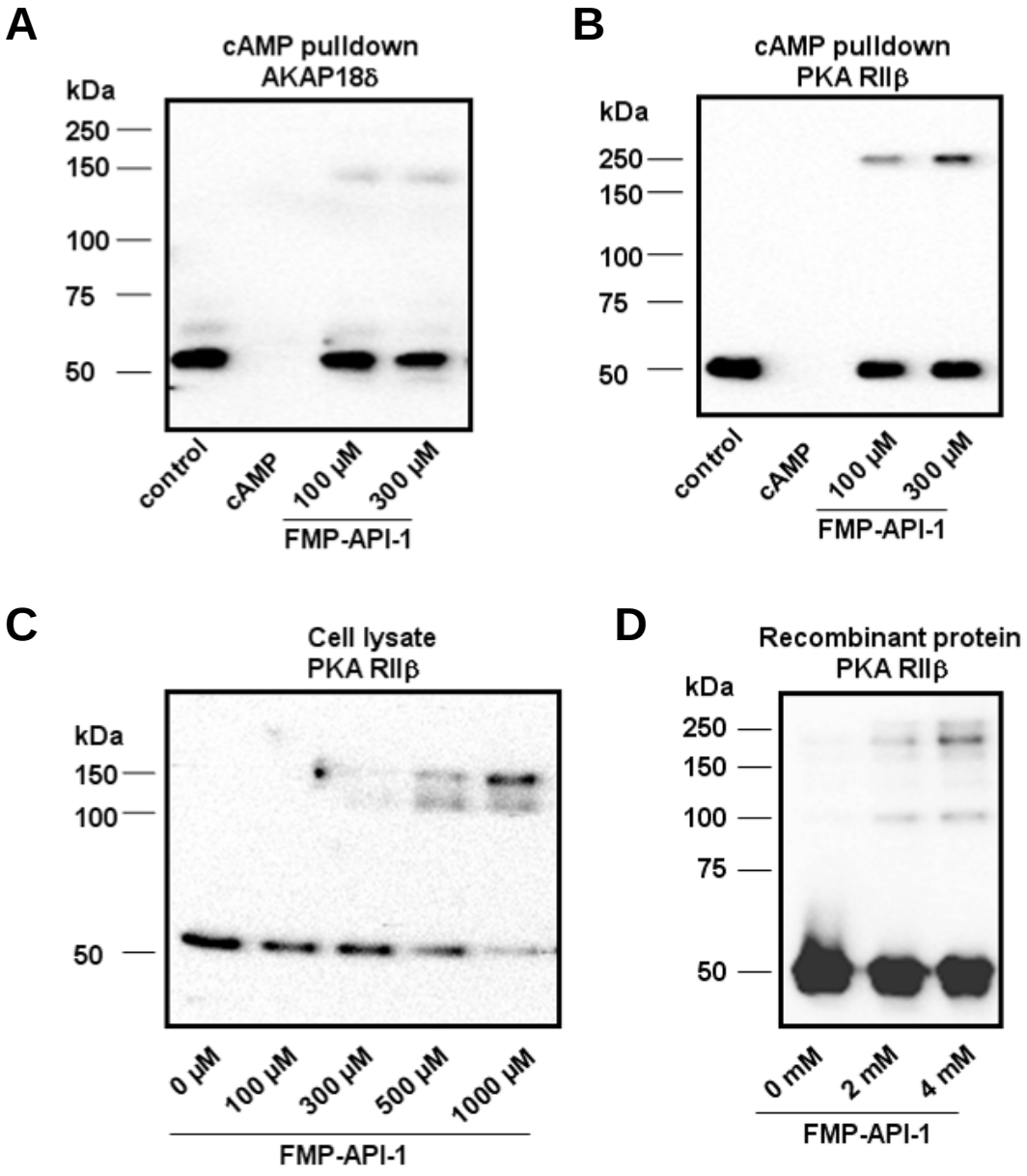

Fig. 3.14: FMP-API-1 induces formation of high molecular weight complexes involving RIIβ. A, B. Neonatal rat cardiac myocytes were treated with DMSO (control) or FMP-API-1 as indicated. cAMP indicates the negative control with excessive cAMP (50 mM). cAMP-agarose pulldowns from the cell lysates were separated by SDS-PAGE and blotted onto PVDF membranes. The AKAP18δ was detected with rabbit AKAP18δ-specific (A18δ4) and anti-rabbit peroxidase-conjugated antibodies (A) and RIIβ with mouse RIIβ-specific and anti-mouse peroxidase-conjugated antibodies (B). C. Neonatal rat cardiac myocytes were treated with FMP-API-1 in the indicated concentrations, and lysates of the cells were separated by SDS-PAGE and analysed by Western blotting with RIIβ-specific antibody as in panel B. D. Recombinant PKA-RIIβ protein was purified (1.2 µM) and incubated with FMP-API-1 as indicated. The samples were analysed by Western blotting as in panel B.

3.10 FMP-API-1 increases PKA-activation, cAMP levels, and PKA substrate phosphorylation

Since it is known that RI subunits form covalent dimers *via* disulphide bridges upon exposition to oxidants, leading to cAMP-independent activation of PKA in cardiac myocytes[10], a series of experiments was conducted to investigate the compound's influence on PKA activity and downstream signalling events.

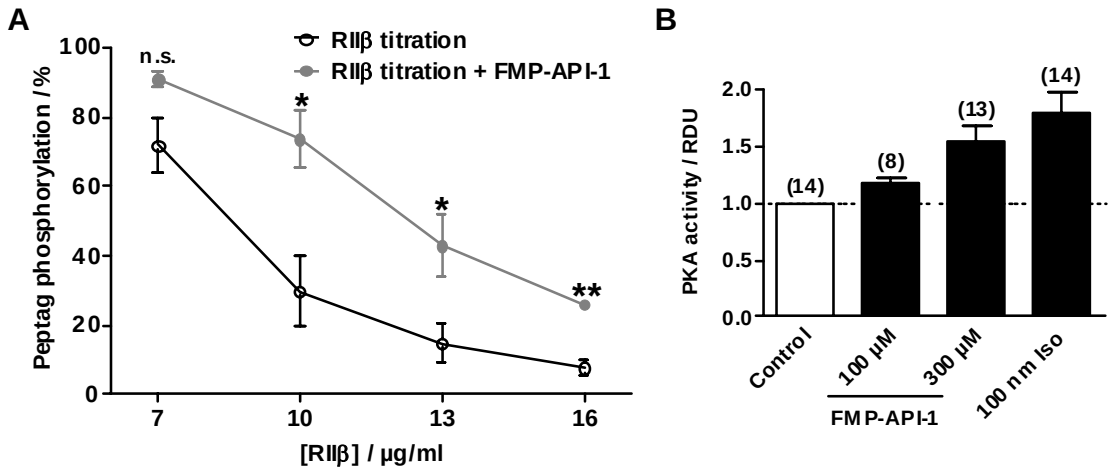

Fig. 3.15: FMP-API-1 activates PKA *in vitro* and in cells. A. PKA catalytic subunit activity was measured by phosphorylation of a fluorescence-labelled substrate peptide, separation of phosphorylated from non-phosphorylated peptide by agarose gel electrophoresis and semiquantification by densitometry. The assay was carried out in the presence of different RIIβ concentrations as indicated, and in the absence and presence of FMP-API-1 (1 mM). The assay was carried out in absence of cAMP (n = 3, means ± SEM; n.s., not significant; *, P < 0.05; **, P < 0.01). B. Neonatal rat cardiac myocytes were treated with DMSO (control), 100 or 300 µM FMP-API-1 or 100 nM isoproterenol (Iso) as indicated. PKA activity was measured from cell lysates as in panel A. RDU, relative density units. Numbers in brackets indicate the number of experiments; means ± SEM.

PKA activity was determined by an assay based on PKA phosphorylation of a fluorescent peptide-substrate in the absence of cAMP. The activity of PKA was diminished by adding RIIβ subunits in increasing amounts (7-16 µg/ml; Fig. 3.15A). In the presence of FMP-API-1 (1 mM), PKA activity was generally higher, with a maximum of 2.5-fold higher activity at an RIIβ concentration of 10 µg/ml. The decreased ability of RIIβ to inhibit the catalytic subunits in the presence of FMP-API-1 suggests that the compound binds to RIIβ and inhibits binding of the catalytic subunit. Alternatively, in combination with the observed oligomerisation, the compound may cause a cAMP-independent activation

mechanism similar to the one of type I PKA previously observed in cardiac myocytes upon peroxide treatment[10].

PKA activity was determined in lysates from neonatal rat cardiac myocytes treated with FMP-API-1 (100 or 300 µM) or isoproterenol (100 nM Iso; Fig. 3.15B). Isoproterenol served as a positive control to activate PKA *via* the β-adrenoceptor, and led to a 1.7-fold increase in PKA activity. FMP-API-1 alone also caused an increase in PKA activity (1.5-fold at 300 µM FMP-API-1).

Next, the influence of FMP-API-1 on the intracellular cAMP level was assessed. Lysates from cells stimulated with isoproterenol (10^{-8}-10^{-5} M) in the absence and presence of FMP-API-1 were subjected to radioimmunoassay (RIA) to determine the cAMP concentration (Fig. 3.16A). Surprisingly, the effectivity of isoproterenol to induce cAMP synthesis was increased by one order of magnitude in the presence of 50 µM FMP-API-1, leading to a decrease of the EC_{50} from 724 nM to 95 nM. A possible explanation for the increase in cAMP synthesis is the inhibition of the interaction between AKAP150 and PKA also found in cardiac myocytes (see Fig. 3.6A). In rat brain extract it was shown that AKAP150 interacts with adenylyl cyclase V/VI, and that PKA-mediated phosphorylation of the cyclase leads to its inhibition, thereby creating a negative feedback loop limiting the cAMP synthesis by the cyclase[5]. The disruption of such an AKAP-PKA complex in cardiac myocytes by FMP-API-1 explains the results depicted in Fig. 3.16A. However, in that case it would be expected that only the cAMP synthesis stimulated *via* signalling pathways involving compartmentalisation are affected by FMP-API-1, i.e. only pathways in which AKAPs are involved.

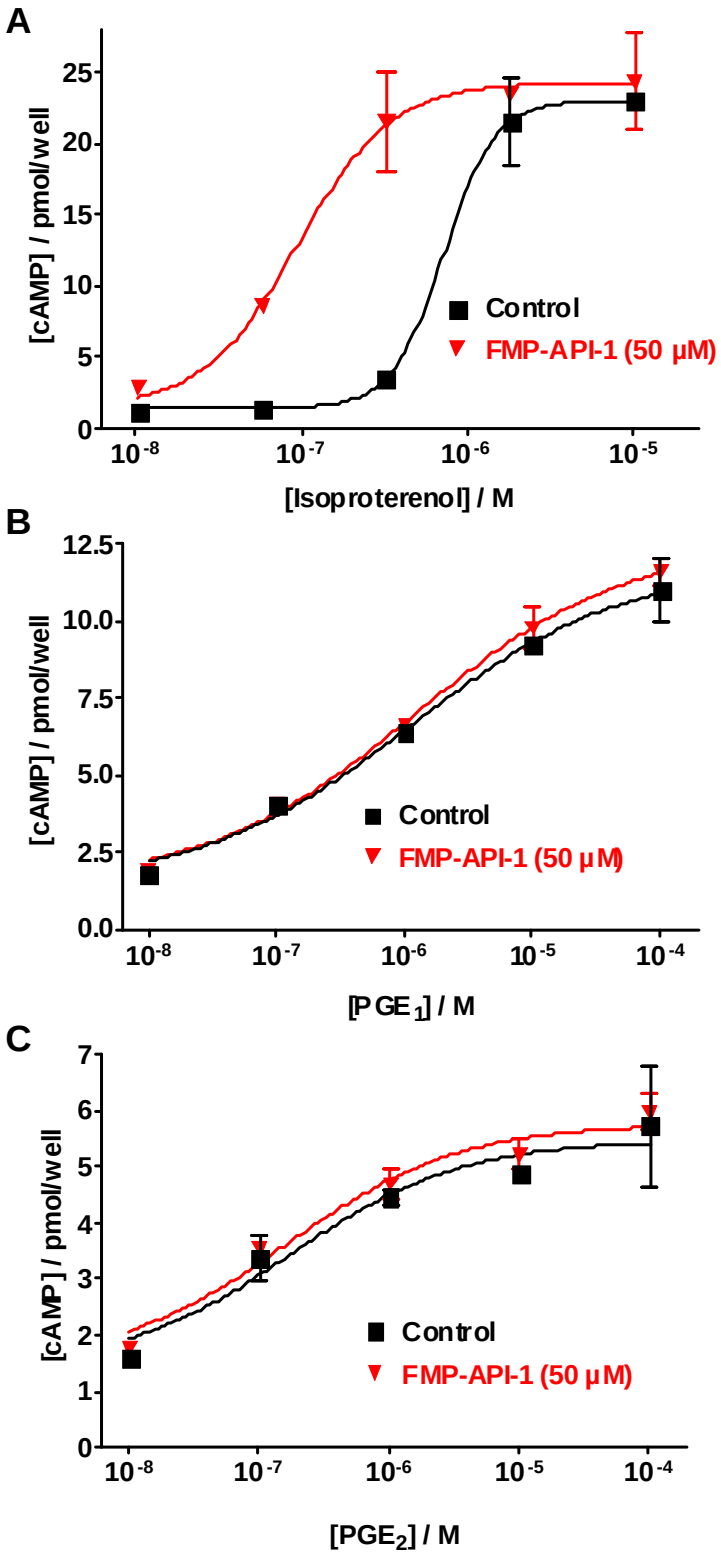

Fig. 3.16: FMP-API-1 influences cAMP levels in isoproterenol-stimulated, but not in prostaglandin-stimulated cardiac myocytes. A-C. Cardiac myocytes were stimulated with isoproterenol or PGE_1 or PGE_2 in the indicated concentrations in absence or presence of 50 µM FMP-API-1. cAMP concentrations in cell lysates were determined by radioimmunoassay. PGE_1, prostaglandin E_1; PGE_2, prostaglandin E_2. n = 3 experiments. Values are means ± SEM.

AKAPs are known to be involved in the β-adrenergic signalling pathway, but for example not in the pathways activated by the prostaglandins PGE_1 and PGE_2. These agonists activate GPCRs and ACs, but while PGE_1 leads to a mainly cytosolic rise in cAMP concentration, isoproterenol does so in the microsomal fraction[49]. For neonatal rat cardiac myocytes discrete microdomains of high cAMP concentration develop in response to β-adrenergic stimulation[119,162]. To characterise the influence of FMP-API-1 on PGE-induced cAMP signalling, the cAMP concentration measurements were carried out with cardiac myocytes stimulated by PGE_1 and PGE_2 (Fig. 3.16B, C). FMP-API-1 did not change the PGE_1- or PGE_2-mediated increases in cAMP concentration, confirming that it targets compartmentalised cAMP signalling.

Next it was tested whether FMP-API-1-induced activation of PKA and the generally increased cAMP-levels lead to phosphorylation of PKA substrates (Fig. 3.17). In cardiac myocytes, a major target of PKA is phospholamban (see introduction), which is phosphorylated upon β-adrenergic stimulation. Phosphorylated phospholamban (p-PLB) was detected with a p-PLB-specific antibody and compared to calsequestrin as a loading control (Fig. 3.17A). When the β-adrenergic pathway was activated by isoproterenol (100 nM), the detectable p-PLB was increased by a factor of 14. FMP-API-1 alone (100 or 300 µM) increased the amount of p-PLB up to 3- or 9-fold, respectively.

Fig. 3.17B shows that both the Iso- and FMP-API-1-induced PLB phosphorylation are largely prevented by the PKA inhibitor H-89[20] (30 µM), suggesting that the increase in phosphorylation is due to PKA activation.

To clarify whether FMP-API-1 increases PLB phosphorylation through inhibition of phosphatases, a protein phosphatase assay was conducted, measuring the activity of phosphatases in the absence and presence of FMP-API-1. The assay is based on dephosphorylation of a substrate peptide with a subsequent colorimetric reaction of the released free phosphate (Fig. 3.17C). Lysates from FMP-API-1-treated cardiac myocytes and recombinant calcineurin, one of the major phosphatases expressed in cardiac myocytes[103], were tested. Concentrations of up to 300 µM FMP-API-1 did not affect the activity of phosphatases compared to treatment with the solvent DMSO.

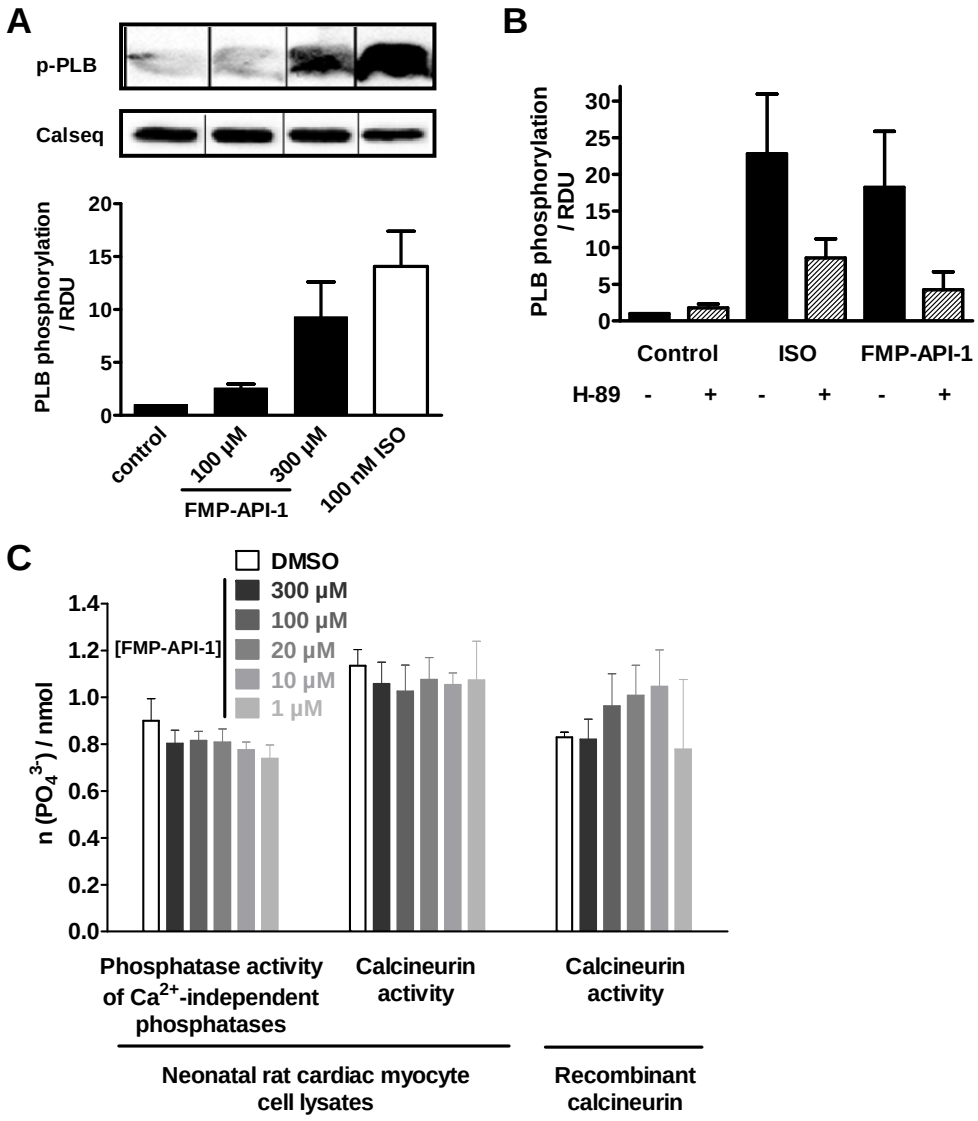

Fig. 3.17: Effects of FMP-API-1 on PKA-phosphorylation of phospholamban (PLB) and on phosphatase activity in cardiac myocytes. A. Cardiac myocytes were treated with DMSO (control), FMP-API-1 (300 µM) or isoproterenol (100 nM). Lysates of the cells were separated by SDS-PAGE and subjected to Western blot analysis with an anti-phospho-phospholamban-specific (p-PLB) or – as loading control – calsequestrin-specific (Calseq) antibody (upper panel). Results are representative of 12 experiments. Semiquantification of the detected blots was performed by densitometry (RDU, relative density units. n = 12, means ± SEM, lower panel). B. Cardiac myocytes were treated with DMSO (control), FMP-API-1 (100 or 300 µM) or isoproterenol (100 nM) in the absence or presence of the PKA-inhibitor H-89. Lysates of the cells were separated by SDS-PAGE and subjected to Western blot analysis as in panel A. Semiquantification of the detected blots was performed by densitometry (RDU, relative density units. n = 4, means ± SEM, lower panel). C. Cardiac myocytes or recombinant calcineurin were treated with DMSO or FMP-API-1 as indicated. Cell lysates or recombinant calcineurin were analysed for phosphatase activity on a substrate peptide and quantification of the released free phosphate with malachite green (n = 4, means ± SEM).

3.11 A structural derivative of FMP-API-1 displays higher activity at lower concentrations

Derivatives of FMP-API-1 were synthesised to obtain insight into the structure activity relationship (SAR). A selection of the synthesised compounds is shown in Fig. 3.18A.

The derivatives were tested in the competitive SPR assay to measure their inhibitory activity on AKAP-PKA interactions. Compounds 1025, 1026 and 1030 were found to be inactive (1026 shown in Fig. 3.18B), whereas the other compounds were active. Compound 1028 inhibited the interaction between AKAP18δ-L314E and RIIα by 25 % at 25 µM, and 1027 by 35 %.

Next, the most active compound 1027 was subjected to the established SPR measurements, revealing that it binds directly to RIIα (Fig. 3.18C). It bound in an additive fashion together with the peptide Ht31 (Fig. 3.18D). Thus, 1027 binds to RIIα directly and allosterically, thereby inhibiting AKAP-PKA interactions.

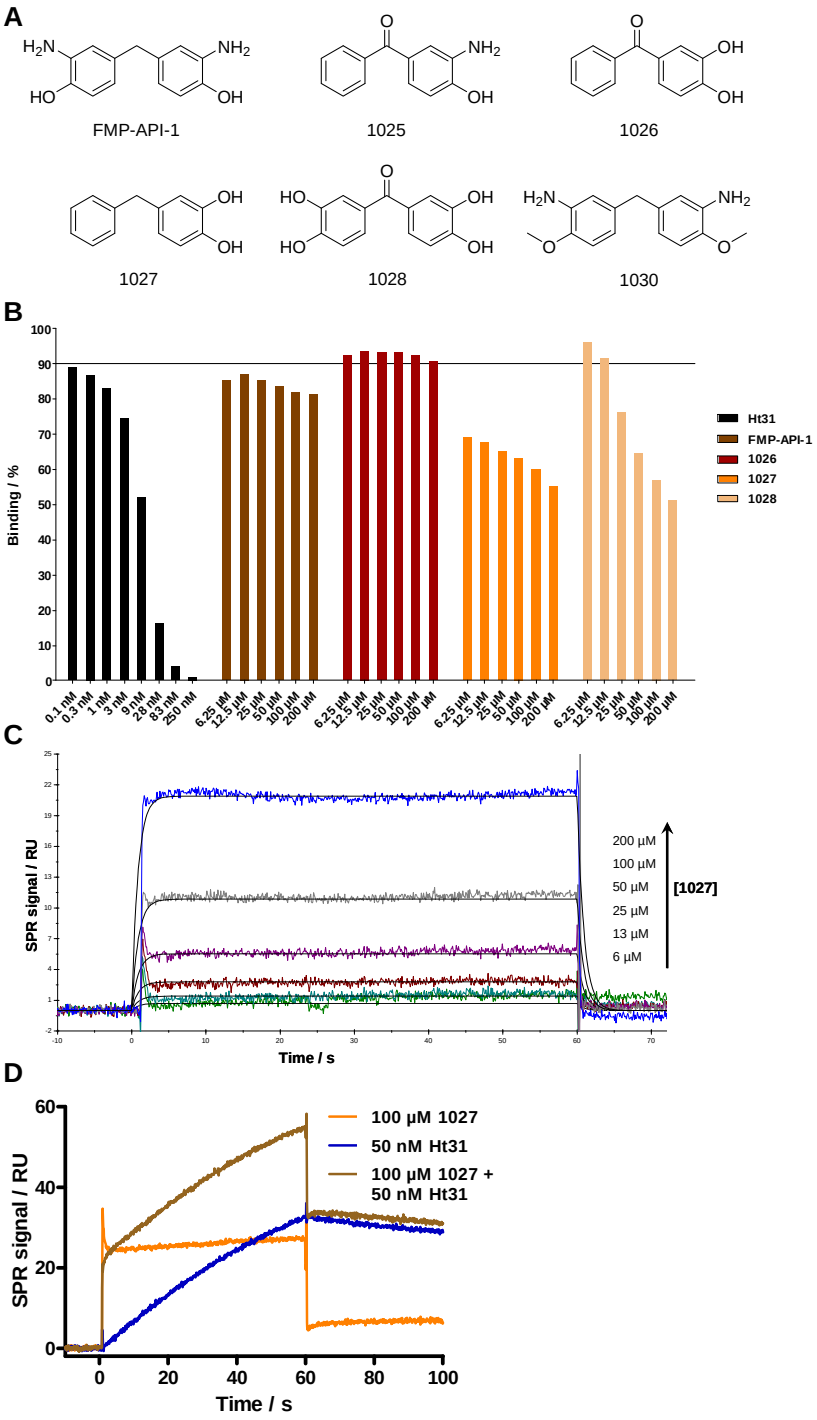

Fig. 3.18: Analysis of FMP-API-1 derivatives. A. Chemical structures of small molecules derived from FMP-API-1. B. RIIα was added to an AKAP18δ-L314E-coated SPR sensor chip in the presence of the AKAP-PKA anchoring disruptor peptide Ht31 or the small molecules in the indicated concentrations to test for their inhibitory effect on AKAP-PKA interactions. C. The derivative 1027 was added in the indicated concentrations to SPR sensor chips covalently coated with RIIα subunits to assess direct binding to the protein. D. The peptide Ht31 and the small molecule 1027 bind additively to RIIα. Association and dissociation of 1027 (100 µM) and Ht31 (50 nM) – either alone or in combination – were measured by SPR using a sensor chip coated with full length RIIα. RU, response units.

3.12 DTT seems to influence the binding of compounds to RIIα

The D/D-domains of RI subunits are known to form disulphide-bridged covalent dimers under oxidative conditions, which are cleaved under reducing conditions (e.g. in the presence of DTT)[10]. Dimerisation leads to altered subcellular localisation, cAMP-independent activation of PKA and downstream substrate phosphorylation. The mechanism is thought to serve as a redox-sensor for cardiac oxidative stress[11]. Although the D/D-domain of RII subunits does not contain the cysteine residues relevant for the disulphide bridge formation in RI subunits (Cys17 and Cys38 in rat RIα), SDS-resistant dimer formation was observed upon treatment of recombinant RII subunits or cell lysates with FMP-API-1 (Figs. 3.9D and 3.14). To clarify the influence of reductive conditions on the FMP-API-1-mediated effects, competitive SPR experiments were repeated in the presence of the reducing agent DTT.

RIIα was preincubated with the compounds FMP-API-1 or 1027 for 2 h in the presence or absence of 5 mM DTT, prior to analysing its binding to SPR chips coated with AKAP18δ-L314E (see above, Figs. 3.8 and 3.18B). The figures 3.19A and B show that the inhibitory effect of both FMP-API-1 and 1027 is abolished by the preincubation with DTT, suggesting that oxidative conditions favor the inhibitory activity of the compounds on AKAP-PKA interactions.

For 1027, it is possible that oxidative conditions facilitate an oxidation of the catechol moiety to a more reactive diketone irreversibly reacting with primary amino or sulphhydryl groups of amino acids (e.g. lysine or cysteine) to a covalent product[131]. However, this possibility was ruled out by mass spectrometric analyses of RIIα incubated with 1027. It was searched for masses possibly assignable to peptides covalently modified by 1027. Matching peptides were then sequenced, but for none of their amino acids a covalent modification was confirmed.

In addition, several C-terminal deletion mutants of RIIα were constructed, expressed and purified as GST-fusion proteins, and also subjected to SPR analyses after incubation with compound 1027 (Fig. 3.19C). The compound inhibited the interaction of all C-terminal RIIα deletion mutants including RIIα(1-156) with AKAP18δ-L314E. However, the shortest C-terminal deletion mutant, RIIα(1-87), representing an extended D/D domain, was only inhibited by 20 %, compared to at least 40 % for the other deletion mutants. The results were in

line with the previous HSQC-NMR measurements (Fig. 3.10), and mapped the binding site to be C-terminal of amino acids 1-87. Since also the AKAP-interaction of the variant RIIα(1-156) was inhibited by the small molecule, this experiment confined the binding site to a region between amino acids 88 and 156 of RIIα.

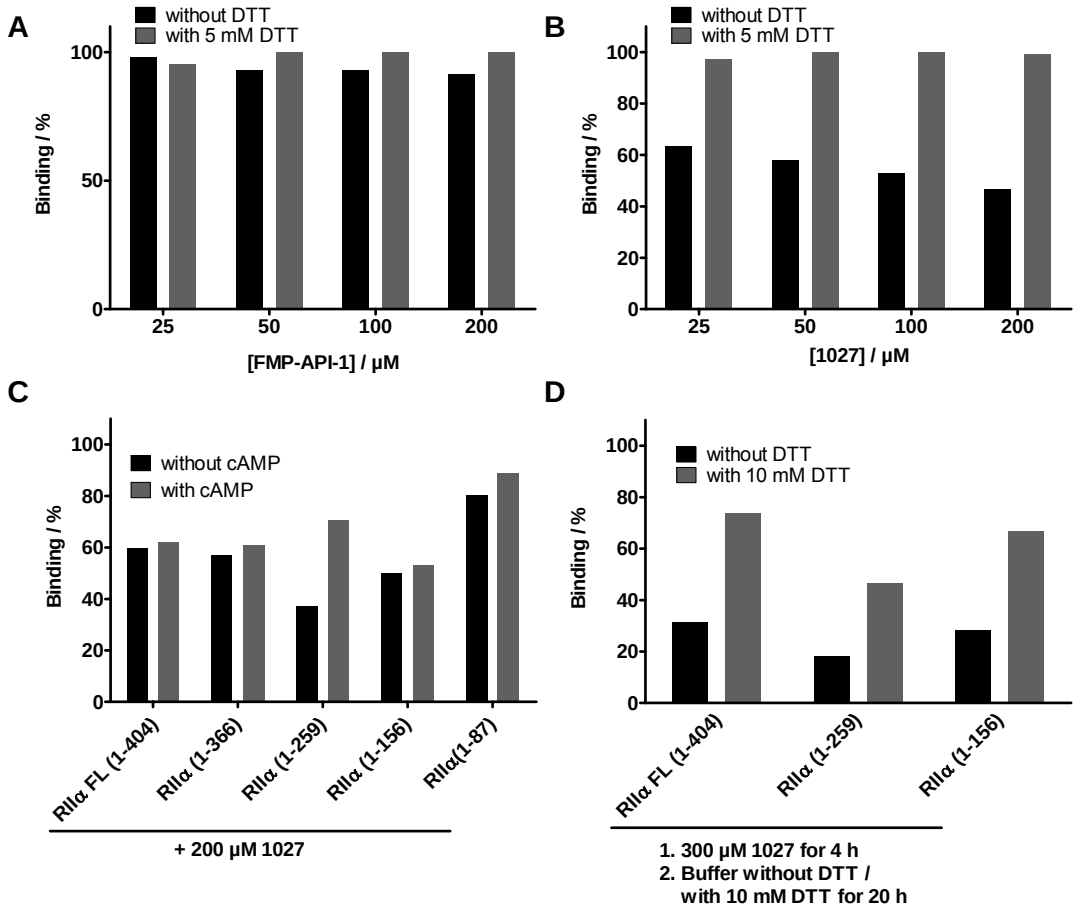

Fig. 3.19: Influence of reductive conditions or cAMP on activity of FMP-API-1 and 1027 to inhibit AKAP-PKA interactions. A, B. RIIα binding to AKAP18δ-L314E-coated SPR sensor chips was analysed in the presence of the indicated concentrations of FMP-API-1 (A) or 1027 (B) and in absence or presence of DTT (5 mM). C. The indicated RIIα constructs were preincubated with 1027 (200 µM) and cAMP (10 µM) for 14 h and binding was analysed on AKAP18δ-L314E-coated SPR sensor chips. D. The indicated RIIα constructs were first preincubated with 1027 (300 µM) for 4 h and then transferred into fresh buffer with or without DTT (10 mM) for 20 h to test for reversibility of the inhibitory effect through DTT. Binding of the RIIα constructs was analysed on AKAP18δ-L314E-coated SPR sensor chips.

To further clarify the influence of reductive conditions, it was also tested whether the inhibitory effect of 1027 was reversible by subsequent incubation with DTT. RIIα was first incubated with 300 µM 1027 for 4 h, and subsequently

with or without 10 mM DTT for 20 h. (Fig. 3.19D). Analysis by SPR revealed that DTT reduced the inhibition of RIIα-binding to AKAP18δ-L314E compared to the non-treated RIIα, although complete reversibility of the inhibitory effect of 1027 was not observed. Thus, DTT lowers the compound-mediated inhibitory effect by 50-60 % when applied after the compounds, but does not completely abolish it.

The influence of cAMP on the inhibitory effect of the small molecule was analysed in a further experiment. The RIIα(1-156) construct contained only four amino acids of the cAMP binding domain A (amino acids 153-242), therefore binding of 1027 to a cAMP binding domain – thereby causing the observed effects, e.g. activation of PKA – was unlikely. Indeed, all RIIα deletion mutant interactions with AKAP18δ-L314E besides the extended D/D-domain RIIα(1-87) were inhibited by 1027 in the presence of cAMP, excluding that 1027 causes its effects by binding to a cAMP binding domain (Fig. 3.19C). However, the inhibitory effect of 1027 on the construct RIIα(1-259) was markedly decreased in presence of cAMP.

3.13 Search for new chemophores for the inhibition of AKAP-PKA interactions

The analysis of FMP-API-1 and its derivative 1027 revealed promising characteristics both in cell assays and regarding the binding to regulatory PKA subunits. However, due to the binding to R subunits the compounds act as global inhibitors of PKA anchoring, and FMP-API-1 leads to generally increased cAMP levels and PKA activation in cardiac myocytes. These properties make them important new tools to study cellular signalling, but limit their potential as lead structures for drug development. Desirable are small molecules inhibiting specific AKAP-PKA interactions. To provide a basis for the search of new chemophores by high throughput screening, and also for the analysis of AKAP-PKA interactions in general, an assay based on fluorescence anisotropy was developed.

The prerequisite for a fluorescence anisotropy (FA) assay is direct interaction of two binding partners different in size. The smaller binding partner is labelled with a fluorescent tag, e.g. fluorescein. For this purpose, the anchoring disruptor (and RII-binding) peptide AKAP18δ-wt[64], comprising the wildtype RII-binding

domain of AKAP18δ, was coupled to fluorescein (F-AKAP18δ-wt) or left unmodified. A constant concentration of 10 nM was chosen for the peptide F-AKAP18δ-wt. At this concentration, the fluorescent species is present in limiting amount to obtain a high degree of sensitivity while allowing robust detection by the plate reader.

RIIα was added in increasing concentrations (0.25 to 500 nM), and the microplate was incubated for 30 min at room temperature (Fig. 3.20A). Fitting of the measured fluorescence anisotropy data to a one site binding model led to the binding curve with a K_d of 4.4 ± 0.5 nM for RIIα, representing the binding of the F-peptide to RIIα depending on the amount of RIIα present in the solution. A good compromise between the two values crucial to the sensitivity of the assay, the K_d and the maximum fluorescence anisotropy signal, is essential for the assay performance. Therefore, a concentration of 20 nM RIIα (red data point in Fig. 3.20A) was chosen for further experiments.

To detect whether the measured interaction can be inhibited competitively, unlabelled AKAP18δ-wt peptide was added in increasing concentrations (2.5 pM to 250 µM) to constant concentrations of RIIα (20 nM) and F-AKAP18δ-wt peptide (10 nM; Fig. 3.20B). A one site competition model was fitted to the data, leading to the inhibition curve shown in Fig. 3.20B with an IC_{50} of 16.8 ± 1.0 nM.

Next, suitable control reactions for fluorescence anisotropy measurements were established (Fig. 3.20C). RIIα (20 nM) was added to F-AKAP18δ-wt (10 nM) to obtain a standard binding value. The 2:1 ratio matches the dimer formation of RIIα subunits required for binding to the AKAP-derived peptide. RIIα (240 nM) was added to obtain a maximum binding signal (according to Fig. 3.20A, saturated binding is achieved with concentrations larger than 50 nM). For competitive inhibition of the peptide-RIIα interaction, the non-labelled peptide AKAP18δ-wt (25 nM) was added to obtain approximately 50 % inhibition, and a concentration of 2.5 µM was added to obtain complete inhibition. As negative control, a proline-substituted version of the AKAP18δ-derived peptide termed AKAP18δ-PP was used in the same concentrations as the wt-peptide for the competition. This peptide does not form an α-helix due to the disturbing proline residues and can thus not bind to regulatory subunits.

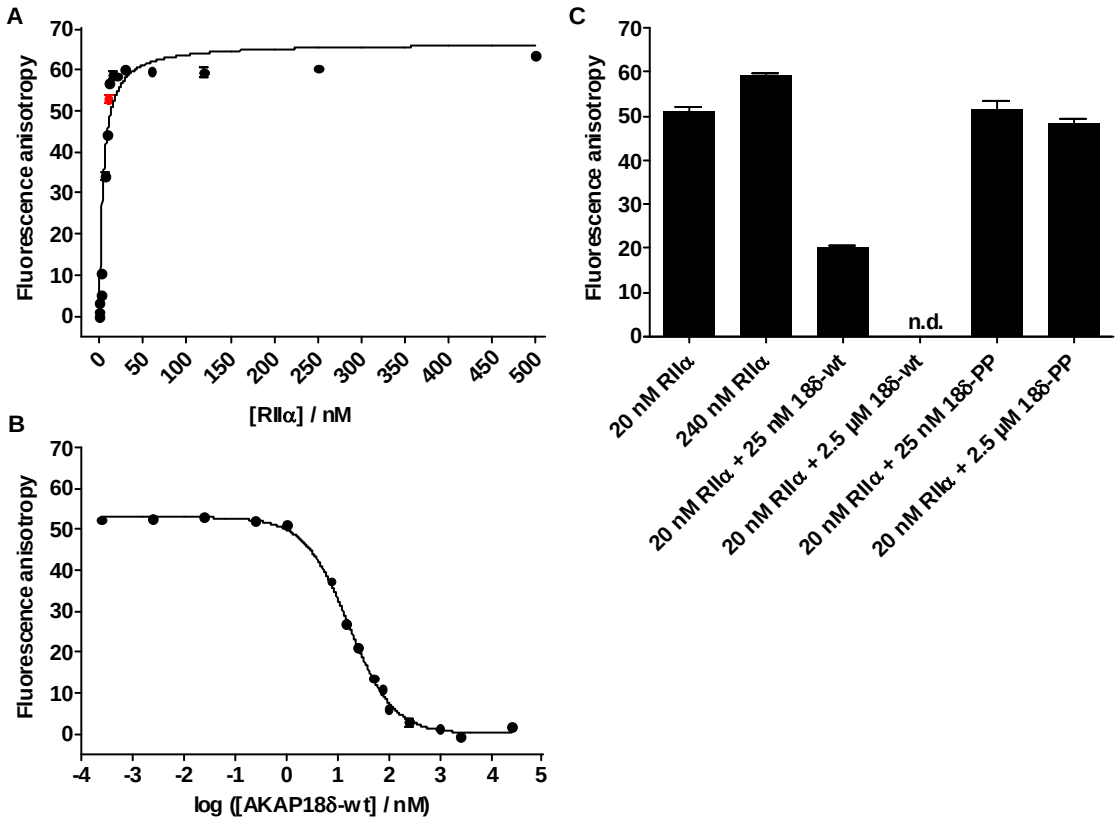

Fig. 3.20: A fluorescence anisotropy-based assay to measure AKAP-PKA interactions. A. RIIα (0.25-500 nM) was added to the fluorescein-tagged peptide F-AKAP18δ-wt (10 nM) and incubated for 30 min at room temperature. Fluorescence anisotropy was measured in a plate reader and corrected for background. A curve was fitted to the data based on a one-site binding model. n = 3, means ± SEM. B. RIIα (20 nM) was preincubated with 2.5 pM – 250 µM non-tagged AKAP18δ-wt peptide. After addition of 10 nM F-AKAP18δ-wt and 30 min incubation, fluorescence anisotropy was assessed in a plate reader. A curve was fitted to the data based on a one-site competition model. n = 3, means ± SEM. C. RIIα (20 or 240 nM) was preincubated with non-tagged peptides as indicated. After addition of 10 nM F-AKAP18δ-wt and 30 min incubation, fluorescence anisotropy was assessed in a plate reader. n = 3, means ± SEM. n.d., not detectable.

Next, it was tested whether the interaction between the AKAP18δ-derived F-peptide and RIIα could be competitively inhibited by the small molecules FMP-API-1-7 identified in the ELISA-based screening performed previously (Fig. 3.1). Increasing concentrations of the primary screening hit compounds or of the non-labelled inhibitory peptide AKAP18δ-L314E were added to the RIIα-F-AKAP18δ-wt complex (Fig. 3.21). However, all compounds besides 990 and the peptide partially precipitated upon addition to the assay buffer (TBS-T). At least a fraction of the small molecules remained dissolved as judged by the colour of the serial dilutions, which decreased together with the small molecule

concentration. The non-labelled peptide led to concentration-dependent inhibition (IC_{50} = 25.6 ± 1.2 nM) of the interaction, validating the assay (Fig. 3.21A). The small molecules failed to inhibit the peptide-protein interaction to the same extent as they did in the ELISA assay. The only striking changes in fluorescence anisotropy were caused by the compounds FMP-API-4 and -5. While FMP-API-4 led to a decreased signal only at the highest concentration of 2.5 mM, the latter increased the signal by 60 %. The intrinsic fluorescence of FMP-API-5 (Fig. 3.21C) disturbs the actual fluorescence anisotropy measurements, although a fluorescence intensity increase is also observed for the inhibitory non-labelled peptide AKAP18δ-L314E.

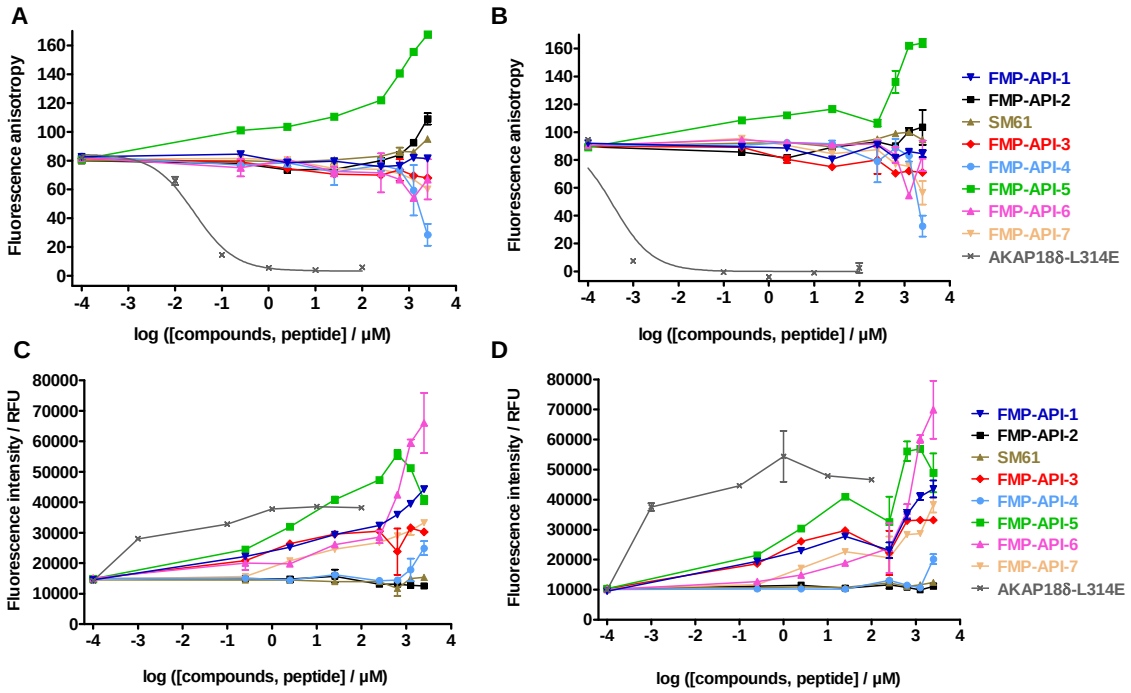

Fig. 3.21: The hits of the ELISA-based screening, FMP-API-1 to -7, were analysed in a fluorescence anisotropy assay. A, B. RIIα (20 nM) was preincubated with the small molecules or the peptide AKAP18δ-L314E in the indicated concentrations. After addition of the fluorescein (F)-labelled peptide F-AKAP18δ-wt (10 nM, A) or F-AKAP18δ-L314E-D298A (10 nM, B) and incubation for 30 min, fluorescence anisotropy was measured in a plate reader. C, D. Fluorescence intensity was measured in parallel to fluorescence anisotropy in panels A and B. RFU, relative fluorescence units.

Substitutions of amino acids in positions of the AKAP18δ-derived peptides important for the formation of hydrogen bonds and salt bridges with the D/D-domain by alanine decrease binding affinity to RIIα[64]. The AKAP18δ-L314E-D298A mutation was shown to have the lowest binding affinity[64]. For this rea-

son, the fluorescence anisotropy assay was repeated with a fluorescein-labelled version of that peptide (Fig. 3.21B, D). Inhibition of the interaction with the non-labelled AKAP18δ-L314E peptide confirmed the weaker affinity of the F-AKAP18δ-L314E-D298A peptide (IC_{50} = 0.4 ± 2.2 nM), but again the compounds failed to inhibit.

3.14 High throughput screening of a small molecule library with a fluorescence anisotropy-based assay

A second round of screening of a newly available library containing new chemical scaffolds was conducted to broaden the chemical basis for the development of potent small molecular AKAP-PKA inhibitors. The established fluorescence anisotropy assay was employed for the screening, providing the chance to find different chemical lead structures (chemotypes) and inhibitory mechanisms.

The control reactions to include on each screening microtiter plate consisted of background determination (without RIIα), 100 % binding value (20 nM RIIα), upper signal limit (240 nM RIIα) and validation reactions with the peptides AKAP18δ-wt and AKAP18δ-PP (17 nM and 2.5 µM, respectively). The concentration of 17 nM is expected to inhibit the interaction by 50 %, and 2.5 µM to inhibit completely. These expected results were obtained, as can be seen from the control summary panels on the analysis sheets (example in Fig. 3.22 and appendix C).

For the screening, all wells on a 384-well microtiter plate were initially filled with 5 µl compound solution from the library plates. In columns 1-22, 4 µl F-AKAP18δ-wt peptide and finally 1 µl RIIα solution were added, resulting in a total volume of 10 µl/well with concentrations of 20 nM RIIα, 10 nM F-AKAP18δ-wt peptide and 20 µM compound. The controls in columns 23-24 were added as indicated in Table 2.1. After 15 min incubation time the fluorescence anisotropy was measured in a plate reader.

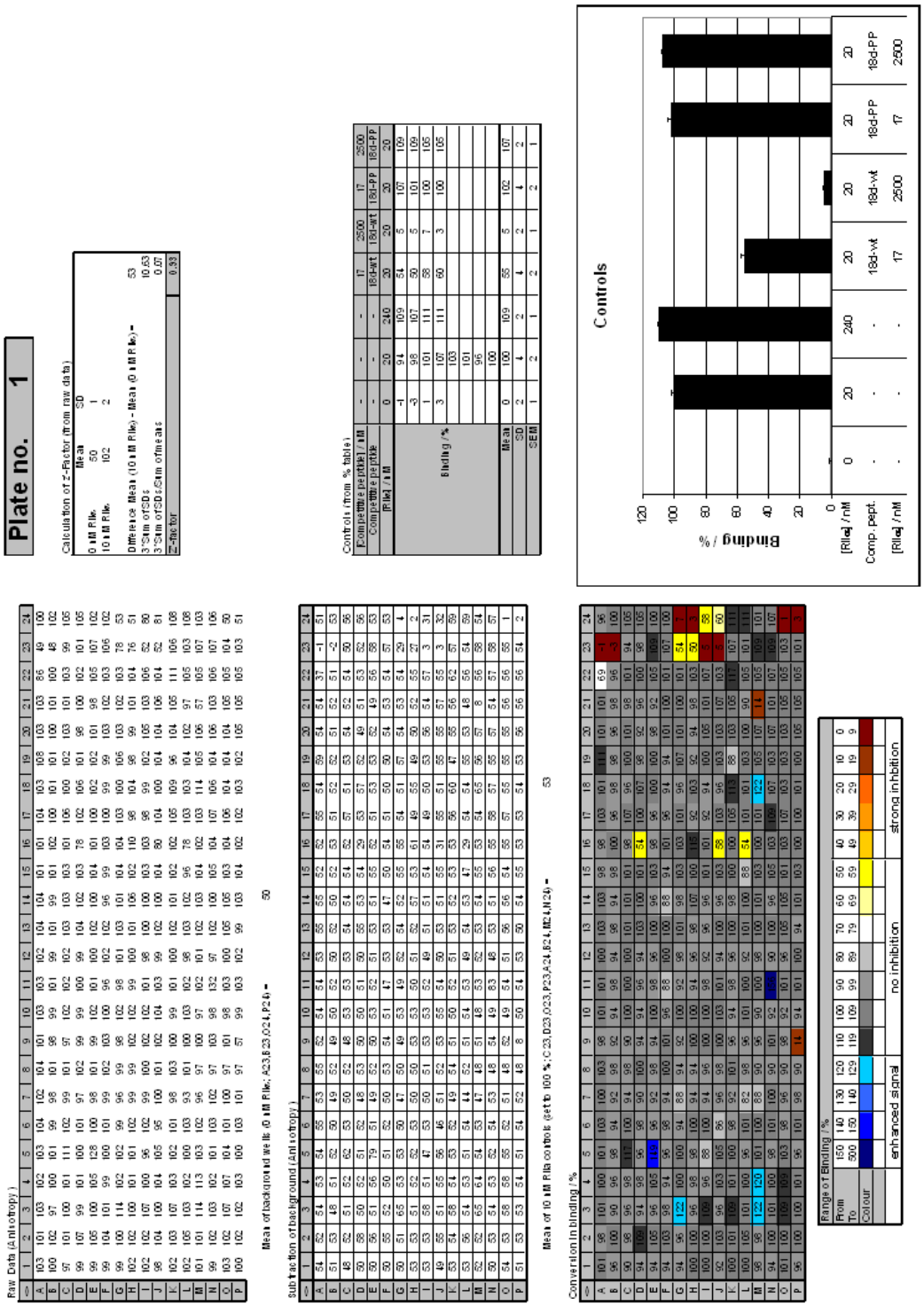

Fig. 3.22: Analysis of the fluorescence anisotropy-based high throughput screening. A representative analysis sheet is shown. The matrix represents a microplate. Depicted are screening raw data (fluorescence anisotropy), data corrected for background and data converted to percentage of binding and colour-coded (lower panels). In addition, the calculation of the z'-factor, and values and graphical analysis of the controls are indicated (upper panels). For full details of all 48 screening microplates see appendix C.

A representative analysis sheet for a measured screening plate is shown in Fig. 3.22. The left panels represent the plate matrix, with fluorescence anisotropy raw data, the data corrected for background as determined from the controls without RIIα, the data converted to percentage of binding compared to the 100 % controls, and the color code legend for the percentage matrix. The latter serves as an indicator for active compounds. The right panels indicate the plate number, calculation of the z'-factor (see below), summary of controls in table and text form. To ease the analysis of the large amounts of data generated by the screening, all parts of the analysis sheet were connected to the raw data using cell links for the calculations and a macro for the color code. The results for all 48 screening microtiter plates are listed in Appendix C.

The z'-factor is a measure for the quality of a high throughput screening (HTS) assay. It reflects both the dynamic range of the assay signal and the signal measurement variation as expressed by the standard deviation[165]. In Fig. 3.23 the z'-factors for all screening plates are summarised. For all plates, the factor was above 0.5, classifying the assay as "excellent"[165].

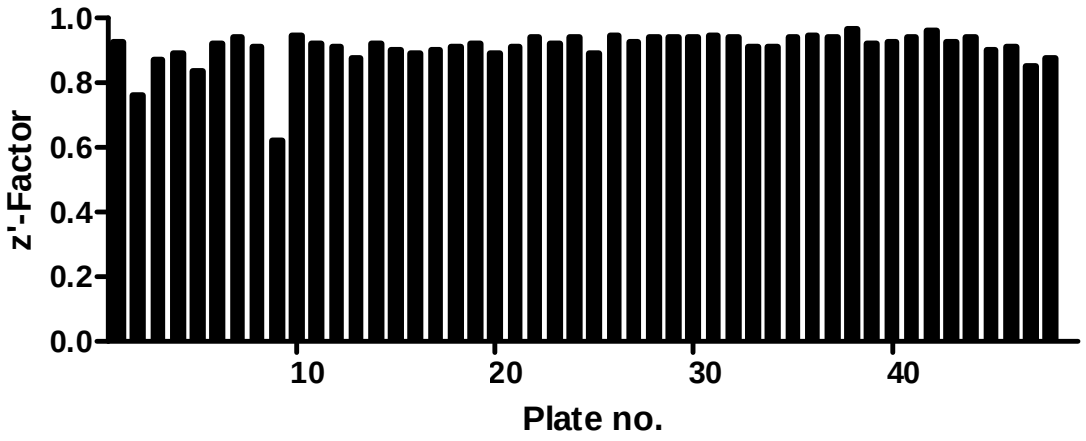

Fig. 3.23: z'-factors for all screening microplates. The z'-factor reflects both the dynamic range of the assay signal and the signal measurement variation as expressed by the standard deviation[165].

After completion of the screening, the calculated RIIα-AKAP18δ-wt binding values in the presence of all compounds were summarised in one table, together with compound identification numbers (ID), plate numbers, positions on plates, and the measured fluorescence intensities. Compounds that caused the RIIα-F-AKAP18δ-wt binding to be decreased by at least 25 % compared to the controls

were considered as hits and subjected to hit validation. To identify false positives, the upper fluorescence intensity limit was set to 45,000 relative fluorescence units (RFU) to exclude compounds with intrinsic fluorescence. The compounds affected by the latter criterion were retested manually, but none of them proved to be active. Overall, 25 out of the original 16671 compounds fulfilled the criteria, shown in table 3.3. The first four compounds led to a negative binding value, meaning that binding in the presence of the compounds was higher than without. Because such compounds could increase the AKAP-PKA interaction, they are also useful as tools to probe biological systems, and were taken into account as well.

Table 3.3: Hits identified in the fluorescence anisotropy-based screening. Comp_ID, compound identification number. Position, position on microplate. Plate no., number of microplate in library. Binding / %, calculated binding value for the RIIα-AKAP18δ-wt interaction in the presence of compounds (20 µM). F-I, fluorescence intensity. RFU, relative fluorescence units.

Comp_ID	Position	Plate no.	Binding / %	F-I / RFU
31917	M19	91	-35	43736
29489	A22	84	-9	39845
30193	A22	86	-2	40786
35825	A22	102	-1	40481
34065	A22	97	2	43571
29695	O12	85	31	37147
26983	G19	77	52	38865
27515	K8	79	55	23320
36452	D17	104	59	42422
28769	A21	82	65	40382
31051	K9	89	68	40536
31633	A2	91	69	25192
28743	G19	82	69	41157
36430	N15	104	70	43624
24487	G17	70	70	34936
26848	P10	77	73	37466
25758	N8	74	74	38625
25944	H20	74	74	38655
32663	G22	93	75	39707
26620	L18	76	75	40411
34962	B12	100	75	31775
27068	L2	78	75	35356
27081	I3	78	75	33574
27085	M3	78	75	35299
25770	J9	74	75	37723

For the first validation step, the fluorescence anisotropy assay was repeated. Serial dilutions of all 25 hits were prepared to obtain final concentrations from 2.5 to 200 µM. RIIα and F-AKAP18δ-wt peptide were added as described above to test which compounds would have concentration-dependent effects on the

binding. In Fig. 3.24A, the resulting concentration-dependency of only the active compounds is shown, the inactive compounds had no influence on the binding and were thus considered false positives.

While compounds 36430 and 36452 led to a concentration-dependent inhibition of up to 90 % and 34962 and 27515 of up to 60 % of the RIIα-F-AKAP18δ-wt interaction (compared to complete inhibition by the control peptide AKAP18δ-wt), the compound 27085 apparently led to an increase in binding by 180 %.

Since signal changes in fluorescent assays may also be caused by a potential intrinsic fluorescence of compounds, the fluorescence intensity was analysed (Fig. 3.24B). According to these data, the fluorescence intensity increased with compound concentration to up to 3-fold for the compounds 36430 and 36452. 27085 and 34962 led to intensity increases of up to 2- and 1.3-fold, respectively, while 27515 caused a decrease in fluorescence intensity of up to 0.6-fold. The peptide did not affect the fluorescence intensity.

The previously established ELISA was used as secondary assay to measure the activity of the identified compounds. The compounds evaluated positively in the fluorescence anisotropy assay were applied in final concentrations from 0.5 to 150 µM to the above described ELISA with full length RIIα and GST-AKAP18δ. Again, the AKAP18δ-wt peptide served as a positive control. As the resulting graph in Fig. 3.24C shows, none of the compounds proved to be active in this assay, while the peptide led to a decrease in binding as expected. However, the ELISA assay is a solid phase assay, while the fluorescence anisotropy assay is carried out in solution. Thus, the identified small molecules should be analysed in further assays, e.g. by solution NMR, in order not to miss any weak binders that could be otimised subsequently by medicinal chemistry.

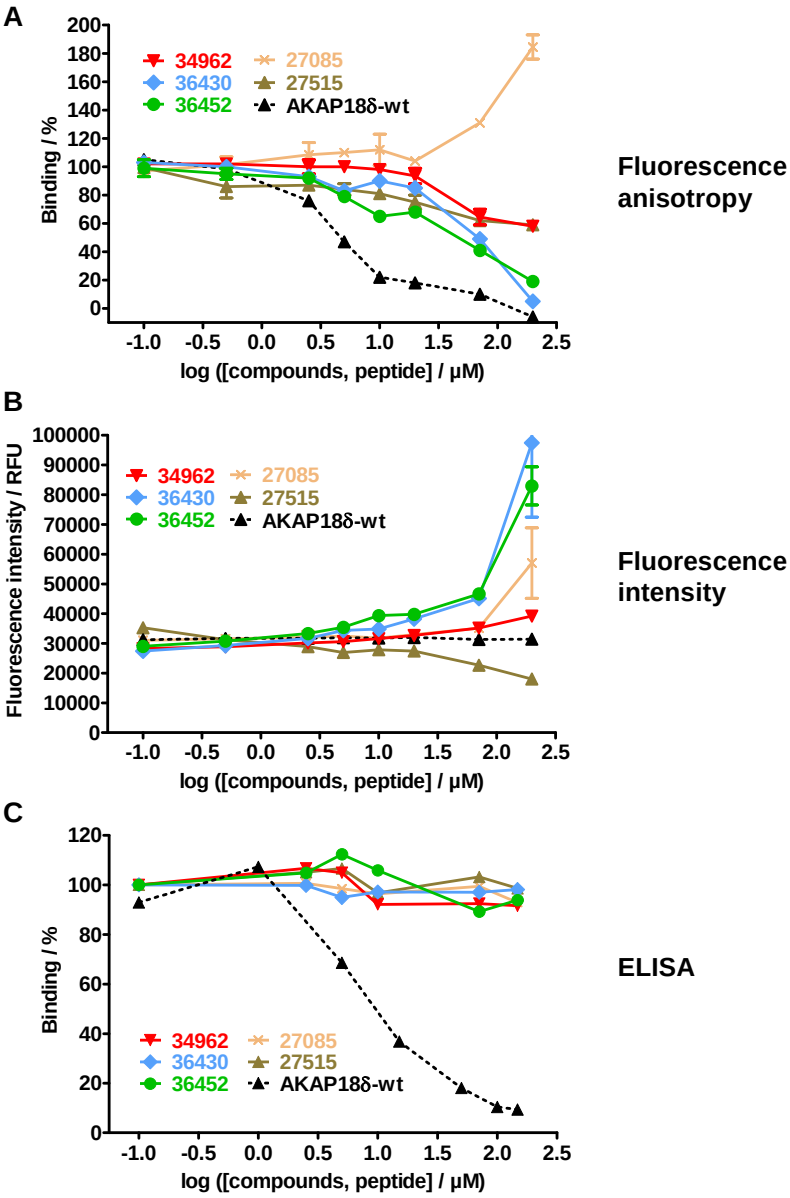

Fig. 3.24: Validation of the hit compounds identified in the fluorescence anisotropy-based high-throughput screening. A. 20 nM RIIα were preincubated with the non-labelled peptide AKAP18δ-wt or with the small molecules in the indicated concentrations for 15 min. 10 nM F-AKAP18δ-wt were added and incubated for 30 min. Fluorescence anisotropy was measured in a plate reader and normalised to 100 % binding controls. B. Fluorescence intensity values to the anisotropy measurement of panel A. RFU, relative fluorescence units. C. Microtiter plates were coated with RIIα (25 nM). Free binding sites were blocked and GST-AKAP18δ (10 nM) was added in the presence of the peptide or compounds in the indicated concentrations. After washing, the bound AKAP18δ was detected by incubation with rabbit AKAP18δ-specific and peroxidase-conjugated anti-rabbit antibody, followed by incubation with a luminol-containing peroxidase substrate solution. Chemiluminescence intensity was measured in a plate reader.

4 Discussion

AKAPs introduce specificity into cellular signalling by compartmentalising key pathway components. A common approach to study this signalling is targeted disruption of interactions and monitoring downstream effects, e.g. GPCR-agonist-induced changes of PKA substrate phosphorylations. Well established and commonly used for this purpose are anchoring disruptor peptides, which mimic the RII-binding domain of AKAPs and thus displace regulatory PKA subunits from their respective subcellular sites. Efforts have been undertaken to obtain peptides specific for regulatory subunit isoforms like the RI-anchoring disruptor (RIAD)[15,143] which preferentially disrupts AKAP-RI interactions (K_d(RI) = 1 nM *vs.* K_d(RII) = 1760 nM) in addition to the non-RI/RII-selective, but high-affinity peptides Ht31, $AKAP_{IS}$ and the AKAP18δ-derived peptides (with K_d-values in the low nanomolar range)[2,64].

Alternative tools to study signalling processes by disruption of protein-protein interactions are small organic molecules. Such molecules are well suited for cell experiments because of their potentially high membrane-permeability. However, newly identified small molecules need to be well characterised regarding their target and their mode of action before they can be used as research tools. In this work, small molecules that were identified in a high-throughput ELISA screening[22] (Fig. 3.1) were characterised towards their effects on compartmentalised cAMP signalling.

4.1 FMP-API-1 binds allosterically to RII, inhibits AKAP-PKA interactions and activates PKA

FMP-API-1, one of the small molecules identified in the high-throughput ELISA screening (Fig. 3.1), activates PKA by a previously unknown, cAMP-independent mechanism (Fig. 3.15). The activation is associated with disruption of AKAP-PKA interactions (Figs. 3.1B, 3.6 and 3.8). FMP-API-1 and its chemical derivative 1027 bind directly and reversibly (Figs. 3.9, 3.11 and 3.18) to RII subunits; presumably between amino acid residues 88 and 156 (Figs. 4.1 and 3.19C) and thus apparently outside the cyclic nucleotide binding (CNB) domains (CNB-A = amino acids 155-244, CNB-B = 277-374 in human RIIα[160]). This ex-

cludes a direct competition of FMP-API-1 with cAMP for the CNB domains, which could potentially also lead to activation of PKA in the absence of cAMP.

4.1.1 Binding sites of the small molecules in PKA regulatory subunits

The optimal way to define the binding site and clearify the detailed mechanism of action of FMP-API-1 would be to solve the x-ray structure of the FMP-API-1-RIIα complex. The three-dimensional structure of RIIα is well defined on the basis of NMR and x-ray structures (Fig. 4.1), but only for the part comprising amino acids 91-391, or for the D/D-domain alone (amino acids 1-44)[42,71,107,113,114,160]. A structure of a full length RIIα dimer including the D/D-domain has not been obtained so far. However, according to the data shown here, such a complete structure would be required to assess the mechanism of action of FMP-API-1 on the molecular level, since it binds outside the D/D-domain, but inhibits AKAP binding to the D/D domain by an allosteric mechanism. Solving a structure of FMP-API-1 bound to full-length RIIα was beyond the scope of this PhD thesis. However, the existing structures and knowledge on functional details of PKA permit speculations on the molecular mechanism of FMP-API-1 binding to RIIα and influencing PKA activation and AKAP binding.

Based on the experimental results summarised above, binding sites for FMP-API-1 are likely to be located in the linker region including the inhibitor region, but, as described in the following, possibly also in the αB/αC helix in CNB-A and the αB helix in CNB-B of RIIα (Fig. 4.1). Binding to any of these sites might lead to the observed effects in the cellular and *in vitro* biological systems studied in this work.

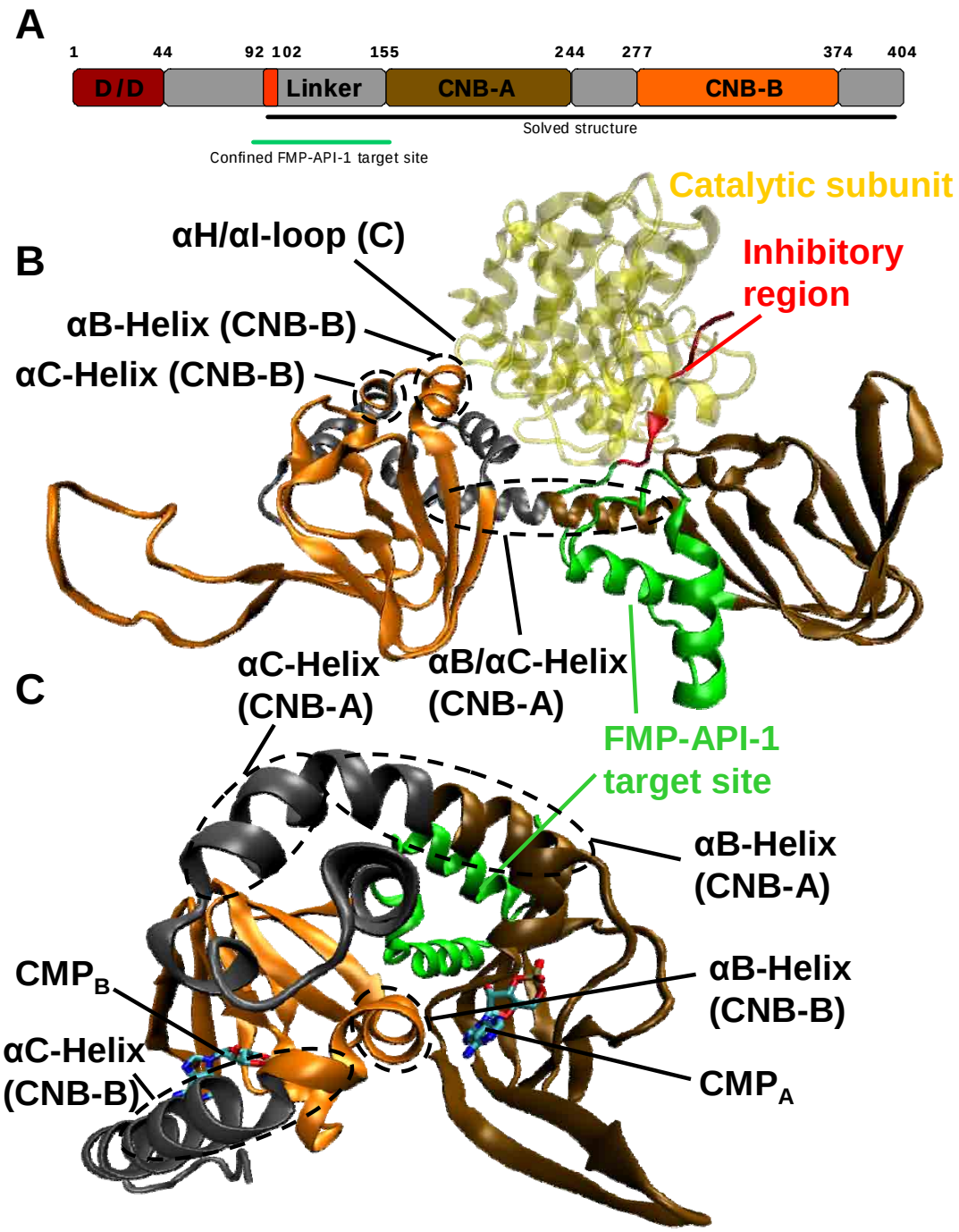

Fig. 4.1: Scheme and structure of the PKA-RII subunit in dissociated and catalytic subunit-associated state. A. Location of the domains described in the text within RIIα. The numbers indicate the amino acids in human RIIα. Colours indicate the position of the domains in the structures. D/D, docking and dimerisation domain; CNB, cyclic nucleotide binding domain. B. Structure of mouse RIIα(91-391) in complex with Cα. The structure and position of the catalytic subunit is indicated in yellow. C. Structure of rat RIIβ(130-412) with two molecules adenosine-3',5'-cyclic-monophosphate (CMP) bound to the CNB-domains. Coloured parts correspond to the homologous parts in human RIIα. For sequence alignment, see appendix B. Structures based on PDB data sets 2QVS[160] (B) and 1CX4[28] (C); graphical representations adapted with VMD[62].

An obvious target for FMP-API-1 is the linker region connecting the D/D domain (1-44) which mediates AKAP binding with the CNB domains (155-374). This region is known to be highly disordered in dissociated dimers[83], hence a structure of a dimer including the region has not been solved. The linker region contains an inhibitory site[150] that is a substrate for the catalytic (C) subunit. This inhibitory site (amino acid residues 92-102, in human RIIα; Fig. 4.1), binds to the active site cleft of the C subunit in the holoenzyme. It is solvent-exposed in the R subunit when dissociated from the C subunit and thus represents a possible binding site in line with the data presented above. Binding of a small molecule to free R subunits could prevent the inhibitory function of this part of the protein or its docking to the catalytic subunit. This could lead to a shift of the binding equilibrium C-RII ⇆ C + RII towards the direction of the dissociated state and hence to activation of C subunits, thereby explaining the measured increase in catalytic activity (Fig. 3.15). Importantly, this target region is located within the deletion construct RIIα(1-156). The binding of this construct to AKAPs is impaired in the presence of the compound 1027 (Fig. 3.19C).

However, other explanations for the observed activation of PKA are conceivable. For FMP-API-1 and 1027 they are unlikely, because they would require compound-binding to RIIα C-terminally of amino acid 156. However, these possible mechanisms could be valuable for future experiments and are thus discussed in the following.

Activation of PKA is known to be associated with conformational changes in the regulatory subunits[70,160] that occur upon binding of cAMP (Fig. 4.1B and C). Since binding of the compound triggers activation of the kinase, which requires dissociation of catalytic subunits, a major conformational change in the holoenzyme is also likely to occur in this case.

Changes in the helical subdomains in both cyclic nucleotide binding domains (CNB-A, 155-244 and CNB-B, 277-374; Fig. 4.1) take place during the transition from the C subunit-bound state to the dissociated state, causing overall conformational changes in the R subunit. In CNB-A a helix switch takes place, in which the integrated αB/αC helix (232-256) is kinked into the discrete αB and αC helices[160] (Fig. 4.1C). Consequently, both CNB domains are moving closer towards each other. The surface formed by the αB/αC helix in CNB-A represents a major interacting surface for docking to the C subunit as well as to the

Glu-rich linker region of RII (located downstream of the inhibitor region, Glu109-Glu112). Many of its residues are exposed to solvent in the dissociated, cAMP-bound state (Fig. 4.1C) but interact with the C subunit in the holoenzyme (Fig. 4.1B)[160], and are thus possible targets for FMP-API-1.

Another possible compound binding site in CNB-B is the B-domain's B-helix (362-370), since it directly interacts with the bound cAMP in CNB-A, and conformational changes in this helix may be directly transmitted to the C-helix of CNB-B, which follows directly in the sequence (371-379) and forms a lid for the bound cAMP in the B-domain, enabling extensive interactions between A- and B-domain[27] (Fig. 4.1). In the holoenzyme, the B-helix of the CNB-B domain docks onto the αH-αI loop of the catalytic subunit. Thus, binding of FMP-API-1 at this site may interfere with holoenzyme formation and catalytic subunit inhibition.

4.1.2 Conformational changes in RII subunits induced by cAMP-binding

A further mechanism explaining the PKA-activation might be given by the fact that cAMP binding to R subunits takes place in a cooperative fashion: one cAMP molecule needs to bind first to CNB-B before another one binds to CNB-A[26]; small molecule-mediated interference with the cooperative cAMP binding/dissociation process might disturb the binding and inactivation of catalytic subunits. However, SPR measurements showed, that the presence of cAMP does not alter the inhibitory activity of 1027 on AKAP-PKA interactions (Fig. 3.19C). Only the RIIα(1-259) construct binds weaker to the AKAP-peptide in presence of cAMP than without, which might be explained by the conformational changes taking place during the cAMP binding. Since the protein contains the complete CNB-A domain, cAMP could bind and cause conformational changes altering the 1027 binding site. Hence, the small molecule is less effective in the presence of cAMP. However, it is not known, why the AKAP-binding of the longer constructs of RII which contain the CNB-A domain too is not as strongly inhibited.

4.1.3 Crosslinking of regulatory subunits

The FMP-API-1-induced oligomerisation of RII subunits (Fig. 3.14) may participate in inducing the conformational change leading to dissociation of catalytic subunits. PKA-RI subunits have been shown to stabilise their dimerisation by

disulphide-bridge formation connecting cystein residues Cys16 and Cys37 in different RI molecules[82] under oxidative conditions, which increases the catalytic activity of the kinase. As a functional consequence of RI dimerisation contractility of cardiac myocytes is increased[10]. Although RII subunits do not contain cysteines at the homologous sequence positions, FMP-API-1 might lead to dimerisation by a yet undefined mechanism, e.g. by crosslinking regulatory subunits, causing catalytic subunit dissocation, activation and increased substrate phosphorylation as observed (Figs. 3.15 and 3.17). However, covalent reactions with cysteines could not be found in mass spectrometry analyses of RIIα incubated with FMP-API-1 or 1027 and would be contradictory to the identified reversible binding mode (Fig. 3.9).

When the structures of 1027 and FMP-API-1 (Fig. 3.18A) are compared, it becomes clear that unlike 1027 the structure of FMP-API-1 is symmetric and comprises functional groups at both phenyl rests. Since many established crosslinkers, e.g. disuccinimidyl suberate (DSS) or bis(sulfosuccinimidyl)suberate (BS3)[95], are bifunctional symmetric molecules, it could be reasoned that the high molecular weight complexes containing RII subunits observed in presence of FMP-API-1 (Fig. 3.14) are caused by a crosslinking reaction of one molecule FMP-API-1 with two molecules RII. However, the binding of FMP-API-1 to RII is reversible in contrast to classic crosslinking reactions (Fig. 3.9). In addition, the derivative 1027 seems to bind RII in the same way as FMP-API-1 (Fig. 3.18), but is not symmetric. The formation of high molecular weight complexes in the presence of 1027 has not been determined.

Recombinant PKA was found activated by FMP-API-1 cAMP-independently (Fig. 3.15A). The molecular mechanism underlying this observation could be based on the dimerisation of regulatory PKA subunits that occurs in the presence of FMP-API-1 (Fig. 3.14), explaining the increase in PKA activity. Alternatively, it could be caused by the induced dissociation of regulatory and catalytic subunits (see above).

4.1.4 The allosteric binding mode of FMP-API-1 and its influence on AKAP binding to RII

FMP-API-1 binds outside the D/D-domain (Fig. 3.10), and thus outside the surface determining AKAP-PKA interactions. Therefore, the mode of disruption of

AKAP-PKA interactions is different for FMP-API-1 and PKA anchoring disruptor peptides such as Ht31 and AKAP18δ-derived peptides. Whereas the peptides bind and block the D/D domain and thereby target the interaction site directly, FMP-API-1 interferes by allosterically binding to RII subunits.

Interestingly, phosphorylation of the RIIα inhibitor region (92-101) at Ser99 may alter AKAP binding to the D/D domain. If Ser99 in the inhibitor region is auto-phosphorylated by the catalytic subunit upon activation of the kinase, not only the cAMP-induced dissociation of the holoenzyme is increased[34], but also the affinity of RII for peptides representing RII-binding domains of several AKAPs, with the greatest increase for the AKAP18-peptide[163]. Thus the AKAP binding to RII is regulated, and this regulation could be modulated by FMP-API-1 and 1027, leading to reduced interaction.

4.1.5 The focussed library derived from FMP-API-1 permits first structure-activity-relationship conclusions

Since 1027 does not contain any amino groups in contrast to FMP-API-1, they seem to be unimportant for the mode of action. From the structure of the inactive compound 1030, differing from FMP-API-1 only in the methoxy- (-O-CH_3) instead of hydroxyl (-OH)-groups, it can be concluded that the hydroxyl groups are relevant for the binding to RIIα. Probably, the hydroxyl groups serve as H-bond donors, facilitating the interaction of the compound with H-bond acceptors in RIIα. One possible acceptor could be Ser99, the phosphorylation site in the inhibitory region of RIIα. From the structure and activity of 1028 it can be concluded, that introduction of a keto function at the central methylene group connecting the two aromatic systems reduces the activity. This may be caused by the decreased flexibility in the centre of the molecule.

When the structures and activities of 1026, 1027 and 1028 are compared, the lack of activity of 1026 is surprising, since it has the same structural features as 1028 and is more compact than 1028. Taken together, more derivatives and investigations of their activities are needed for a detailed analysis of the SAR.

4.1.6 Characteristics of AKAP-PKA interaction surfaces and small molecules

The surface area involved in the interaction of $AKAP_{IS}$ with RIIα is 1433 $Å^2$, thus being close to the range of a classic protein-protein interaction (1500-

3000 Å^2)[42,56]. The molecular details of AKAP-PKA interactions as known from the structures solved by NMR or X-ray structure analysis (for AKAP-derived peptides in complex with the D/D-domain[42,113,114]) show that there are no hot-spots as described for many protein-protein-interactions (see section 1.7), but rather an interface consisting of a consensus motif forming an amphipathic α-helix (the RII-binding domain of AKAPs) interacting with the shallow hydrophobic groove formed by the dimerised regulatory subunit D/D domain.

A small molecule of 230 Da (as FMP-API-1) can probably not occlude such a hydrophobic interaction surface to compete with the native high-affinity interaction, but an allosterically binding molecule exhibiting its effect *via* conformational changes or by influencing the 1:2 stoichiometry of the AKAP-PKA complex could be effective.

Examples in which allosteric modes of action of small molecules were demonstrated are the cancer drug taxol, which stabilises microtubules by binding to α-tubulin[161], and a small molecule binding to inducible nitric oxide synthase (iNOS) blocking dimerisation and hence NO synthesis by allosterically disrupting the protein-protein interaction at the dimer interface[97].

4.2 The identified compounds are active in cell-based assays

4.2.1 Interference with compartmentalised cAMP signalling in cardiac myocytes

FMP-API-1 was applied to primary cultured neonatal rat cardiac myocytes to analyse its effects on cAMP signalling in cells. The pulldown experiments with cAMP-agarose (Fig. 3.6) showed that lower amounts of AKAP18δ and AKAP150 were precipitated in the presence of FMP-API-1, while the amount of precipitated RII subunits remained unaffected, suggesting that FMP-API-1 does not act as a cAMP competitor. This is in line with the data obtained in SPR measurements (Fig. 3.19C). Presumably, this RII-binding compound acts globally on all AKAP-PKA interactions. At the same time this experiment shows that FMP-API-1 permeates the plasma membrane of cardiac myocytes.

A functional consequence of the AKAP-PKA disruption inside the myocytes is the failure of the β-adrenoceptor agonist isoproterenol to increase L-type Ca^{2+}-channel currents, an event that requires PKA-anchoring to the channel by

AKAP18α (Fig. 3.7a)[59-61]. Return of the current inducibility after washing out FMP-API-1 supports the reversible binding mechanism shown by SPR and STD-NMR (Fig. 3.9).

The inhibitory effect of AKAP-PKA disruption on the L-type Ca^{2+}-channel current was also observed upon treatment of cardiac myocytes with the anchoring disruptor peptides Ht31 and AKAP18δ-L314E[60,61,64]. The peptides also effectively displace PKA activity from already precipitated AKAPs. For example, the peptides displace RII subunits from AKAPs located on aquaporin-2-bearing vesicles[64]. However, biochemical evidence for the disruption of AKAP-PKA interactions through peptides for example from pulldown or immunoprecipitation experiments from peptide-treated living cells is lacking.

FMP-API-1 was applied in a concentration of at least 100 µM to measure disruption of AKAP-PKA interactions in cardiac myocytes by cAMP-agarose pulldown. In contrast, physiological effects were observed at several fold lower concentrations. The IC_{50} value for the inhibition of β-adrenoceptor-induced increases of L-type Ca^{2+} channel currents was 5.6 µM. A possible explanation for this difference is that in the pulldown intact cells are treated with the compound. In this setup FMP-API-1 has to permeate the plasma membrane, while in the patch clamp experiments it is introduced into the cells directly *via* the patch clamp pipette.

To exclude that FMP-API-1 acts directly on the L-type Ca^{2+}-channel, the direct agonist Bay-K8644 was included into the patch clamp setup (Fig. 3.7B). While the isoproterenol-induced current increase could be inhibited by FMP-API-1 as before, Bay-K8644 still induced the channel current after FMP-API-1 treatment, showing that the channel currents are inducible, and that inhibition of the AKAP18α-PKA interaction at the channel is most likely the underlying mechanism of the inhibitory effect.

A further observation in cardiac myocyte cell cultures was the elevation of cAMP levels in response to a combination of FMP-API-1 and isoproterenol compared to isoproterenol stimulation alone by one order of magnitude (EC_{50} shift from 724 to 95 nM; Fig. 3.16A). This observation may be explained by interference with the negative feedback loop based on the interaction of AKAP79/150 with adenylyl cyclase (AC) V/VI, which has so far only been detected in rat brain extracts. Upon activation of AC, the cAMP level rises and

activates PKA anchored by AKAP79/150, which in turn phosphorylates AC, thereby inhibiting it, limiting cAMP synthesis and thus PKA activation. Disruption of this AKAP-PKA complex by FMP-API-1 (Fig. 3.6A) most likely interrupts the negative feedback loop, leading to prolonged cAMP synthesis.

However, the increased cAMP levels cannot be hold responsible for the increased PKA activity found in cardiac myocytes treated with FMP-API-1 (Fig. 3.15B), because for an increase in cAMP synthesis the β-agonist isoproterenol is required (Fig. 3.16A), while for PKA activation it is not. Furthermore, recombinant PKA is activated by FMP-API-1 in absence of cAMP. The dual action – activation of PKA and ablation of AKAP-PKA interactions – turns FMP-API-1 into a new tool to study the compartmentalisation of cAMP signalling.

The phospholamban phosphorylation found in FMP-API-1-treated cardiac myocytes (Fig. 3.17A) is most likely a consequence of the increased PKA activity. Phospholamban is phosphorylated upon FMP-API-1-treatment of the cells independently of isoproterenol stimulation, indicating that the cAMP-independent PKA-activation mechanism contributes largely to the overall effect. In addition, the detected phosphorylation of phospholamban can be inhibited by 75 % through the PKA-inhibitor H-89, largely excluding the involvement of other kinases (Fig. 17B). The remaining phosphorylation might be explained by imperfect phospho-antibody specificity. While PKA phosphorylates Ser16, Thr17 is phosphorylated by calmodulin-dependent kinase, so that the phosphorylation detected in presence of H-89 could be the one at Thr17. There was no effect of FMP-API-1 on the activity of phosphatases important for the regulation of contraction in cardiac myocytes, e.g. PP1 (Fig. 3.17C), excluding increased phospholamban phosphorylation due to the inhibition of protein phosphatases.

4.2.2 The possible influence of FMP-API-1 on cAMP signalling in failing hearts

Some AKAP-PKA interactions may be regulated (see sections 3.8 and 4.1.4) by PKA-phosphorylation of regulatory subunits. The study by Manni *et al.*[90] showed that less AKAP18α is co-immunoprecipitated with a non-phosphorylated RII mimic when compared to a constitutively PKA-phosphorylated mimic or wildtype RII. Since RII phosphorylation is reduced in heart failure[164], this could imply generally decreased compartmentalisation of PKA by AKAPs in failing cardiac

myocytes. This condition may cause decreased PKA-mediated protein phosphorylation (e.g., of phospholamban) and thus impaired contractility. Considering the observed effects of FMP-API-1 (e.g., increase in phospholamban phosphorylation), the application of the compound may lead to a rescue of the reduced RII phosphorylation in heart failure by generally increasing cAMP levels and PKA activation. However, further detailed characterisation in cell models and *in vivo* is required, e.g. with more phospho-antibodies.

A consequence of phospholamban phosphorylation, and thus also of the effect of FMP-API-1, is an increase in contractility due to faster reuptake of Ca^{2+}, potentiating the next contraction. Furthermore, FMP-API-1-treatment should lead to faster relaxation after contraction. An increase in contractility is also known to be caused by stimulation of the β-adrenergic pathway in cardiac myocytes[30]. A small molecule acting beyond the β-adrenergic receptor could cause fewer or less severe adverse drug effects than stimulation of all signalling events downstream of the receptor.

4.2.3 Inhibition of the AQP2 shuttle in IMCD cells

The redistribution of AQP2 in renal collecting duct principal cells following hormonal stimulation by AVP represents an example for a physiological process dependent on the compartmentalisation of cAMP signalling. Direct inhibition of PKA by H-89, or the displacement of PKA from AKAP signalling complexes by anchoring disruptor peptides, prevents activation of the shuttle[52,74,110,147].

Primary cultured rat inner medullary collecting duct (IMCD) cells maintain a functional AQP2 shuttle[91], and were treated with the compounds FMP-API-2, -3, and -7. All three inhibited the AQP2-shuttle after 30 min incubation (Fig. 3.2C, D, H), suggesting that the compounds entered the cells. FMP-API-2 showed the most pronounced effect. Additionally, its action was reversible by washing the treated cells with fresh culture medium (Fig. 3.3). These observations argue for a specific, directed effect of the compound and a reversible binding mechanism to its target protein. However, Western blot and RII overlay analysis of protein complexes coprecipitated with regulatory PKA subunits from IMCD cell or inner medulla lysates by cAMP-agarose led to ambiguous results. Likewise, FMP-API-2 and its derivatives failed to inhibit the interaction of RIIα with AKAP18δ-

derived peptides in SPR measurements, confirming that AKAP-PKA interactions are not the target of FMP-API-2 and its derivatives.

Nevertheless, FMP-API-2 and its derivatives are interesting lead structures due to their clear inhibitory effect on the AQP2 shuttle. Their molecular target in the cell needs to be identified, and experiments for this purpose are ongoing. For example, the target could be identified using a matrix-conjugated version of FMP-API-1 and subsequent mass-spectrometric analysis of pulldown experiments from IMCD cells. The identification of the target will enable further structure-activity-relationship (SAR) studies, and chemical improvement by synthesis of focussed libraries, as it was done with FMP-API-1.

4.2.4 Applications for small molecule AQP2 shuttle inhibitors

It was shown in patients that in heart failure, liver cirrhosis and hypertension, but also during pregnancy, water retention caused by upregulation of AQP2 may occur, leading to water retention[1,67,92,127-129]. Water retention is so far treated with diuretics and aquaretics. Diuretics indirectly increase water excretion *via* the kidneys by inhibiting Na^+-, K^+- and Ca^{2+}-ion transporters, which are required for urine concentration. However, the resulting loss of electrolytes causes severe side effects such as hypotension and increased risk of thrombosis.

Aquaretics are a novel class of drugs known as vaptans that lack the side effects caused by the disturbance of electrolyte homeostasis. Vaptans are vasopressin receptor-selective antagonists[96,118,125,134]. Long-term studies are missing so far. They lead to increased water excretion and represent a potential replacement for conventional diuretics. Possible unwanted side effects during the treatment with vaptans are hypotension, thirst and hypernatraemia[24].

However, vaptans had no positive influence on the mortality of patients. As one reason for this their severe side effects were suggested[24]. This underpins the importance to develop compounds with less severe side effects. Small molecules directly inhibiting the AQP2 shuttle without affecting all signalling pathways emanating from the V2 receptor would lower the risk of unwanted side effects. Aside from this, a mirror-image oligonucleotide binding and inhibiting AVP was developed as aquaretically active agent, but is not approved as a drug[118].

Since the identified compound FMP-API-2 and its derivatives inhibit the AQP2 shuttle in renal collecting duct principal cells and thereby most likely lead to increased water excretion, it seems to be feasible to develop them into a novel class of aquaretics, if they are specific for their target.

4.3 Fluorescence anisotropy is a quick, solution-based method to characterise AKAP-PKA interactions

The ELISA-based assay used for the first high throughput screening (Fig. 3.1) is a reliable but longsome assay due to the many steps involved. In order to circumvent the drawback, a fluorescence anisotropy (FA) assay was established to measure AKAP-PKA interactions (Fig. 3.20). This method allows to measure interactions in solution, which is closer to the physiological situation in cells and allows true binding steady state analysis of interactions.

When the anchoring disruptor peptides were used to competitively inhibit the AKAP-peptide-RIIα interaction (Figs. 3.20 and 3.21), the FA assay proved to be a reliable and fast method to quantify the effects of the peptides. Other advantages are the lack of multiple incubation and washing steps and low reagent requirements. These characteristics make the FA assay suitable for automation and therefore for high throughput screening.

The ELISA is more sensitive compared to FA, because it is based on one interaction partner bound to a solid phase. Unbound ligands are removed by washing steps. While FA permits a more direct readout, the ELISA has the advantage to enrich the binding partner and the specific antibodies to the antigen, and to amplify the readout signal by employing an enzymatic reaction for detection (here, the peroxidase-catalysed oxidation of luminol to produce light).

The interaction between full length AKAP18δ and RIIα is a high affinity interaction with a K_d of 31 nM (determined by SPR[52]), but when instead of full length AKAP18δ only a peptide representing its RII-binding domain is used, the K_d drops by an order of magnitude to 0.4 nM (SPR[64]). This high-affinity interaction is hardly expected to be disrupted by the low affinity small molecules identified by the ELISA (as indicated by their IC_{50} values in the micromolar range; Fig. 3.1 and Table 3.1). In combination with the lower sensitivity this explains why the FA assay did not confirm the activity of the small molecules identified by the ELISA (Fig. 3.21) in addition to their limited solubility in the FA assay buffer.

In view of its advantages, the FA assay established in this work will proof as a valuable tool to characterise newly developed peptides or peptidomimetics with regard to RII-binding.

5 Summary

A-kinase anchoring proteins (AKAPs) tether the cAMP-dependent protein kinase (PKA) to subcellular structures in proximity to its substrates, providing the basis for compartmentalised cAMP signalling. In order to study the relevance of specific protein-protein interactions within compartmentalised cAMP signalling networks, it was aimed to establish small molecules disrupting AKAP-PKA interactions. An ELISA-based screening of a library containing 20,000 diverse, drug-like small molecules was conducted. Two of the identified hits inhibiting the AKAP18δ-PKA interaction concentration-dependently (FMP-API-1 and -2, IC_{50} values of 23 and 1 µM, respectively) were characterised.

AKAP-mediated PKA-anchoring to AQP2-bearing vesicles is a prerequisite for the vasopressin-induced translocation of aquaporin (AQP2) into the plasma membrane of rat renal primary principal cells. Immunomicroscopic analysis revealed that FMP-API-2 (100 µM) completely, but reversibly inhibited the translocation. However, the AKAP-PKA interaction could not be confirmed as the target of FMP-API-2, which will have to be defined in future work.

Disruption of AKAP-PKA interactions in cells was shown for FMP-API-1. cAMP-agarose pulldowns (enriching cAMP-binding proteins and their interaction partners) from compound-treated (100 µM) neonatal rat cardiac myocytes contained 60 % less coprecipitated AKAP18δ and AKAP150. β-adrenoceptor-induced increases of L-type Ca^{2+}-channel currents in cardiac myocytes, depending on the AKAP18α-PKA interaction, were abolished in presence of FMP-API-1.

Biomolecular interaction analyses (by surface plasmon resonance; SPR) confirmed the inhibition of AKAP-PKA interactions through FMP-API-1 *in vitro*. In addition, SPR revealed direct binding of FMP-API-1 to PKA-RIIα subunits, which was confirmed by saturation transfer difference nuclear magnetic resonance (STD-NMR), a ligand-observed method to study protein-ligand interactions. The AKAP-derived peptide Ht31 binds to the docking and dimerisation (D/D) domain of RIIα, responsible for regulatory PKA-subunit dimerisation and AKAP-binding. SPR measurements showed additive binding of FMP-API-1 and Ht31 to RIIα, suggesting an allosteric binding mechanism for FMP-API-1. 1027, a chemical derivative of FMP-API-1, inhibits the AKAP-PKA interaction more effectively than FMP-API-1 while binding RIIα in the same fashion. By using RIIα deletion mutants, the binding region of 1027 was confined to amino acids 88-156 of RIIα. It includes the inhibitory motif (92-102), which binds to and inhibits catalytic PKA subunits. This provides a possible explanation for the observed 2.5-fold activity increase of recombinant PKA in presence of FMP-API-1. The activity of cellular PKA was also increased (1.5-fold) as measured by phosphorylation of a peptide substrate. As a consequence of PKA activation, the phosphorylation of phospholamban, an important PKA substrate in cardiac myocytes, was found to be 9-fold increased in the presence of FMP-API-1. β-adrenergic stimulation causes an increase in cAMP concentration in cardiac myocytes, which was enhanced by FMP-API-1 (shifting the EC_{50} from 724 nM to 95 nM). This is explained by disruption of the AKAP150-PKA interaction which is involved in a negative feedback loop limiting cAMP-synthesis by inhibition of adenylyl cyclase through PKA-phosphorylation. Taken together, the small molecule FMP-API-1 binds to PKA-RIIα subunits, inhibits AKAP-PKA-interactions *in vitro* and in cells by an allosteric mechanism and activates PKA. The dual action turns the molecule into a new tool to study compartmentalised cAMP signalling by interference with protein-protein interactions.

Protein-protein interactions are involved in cellular signalling and are thus disease-relevant. Small molecules inhibiting such interactions were characterised in this work. They open new avenues in basic research as well as for future treatments of human diseases including water retention and heart failure.

6 Zusammenfassung

A-Kinase Ankerproteine (AKAPs) verankern die cAMP-abhängige Proteinkinase (PKA) an subzellulären Strukturen in Substratnähe und bilden so die Grundlage für kompartimentierte cAMP-Signalwege. Um die Relevanz spezifischer Protein-Protein-Interaktionen in kompartimentierten cAMP-Signalnetzwerken zu analysieren, sollten kleine Moleküle für die Hemmung von AKAP-PKA-Interaktionen etabliert werden. Es wurde eine 20.000 wirkstoffähnliche kleine Moleküle umfassende Substanzbibliothek mittels eines ELISA-basierten Hochdurchsatzverfahrens durchmustert. Zwei der identifizierten Substanzen, die die AKAP-PKA-Interaktion konzentrationsabhängig hemmen (FMP-API-1 und -2, mit IC_{50}-Werten von 23 µM bzw. 1 µM), wurden näher charakterisiert.
Die AKAP-vermittelte PKA-Verankerung an AQP2-haltigen Vesikeln ist Voraussetzung für die Vasopressin-induzierte Umverteilung von Aquaporin-2 (AQP2) in die Plasmamembran renaler Ratten-Primärzellen. Immunfärbungen zeigten, dass FMP-API-2 (100 µM) die Umverteilung vollständig, aber reversibel hemmt. Allerdings konnte die AKAP-PKA-Interaktion nicht als Angriffspunkt von FMP-API-2 verifiziert werden. Dieser wird in zukünftigen Studien zu definieren sein.
Die Hemmung von AKAP-PKA-Interaktionen durch FMP-API-1 wurde in Zellen bestätigt. cAMP-Agarose-Präzipitationen (zur Anreicherung cAMP-bindender Proteine und ihrer Interaktionspartner) aus FMP-API-1-behandelten (100 µM) neonatalen Rattenherzmyozyten enthielten 60 % weniger kopräzipitiertes AKAP18δ und AKAP150 im Vergleich zu Kontrollen. Der von der AKAP18α-PKA-Interaktion abhängige β-Adrenozeptor-induzierte Anstieg von L-Typ-Ca^{2+}-Kanalströmen in Herzmyozyten wurde durch FMP-API-1 verhindert. Biomolekulare Interaktionsanalysen (mittels Oberflächenplasmonresonanz; SPR) bestätigten die Hemmung von AKAP-PKA-Interaktionen durch FMP-API-1 *in vitro*. Außerdem zeigte SPR die direkte Bindung von FMP-API-1 an PKA-RIIα. Dies wurde durch Sättigungstransfer-Differenz (STD)-NMR bestätigt, einer Methode zur Analyse von Protein-Ligand-Interaktionen. Das AKAP-abgeleitete Peptid Ht31 bindet an die Docking- und Dimerisierungsdomäne (D/D) von RIIα, die für Dimerisierung und AKAP-Bindung regulatorischer PKA-Untereinheiten verantwortlich ist. SPR-Messungen zeigten additive Bindung von Ht31 und FMP-API-1 an RIIα, was einen allosterischen Bindungsmechanismus für FMP-API-1 nahelegt. Das kleine Molekül 1027, ein chemisches Derivat von FMP-API-1, hemmt die AKAP-PKA-Interaktion effektiver als FMP-API-1 und bindet wie dieses an RIIα. Mithilfe von RIIα-Deletionsmutanten wurde die Bindungsregion von 1027 auf die Aminosäuren 88-156 eingegrenzt. Diese beinhaltet das inhibitorische Motiv (92-102) von RIIα, welches die katalytische PKA-Untereinheit bindet und hemmt. Dies erklärt möglicherweise den beobachteten 2,5-fachen Aktivitätsanstieg rekombinanter PKA in Gegenwart von FMP-API-1. Die Aktivität zellulärer PKA wurde ebenfalls verstärkt (1,5-fach), wie durch Phosphorylierung eines Peptidsubstrats ermittelt wurde. Als Konsequenz der PKA-Aktivierung wurde eine 9-fache Verstärkung der Phosphorylierung von Phospholamban, eines wichtigen PKA-Substrats in Herzmyozyten, in Gegenwart von FMP-API-1 festgestellt. β-adrenerge Stimulation verursacht einen Anstieg der cAMP-Konzentration in Herzmyozyten, welcher durch FMP-API-1 verstärkt wurde (wobei sich der EC_{50}-Wert von 724 auf 95 nM reduzierte). Dies kann durch die Inhibition der AKAP150-PKA-Interaktion erklärt werden. Sie ist an einer negativen Rückkopplungsschleife beteiligt, in der Adenylylzyklase durch PKA-Phosphorylierung gehemmt und damit die cAMP-Synthese begrenzt wird.
Zusammengefasst bindet das kleine Molekül FMP-API-1 an PKA-RIIα-Untereinheiten, hemmt AKAP-PKA-Interaktionen *in vitro* und in Zellen mittels eines allosterischen Mechanismus und aktiviert PKA. Diese duale Wirkung macht das Molekül zu einem neuen Werkzeug für die Analyse kompartimentierter cAMP-Signalwege durch Hemmung von Protein-Protein-Interaktionen. Protein-Protein-Interaktionen sind an zellulären Signalwegen beteiligt und daher krankheitsrelevant. In dieser Arbeit wurden kleine Moleküle charakterisiert, die solche Interaktionen hemmen. Sie eröffnen neue Wege sowohl für die Grundlagenforschung als auch für die zukünftige Behandlung menschlicher Krankheiten wie Wasserretention und Herzversagen.

Bibliography

1. Agre,P. & Kozono,D. Aquaporin water channels: molecular mechanisms for human diseases. *FEBS Lett.* **555**, 72-78 (2003).

2. Alto,N.M. *et al.* Bioinformatic design of A-kinase anchoring protein-in silico: a potent and selective peptide antagonist of type II protein kinase A anchoring. *Proc. Natl. Acad. Sci. U. S. A* **100**, 4445-4450 (2003).

3. Arkin,M.R. *et al.* Binding of small molecules to an adaptive protein-protein interface. *Proc. Natl. Acad. Sci. U. S. A* **100**, 1603-1608 (2003).

4. Arkin,M.R. & Wells,J.A. Small-molecule inhibitors of protein-protein interactions: progressing towards the dream. *Nat. Rev. Drug Discov.* **3**, 301-317 (2004).

5. Bauman,A.L. *et al.* Dynamic regulation of cAMP synthesis through anchored PKA-adenylyl cyclase V/VI complexes. *Mol. Cell* **23**, 925-931 (2006).

6. Bengrine,A., Li,J. & Awayda,M.S. The A-kinase anchoring protein 15 regulates feedback inhibition of the epithelial Na+ channel. *FASEB J.* **21**, 1189-1201 (2007).

7. Bichet,D.G. Lithium, cyclic AMP signaling, A-kinase anchoring proteins, and aquaporin-2. *J. Am. Soc. Nephrol.* **17**, 920-922 (2006).

8. Bichet,D.G. Nephrogenic diabetes insipidus. *Adv. Chronic. Kidney Dis.* **13**, 96-104 (2006).

9. Boussiotis,V.A., Freeman,G.J., Berezovskaya,A., Barber,D.L. & Nadler,L.M. Maintenance of human T cell anergy: blocking of IL-2 gene transcription by activated Rap1. *Science* **278**, 124-128 (1997).

10. Brennan,J.P. *et al.* Oxidant-induced activation of type I protein kinase A is mediated by RI subunit interprotein disulfide bond formation. *J. Biol. Chem.* **281**, 21827-21836 (2006).

11. Brennan,J.P. *et al.* Detection and mapping of widespread intermolecular protein disulfide formation during cardiac oxidative stress using proteomics with diagonal electrophoresis. *J. Biol. Chem.* **279**, 41352-41360 (2004).

12. Brooks,H., Lebleu,B. & Vives,E. Tat peptide-mediated cellular delivery: back to basics. *Adv. Drug Deliv. Rev.* **57**, 559-577 (2005).

13. Brown,R.L., August,S.L., Williams,C.J. & Moss,S.B. AKAP7gamma is a nuclear RI-binding AKAP. *Biochem. Biophys. Res. Commun.* **306**, 394-401 (2003).

14. Burns-Hamuro,L.L. *et al.* Designing isoform-specific peptide disruptors of protein kinase A localization. *Proc. Natl. Acad. Sci. U. S. A* **100**, 4072-4077 (2003).

15. Carlson,C.R. *et al.* Delineation of type I protein kinase A-selective signaling events using an RI anchoring disruptor. *J. Biol. Chem.* **281**, 21535-21545 (2006).

16. Carr,D.W., Hausken,Z.E., Fraser,I.D., Stofko-Hahn,R.E. & Scott,J.D. Association of the type II cAMP-dependent protein kinase with a human thyroid RII-anchoring protein. Cloning and characterization of the RII-binding domain. *J. Biol. Chem.* **267**, 13376-13382 (1992).

17. Carr,D.W. *et al.* Interaction of the regulatory subunit (RII) of cAMP-dependent protein kinase with RII-anchoring proteins occurs through an amphipathic helix binding motif. *J. Biol. Chem.* **266**, 14188-14192 (1991).

18. Carr,D.W., Stofko-Hahn,R.E., Fraser,I.D., Cone,R.D. & Scott,J.D. Localization of the cAMP-dependent protein kinase to the postsynaptic densities by A-kinase anchoring proteins. Characterization of AKAP 79. *J. Biol. Chem.* **267**, 16816-16823 (1992).

19. Checovich,W.J., Bolger,R.E. & Burke,T. Fluorescence polarization--a new tool for cell and molecular biology. *Nature* **375**, 254-256 (1995).

20. Chijiwa,T. *et al.* Inhibition of forskolin-induced neurite outgrowth and protein phosphorylation by a newly synthesized selective inhibitor of cyclic AMP-dependent protein kinase, N-[2-(p-bromocinnamylamino)ethyl]-5-isoquinolinesulfonamide (H-89), of PC12D pheochromocytoma cells. *J. Biol. Chem.* **265**, 5267-5272 (1990).

21. Chiriva-Internati,M. *et al.* AKAP-4: a novel cancer testis antigen for multiple myeloma. *Br. J. Haematol.* **140**, 465-468 (2008).

22. Christian,F. *et al.* Disruption of AKAP-PKA Interactions by Small Molecules. *Poster Presentation at the 15th Protein Kinase Symposium, Oslo, Norway* (2006).

23. Clackson,T. & Wells,J.A. A hot spot of binding energy in a hormone-receptor interface. *Science* **267**, 383-386 (1995).

24. Decaux,G., Soupart,A. & Vassart,G. Non-peptide arginine-vasopressin antagonists: the vaptans. *Lancet* **371**, 1624-1632 (2008).

25. Dell'Acqua,M.L., Dodge,K.L., Tavalin,S.J. & Scott,J.D. Mapping the protein phosphatase-2B anchoring site on AKAP79. Binding and inhibition of phosphatase activity are mediated by residues 315-360. *J. Biol. Chem.* **277**, 48796-48802 (2002).

26. Diller,T.C., Madhusudan, Xuong,N.H. & Taylor,S.S. Molecular basis for regulatory subunit diversity in cAMP-dependent protein kinase: crystal structure of the type II beta regulatory subunit. *Structure.* **9**, 73-82 (2001).

27. Diller,T.C., Madhusudan, Xuong,N.H. & Taylor,S.S. Molecular basis for regulatory subunit diversity in cAMP-dependent protein kinase: crystal structure of the type II beta regulatory subunit. *Structure.* **9**, 73-82 (2001).

28. Diller,T.C., Madhusudan, Xuong,N.H. & Taylor,S.S. Molecular basis for regulatory subunit diversity in cAMP-dependent protein kinase: crystal structure of the type II beta regulatory subunit. *Structure.* **9**, 73-82 (2001).

29. Diviani,D., Soderling,J. & Scott,J.D. AKAP-Lbc anchors protein kinase A and nucleates Galpha 12-selective Rho-mediated stress fiber formation. *J. Biol. Chem.* **276**, 44247-44257 (2001).

30. Dorn,G.W. & Molkentin,J.D. Manipulating cardiac contractility in heart failure: data from mice and men. *Circulation* **109**, 150-158 (2004).

31. Dousa,T.P. Cyclic-3',5'-nucleotide phosphodiesterase isozymes in cell biology and pathophysiology of the kidney. *Kidney Int.* **55**, 29-62 (1999).

32. Dransfield,D.T. *et al.* Ezrin is a cyclic AMP-dependent protein kinase anchoring protein. *EMBO J.* **16**, 35-43 (1997).

33. El-Armouche,A. & Eschenhagen,T. beta-Adrenergic stimulation and myocardial function in the failing heart. *Heart Fail. Rev.* (2008).

34. Erlichman,J., Rosenfeld,R. & Rosen,O.M. Phosphorylation of a cyclic adenosine 3':5'-monophosphate-dependent protein kinase from bovine cardiac muscle. *J. Biol. Chem.* **249**, 5000-5003 (1974).

35. Fink,M.A. *et al.* AKAP-mediated targeting of protein kinase a regulates contractility in cardiac myocytes. *Circ. Res.* **88**, 291-297 (2001).

36. Foged,C. & Nielsen,H.M. Cell-penetrating peptides for drug delivery across membrane barriers. *Expert. Opin. Drug Deliv.* **5**, 105-117 (2008).

37. Frank,B. *et al.* Association of a common AKAP9 variant with breast cancer risk: a collaborative analysis. *J. Natl. Cancer Inst.* **100**, 437-442 (2008).

38. Frank,R. The SPOT-synthesis technique. Synthetic peptide arrays on membrane supports--principles and applications. *J. Immunol. Methods* **267**, 13-26 (2002).

39. Fraser,I.D. *et al.* A novel lipid-anchored A-kinase Anchoring Protein facilitates cAMP-responsive membrane events. *EMBO J.* **17**, 2261-2272 (1998).

40. Fushimi,K., Sasaki,S. & Marumo,F. Phosphorylation of serine 256 is required for cAMP-dependent regulatory exocytosis of the aquaporin-2 water channel. *J. Biol. Chem.* **272**, 14800-14804 (1997).

41. Giesemann,T., Guttenberg,G. & Aktories,K. Human alpha-defensins inhibit Clostridium difficile toxin B. *Gastroenterology* **134**, 2049-2058 (2008).

42. Gold,M.G. *et al.* Molecular basis of AKAP specificity for PKA regulatory subunits. *Mol. Cell* **24**, 383-395 (2006).

43. Gold,M.G., Smith,F.D., Scott,J.D. & Barford,D. AKAP18 contains a phosphoesterase domain that binds AMP. *J. Mol. Biol.* **375**, 1329-1343 (2008).

44. Grantcharova,E. *et al.* The extracellular N terminus of the endothelin B (ETB) receptor is cleaved by a metalloprotease in an agonist-dependent process. *J. Biol. Chem.* **277**, 43933-43941 (2002).

45. Gray,P.C. *et al.* Primary structure and function of an A kinase anchoring protein associated with calcium channels. *Neuron* **20**, 1017-1026 (1998).

46. Gray,P.C., Tibbs,V.C., Catterall,W.A. & Murphy,B.J. Identification of a 15-kDa cAMP-dependent protein kinase-anchoring protein associated with skeletal muscle L-type calcium channels. *J. Biol. Chem.* **272**, 6297-6302 (1997).

47. Hausken,Z.E., Coghlan,V.M., Hastings,C.A., Reimann,E.M. & Scott,J.D. Type II regulatory subunit (RII) of the cAMP-dependent protein kinase interaction with A-kinase anchor proteins requires isoleucines 3 and 5. *J. Biol. Chem.* **269**, 24245-24251 (1994).

48. Hausken,Z.E., Dell'Acqua,M.L., Coghlan,V.M. & Scott,J.D. Mutational analysis of the A-kinase anchoring protein (AKAP)-binding site on RII. Classification Of side chain determinants for anchoring and isoform selective association with AKAPs. *J. Biol. Chem.* **271**, 29016-29022 (1996).

49. Hayes,J.S., Brunton,L.L. & Mayer,S.E. Selective activation of particulate cAMP-dependent protein kinase by isoproterenol and prostaglandin E1. *J. Biol. Chem.* **255**, 5113-5119 (1980).

50. He,M.M. *et al.* Small-molecule inhibition of TNF-alpha. *Science* **310**, 1022-1025 (2005).

51. Henn,V. *et al.* Identification of a novel A-kinase anchoring protein 18 isoform and evidence for its role in the vasopressin-induced aquaporin-2 shuttle in renal principal cells. *J. Biol. Chem.* **279**, 26654-26665 (2004).

52. Henn,V. *et al.* Identification of a novel A-kinase anchoring protein 18 isoform and evidence for its role in the vasopressin-induced aquaporin-2 shuttle in renal principal cells. *J. Biol. Chem.* **279**, 26654-26665 (2004).

53. Henriques,S.T., Melo,M.N. & Castanho,M.A. How to address CPP and AMP translocation? Methods to detect and quantify peptide internalization in vitro and in vivo (Review). *Mol. Membr. Biol.* **24**, 173-184 (2007).

54. Herberg,F.W., Maleszka,A., Eide,T., Vossebein,L. & Tasken,K. Analysis of A-kinase anchoring protein (AKAP) interaction with protein kinase A (PKA) regulatory subunits: PKA isoform specificity in AKAP binding. *J. Mol. Biol.* **298**, 329-339 (2000).

55. Hoffmann,R., Wilkinson,I.R., McCallum,J.F., Engels,P. & Houslay,M.D. cAMP-specific phosphodiesterase HSPDE4D3 mutants which mimic activation and changes in rolipram inhibition triggered by protein kinase A phosphorylation of Ser-54: generation of a molecular model. *Biochem. J.* **333 (Pt 1)**, 139-149 (1998).

56. Hopkins,A.L. & Groom,C.R. The druggable genome. *Nat. Rev. Drug Discov.* **1**, 727-730 (2002).

57. Huang,L.J., Durick,K., Weiner,J.A., Chun,J. & Taylor,S.S. D-AKAP2, a novel protein kinase A anchoring protein with a putative RGS domain. *Proc. Natl. Acad. Sci. U. S. A* **94**, 11184-11189 (1997).

58. Huang,Z., Somanath,P.R., Chakrabarti,R., Eddy,E.M. & Vijayaraghavan,S. Changes in intracellular distribution and activity of protein phosphatase PP1gamma2 and its regulating proteins in spermatozoa lacking AKAP4. *Biol. Reprod.* **72**, 384-392 (2005).

59. Hulme,J.T., Ahn,M., Hauschka,S.D., Scheuer,T. & Catterall,W.A. A novel leucine zipper targets AKAP15 and cyclic AMP-dependent protein kinase to the C terminus of the skeletal muscle Ca2+ channel and modulates its function. *J. Biol. Chem.* **277**, 4079-4087 (2002).

60. Hulme,J.T., Lin,T.W., Westenbroek,R.E., Scheuer,T. & Catterall,W.A. Beta-adrenergic regulation requires direct anchoring of PKA to cardiac CaV1.2 channels via a leucine zipper interaction with A kinase-anchoring protein 15. *Proc. Natl. Acad. Sci. U. S. A* **100**, 13093-13098 (2003).

61. Hulme,J.T., Westenbroek,R.E., Scheuer,T. & Catterall,W.A. Phosphorylation of serine 1928 in the distal C-terminal domain of cardiac CaV1.2 channels during beta1-adrenergic regulation. *Proc. Natl. Acad. Sci. U. S. A* **103**, 16574-16579 (2006).

62. Humphrey,W., Dalke,A. & Schulten,K. VMD: visual molecular dynamics. *J. Mol. Graph.* **14**, 33-38 (1996).

63. Hundsrucker,C. & Klussmann,E. Direct AKAP-Mediated Protein-Protein Interactions as Potential Drug Targets. *Handb. Exp. Pharmacol.* 483-503 (2008).

64. Hundsrucker,C. *et al.* High-affinity AKAP7delta-protein kinase A interaction yields novel protein kinase A-anchoring disruptor peptides. *Biochem. J.* **396**, 297-306 (2006).

65. Hundsrucker,C. *et al.* High-affinity AKAP7delta-protein kinase A interaction yields novel protein kinase A-anchoring disruptor peptides. *Biochem. J.* **396**, 297-306 (2006).

66. Hundsrucker,C., Rosenthal,W. & Klussmann,E. Peptides for disruption of PKA anchoring. *Biochem. Soc. Trans.* **34**, 472-473 (2006).

67. Ivarsen,P. *et al.* Increased urinary excretion of aquaporin 2 in patients with liver cirrhosis. *Gut* **52**, 1194-1199 (2003).

68. Kapiloff,M.S., Jackson,N. & Airhart,N. mAKAP and the ryanodine receptor are part of a multi-component signaling complex on the cardiomyocyte nuclear envelope. *J. Cell Sci.* **114**, 3167-3176 (2001).

69. Kapiloff,M.S., Schillace,R.V., Westphal,A.M. & Scott,J.D. mAKAP: an A-kinase anchoring protein targeted to the nuclear membrane of differentiated myocytes. *J. Cell Sci.* **112 (Pt 16)**, 2725-2736 (1999).

70. Kim,C., Cheng,C.Y., Saldanha,S.A. & Taylor,S.S. PKA-I holoenzyme structure reveals a mechanism for cAMP-dependent activation. *Cell* **130**, 1032-1043 (2007).

71. Kinderman,F.S. *et al.* A dynamic mechanism for AKAP binding to RII isoforms of cAMP-dependent protein kinase. *Mol. Cell* **24**, 397-408 (2006).

72. King,L.S., Kozono,D. & Agre,P. From structure to disease: the evolving tale of aquaporin biology. *Nat. Rev. Mol. Cell Biol.* **5**, 687-698 (2004).

73. Klussmann,E., Maric,K. & Rosenthal,W. The mechanisms of aquaporin control in the renal collecting duct. *Rev. Physiol Biochem. Pharmacol.* **141**, 33-95 (2000).

74. Klussmann,E., Maric,K., Wiesner,B., Beyermann,M. & Rosenthal,W. Protein kinase A anchoring proteins are required for vasopressin-mediated translocation of aquaporin-2 into cell membranes of renal principal cells. *J. Biol. Chem.* **274**, 4934-4938 (1999).

75. Klussmann,E. & Rosenthal,W. Role and identification of protein kinase A anchoring proteins in vasopressin-mediated aquaporin-2 translocation. *Kidney Int.* **60**, 446-449 (2001).

76. Klussmann,E., Rosenthal,W., Rademann,J., Christian,F. & Meyer,S. Non-peptidic inhibitors of AKAP/PKA interaction. PCT/DE2006/000897(WO/2006/122546). 23-11-2006.

77. Klussmann,E. *et al.* An inhibitory role of Rho in the vasopressin-mediated translocation of aquaporin-2 into cell membranes of renal principal cells. *J. Biol. Chem.* **276**, 20451-20457 (2001).

78. Kramer,A. & Schneider-Mergener,J. Synthesis and screening of peptide libraries on continuous cellulose membrane supports. *Methods Mol. Biol.* **87**, 25-39 (1998).

79. Kuwahara,M. *et al.* cAMP-dependent phosphorylation stimulates water permeability of aquaporin-collecting duct water channel protein expressed in Xenopus oocytes. *J. Biol. Chem.* **270**, 10384-10387 (1995).

80. Landsverk,H.B. *et al.* Regulation of anchoring of the RIIalpha regulatory subunit of PKA to AKAP95 by threonine phosphorylation of RIIalpha: implications for chromosome dynamics at mitosis. *J. Cell Sci.* **114**, 3255-3264 (2001).

81. Langeberg,L.K. & Scott,J.D. A-kinase-anchoring proteins. *J. Cell Sci.* **118**, 3217-3220 (2005).

82. Leon,D.A., Herberg,F.W., Banky,P. & Taylor,S.S. A stable alpha-helical domain at the N terminus of the RIalpha subunits of cAMP-dependent protein kinase is a novel dimerization/docking motif. *J. Biol. Chem.* **272**, 28431-28437 (1997).

83. Li,F. *et al.* Consequences of cAMP and catalytic-subunit binding on the flexibility of the A-kinase regulatory subunit. *Biochemistry* **39**, 15626-15632 (2000).

84. Lipinski,C.A., Lombardo,F., Dominy,B.W. & Feeney,P.J. Experimental and computational approaches to estimate solubility and permeability in drug discovery and development settings. *Adv. Drug Deliv. Rev.* **46**, 3-26 (2001).

85. Livnah,O. *et al.* Functional mimicry of a protein hormone by a peptide agonist: the EPO receptor complex at 2.8 A. *Science* **273**, 464-471 (1996).

86. Lundblad,J.R., Laurance,M. & Goodman,R.H. Fluorescence polarization analysis of protein-DNA and protein-protein interactions. *Mol. Endocrinol.* **10**, 607-612 (1996).

87. Lygren,B. *et al.* AKAP complex regulates Ca2+ re-uptake into heart sarcoplasmic reticulum. *EMBO Rep.* **8**, 1061-1067 (2007).

88. Lygren,B. & Tasken,K. The potential use of AKAP18delta as a drug target in heart failure patients. *Expert. Opin. Biol. Ther.* **8**, 1099-1108 (2008).

89. Lynch,M.J. *et al.* RNA silencing identifies PDE4D5 as the functionally relevant cAMP phosphodiesterase interacting with beta arrestin to control the protein kinase A/AKAP79-mediated switching of the beta2-adrenergic receptor to activation of ERK in HEK293B2 cells. *J. Biol. Chem.* **280**, 33178-33189 (2005).

90. Manni,S., Mauban,J.H., Ward,C.W. & Bond,M. Phosphorylation of the cAMP-dependent protein kinase (PKA) regulatory subunit modulates PKA-AKAP interaction, substrate phosphorylation, and calcium signaling in cardiac cells. *J. Biol. Chem.* **283**, 24145-24154 (2008).

91. Maric,K., Oksche,A. & Rosenthal,W. Aquaporin-2 expression in primary cultured rat inner medullary collecting duct cells. *Am. J. Physiol* **275**, F796-F801 (1998).

92. Martin,P.Y. *et al.* Selective V2-receptor vasopressin antagonism decreases urinary aquaporin-2 excretion in patients with chronic heart failure. *J. Am. Soc. Nephrol.* **10**, 2165-2170 (1999).

93. Marx,S.O. *et al.* Requirement of a macromolecular signaling complex for beta adrenergic receptor modulation of the KCNQ1-KCNE1 potassium channel. *Science* **295**, 496-499 (2002).

94. Marx,S.O. *et al.* PKA phosphorylation dissociates FKBP12.6 from the calcium release channel (ryanodine receptor): defective regulation in failing hearts. *Cell* **101**, 365-376 (2000).

95. Mattson,G. *et al.* A practical approach to crosslinking. *Mol. Biol. Rep.* **17**, 167-183 (1993).

96. Mayinger,B. & Hensen,J. Nonpeptide vasopressin antagonists: a new group of hormone blockers entering the scene. *Exp. Clin. Endocrinol. Diabetes* **107**, 157-165 (1999).

97. McMillan,K. *et al.* Allosteric inhibitors of inducible nitric oxide synthase dimerization discovered via combinatorial chemistry. *Proc. Natl. Acad. Sci. U. S. A* **97**, 1506-1511 (2000).

98. McSorley,T. *et al.* Spatial organisation of AKAP18 and PDE4 isoforms in renal collecting duct principal cells. *Eur. J. Cell Biol.* **85**, 673-678 (2006).

99. Meyer,B. *et al.* Saturation transfer difference NMR spectroscopy for identifying ligand epitopes and binding specificities. *Ernst. Schering. Res. Found. Workshop* 149-167 (2004).

100. Meyer,B. & Peters,T. NMR spectroscopy techniques for screening and identifying ligand binding to protein receptors. *Angew. Chem. Int. Ed Engl.* **42**, 864-890 (2003).

101. Meyer,S. *et al.* Structure-Activity Study of Small Molecules as Inhibitors of Protein Kinase A (PKA) - A Kinase Anchoring Protein (AKAP) Interactions. *Poster Presentation at the Frontiers in Medicinal Chemistry Conference, March 18-21, 2007, Berlin, Germany* (2006).

102. Michel,J.J. & Scott,J.D. AKAP mediated signal transduction. *Annu. Rev. Pharmacol. Toxicol.* **42**, 235-257 (2002).

103. Molkentin,J.D. Calcineurin and beyond: cardiac hypertrophic signaling. *Circ. Res.* **87**, 731-738 (2000).

104. Montminy,M.R., Gonzalez,G.A. & Yamamoto,K.K. Regulation of cAMP-inducible genes by CREB. *Trends Neurosci.* **13**, 184-188 (1990).

105. Mooren,F.C. & Kinne,R.K. Intracellular calcium in primary cultures of rat renal inner medullary collecting duct cells during variations of extracellular osmolality. *Pflugers Arch.* **427**, 463-472 (1994).

106. Moreira,I.S., Fernandes,P.A. & Ramos,M.J. Hot spots--a review of the protein-protein interface determinant amino-acid residues. *Proteins* **68**, 803-812 (2007).

107. Morikis,D., Roy,M., Newlon,M.G., Scott,J.D. & Jennings,P.A. Electrostatic properties of the structure of the docking and dimerization domain of protein kinase A IIalpha. *Eur. J. Biochem.* **269**, 2040-2051 (2002).

108. Navedo,M.F. *et al.* AKAP150 is required for stuttering persistent Ca2+ sparklets and angiotensin II-induced hypertension. *Circ. Res.* **102**, e1-e11 (2008).

109. Nedvetsky,P.I. *et al.* Regulation of aquaporin-2 trafficking. *Handb. Exp. Pharmacol.* 133-157 (2009).

110. Nejsum,L.N., Zelenina,M., Aperia,A., Frokiaer,J. & Nielsen,S. Bidirectional regulation of AQP2 trafficking and recycling: involvement of AQP2-S256 phosphorylation. *Am. J. Physiol Renal Physiol* **288**, F930-F938 (2005).

111. Newhall,K.J. *et al.* Dynamic anchoring of PKA is essential during oocyte maturation. *Curr. Biol.* **16**, 321-327 (2006).

112. Newlon,M.G., Roy,M., Hausken,Z.E., Scott,J.D. & Jennings,P.A. The A-kinase anchoring domain of type IIalpha cAMP-dependent protein kinase is highly helical. *J. Biol. Chem.* **272**, 23637-23644 (1997).

113. Newlon,M.G. *et al.* A novel mechanism of PKA anchoring revealed by solution structures of anchoring complexes. *EMBO J.* **20**, 1651-1662 (2001).

114. Newlon,M.G. *et al.* The molecular basis for protein kinase A anchoring revealed by solution NMR. *Nat. Struct. Biol.* **6**, 222-227 (1999).

115. Nielsen,S. *et al.* Aquaporins in the kidney: from molecules to medicine. *Physiol Rev.* **82**, 205-244 (2002).

116. Oliveria,S.F., Dell'Acqua,M.L. & Sather,W.A. AKAP79/150 anchoring of calcineurin controls neuronal L-type Ca2+ channel activity and nuclear signaling. *Neuron* **55**, 261-275 (2007).

117. Perkins,G.A. *et al.* PKA, PKC, and AKAP localization in and around the neuromuscular junction. *BMC. Neurosci.* **2**, 17 (2001).

118. Purschke,W.G., Eulberg,D., Buchner,K., Vonhoff,S. & Klussmann,S. An L-RNA-based aquaretic agent that inhibits vasopressin in vivo. *Proc. Natl. Acad. Sci. U. S. A* **103**, 5173-5178 (2006).

119. Richter,W. *et al.* Signaling from beta1- and beta2-adrenergic receptors is defined by differential interactions with PDE4. *EMBO J.* **27**, 384-393 (2008).

120. Richter,W., Jin,S.L. & Conti,M. Splice variants of the cyclic nucleotide phosphodiesterase PDE4D are differentially expressed and regulated in rat tissue. *Biochem. J.* **388**, 803-811 (2005).

121. Rishi,V. *et al.* A high-throughput fluorescence-anisotropy screen that identifies small molecule inhibitors of the DNA binding of B-ZIP transcription factors. *Anal. Biochem.* **340**, 259-271 (2005).

122. Roehrl,M.H. *et al.* Selective inhibition of calcineurin-NFAT signaling by blocking protein-protein interaction with small organic molecules. *Proc. Natl. Acad. Sci. U. S. A* **101**, 7554-7559 (2004).

123. Roehrl,M.H., Wang,J.Y. & Wagner,G. A general framework for development and data analysis of competitive high-throughput screens for small-molecule inhibitors of protein-protein interactions by fluorescence polarization. *Biochemistry* **43**, 16056-16066 (2004).

124. Roehrl,M.H., Wang,J.Y. & Wagner,G. Discovery of small-molecule inhibitors of the NFAT--calcineurin interaction by competitive high-throughput fluorescence polarization screening. *Biochemistry* **43**, 16067-16075 (2004).

125. Saito,T. *et al.* Acute aquaresis by the nonpeptide arginine vasopressin (AVP) antagonist OPC-31260 improves hyponatremia in patients with syndrome of inappropriate secretion of antidiuretic hormone (SIADH). *J. Clin. Endocrinol. Metab* **82**, 1054-1057 (1997).

126. Schramm,M., Thomas,G., Towart,R. & Franckowiak,G. Novel dihydropyridines with positive inotropic action through activation of Ca2+ channels. *Nature* **303**, 535-537 (1983).

127. Schrier,R.W. & Cadnapaphornchai,M.A. Renal aquaporin water channels: from molecules to human disease. *Prog. Biophys. Mol. Biol.* **81**, 117-131 (2003).

128. Schrier,R.W., Cadnapaphornchai,M.A. & Ohara,M. Water retention and aquaporins in heart failure, liver disease and pregnancy. *J. R. Soc. Med.* **94**, 265-269 (2001).

129. Schrier,R.W., Ohara,M., Rogachev,B., Xu,L. & Knotek,M. Aquaporin-2 water channels and vasopressin antagonists in edematous disorders. *Mol. Genet. Metab* **65**, 255-263 (1998).

130. Schwaerzel,M., Jaeckel,A. & Mueller,U. Signaling at A-kinase anchoring proteins organizes anesthesia-sensitive memory in Drosophila. *J. Neurosci.* **27**, 1229-1233 (2007).

131. Schweigert,N., Zehnder,A.J. & Eggen,R.I. Chemical properties of catechols and their molecular modes of toxic action in cells, from microorganisms to mammals. *Environ. Microbiol.* **3**, 81-91 (2001).

132. Scott,J.D. *et al.* Type II regulatory subunit dimerization determines the subcellular localization of the cAMP-dependent protein kinase. *J. Biol. Chem.* **265**, 21561-21566 (1990).

133. Sculptoreanu,A., Rotman,E., Takahashi,M., Scheuer,T. & Catterall,W.A. Voltage-dependent potentiation of the activity of cardiac L-type calcium channel alpha 1 subunits due to phosphorylation by cAMP-dependent protein kinase. *Proc. Natl. Acad. Sci. U. S. A* **90**, 10135-10139 (1993).

134. Serradeil-Le,G.C. *et al.* Nonpeptide vasopressin receptor antagonists: development of selective and orally active V1a, V2 and V1b receptor ligands. *Prog. Brain Res.* **139**, 197-210 (2002).

135. Sette,C. & Conti,M. Phosphorylation and activation of a cAMP-specific phosphodiesterase by the cAMP-dependent protein kinase. Involvement of serine 54 in the enzyme activation. *J. Biol. Chem.* **271**, 16526-16534 (1996).

136. Shin,D.S., Kim,D.H., Chung,W.J. & Lee,Y.S. Combinatorial solid phase peptide synthesis and bioassays. *J. Biochem. Mol. Biol.* **38**, 517-525 (2005).

137. Sidhu,S.S., Lowman,H.B., Cunningham,B.C. & Wells,J.A. Phage display for selection of novel binding peptides. *Methods Enzymol.* **328**, 333-363 (2000).

138. Skalhegg,B.S. & Tasken,K. Specificity in the cAMP/PKA signaling pathway. Differential expression,regulation, and subcellular localization of subunits of PKA. *Front Biosci.* **5**, D678-D693 (2000).

139. Smith,F.D. & Scott,J.D. Signaling complexes: junctions on the intracellular information super highway. *Curr. Biol.* **12**, R32-R40 (2002).

140. Snyder,H.M., Noland,T.D. & Breyer,M.D. cAMP-dependent protein kinase mediates hydrosmotic effect of vasopressin in collecting duct. *Am. J. Physiol* **263**, C147-C153 (1992).

141. Stefan,E. *et al.* Compartmentalization of cAMP-dependent signaling by phosphodiesterase-4D is involved in the regulation of vasopressin-mediated water reabsorption in renal principal cells. *J. Am. Soc. Nephrol.* **18**, 199-212 (2007).

142. Stokes,J.B., Grupp,C. & Kinne,R.K. Purification of rat papillary collecting duct cells: functional and metabolic assessment. *Am. J. Physiol* **253**, F251-F262 (1987).

143. Stokka,A.J. *et al.* Characterization of A-kinase-anchoring disruptors using a solution-based assay. *Biochem. J.* **400**, 493-499 (2006).

144. Strathmann,M.P. & Simon,M.I. G alpha 12 and G alpha 13 subunits define a fourth class of G protein alpha subunits. *Proc. Natl. Acad. Sci. U. S. A* **88**, 5582-5586 (1991).

145. Sunahara,R.K., Dessauer,C.W. & Gilman,A.G. Complexity and diversity of mammalian adenylyl cyclases. *Annu. Rev. Pharmacol. Toxicol.* **36**, 461-480 (1996).

146. Svoboda,P. *et al.* Biochemistry of transmembrane signaling mediated by trimeric G proteins. *Physiol Res.* **53 Suppl 1**, S141-S152 (2004).

147. Szaszak,M., Christian,F., Rosenthal,W. & Klussmann,E. Compartmentalized cAMP signalling in regulated exocytic processes in non-neuronal cells. *Cell Signal.* **20**, 590-601 (2008).

148. Tang,C., Iwahara,J. & Clore,G.M. Visualization of transient encounter complexes in protein-protein association. *Nature* **444**, 383-386 (2006).

149. Tasken,K. & Aandahl,E.M. Localized effects of cAMP mediated by distinct routes of protein kinase A. *Physiol Rev.* **84**, 137-167 (2004).

150. Taylor,S.S., Buechler,J.A. & Yonemoto,W. cAMP-dependent protein kinase: framework for a diverse family of regulatory enzymes. *Annu. Rev. Biochem.* **59**, 971-1005 (1990).

151. Trotter,K.W. *et al.* Alternative splicing regulates the subcellular localization of A-kinase anchoring protein 18 isoforms. *J. Cell Biol.* **147**, 1481-1492 (1999).

152. Valenti,G., Procino,G., Tamma,G., Carmosino,M. & Svelto,M. Minireview: aquaporin 2 trafficking. *Endocrinology* **146**, 5063-5070 (2005).

153. Vijayaraghavan,S. *et al.* Isolation and molecular characterization of AKAP110, a novel, sperm-specific protein kinase A-anchoring protein. *Mol. Endocrinol.* **13**, 705-717 (1999).

154. Vogtherr,M. & Fiebig,K. NMR-based screening methods for lead discovery. *EXS* 183-202 (2003).

155. Wells,J.A. & McClendon,C.L. Reaching for high-hanging fruit in drug discovery at protein-protein interfaces. *Nature* **450**, 1001-1009 (2007).

156. Widmer,H. & Jahnke,W. Protein NMR in biomedical research. *Cell Mol. Life Sci.* **61**, 580-599 (2004).

157. Willoughby,D., Wong,W., Schaack,J., Scott,J.D. & Cooper,D.M. An anchored PKA and PDE4 complex regulates subplasmalemmal cAMP dynamics. *EMBO J.* **25**, 2051-2061 (2006).

158. Wong,W. & Scott,J.D. AKAP signalling complexes: focal points in space and time. *Nat. Rev. Mol. Cell Biol.* **5**, 959-970 (2004).

159. Wrighton,N.C. *et al.* Small peptides as potent mimetics of the protein hormone erythropoietin. *Science* **273**, 458-464 (1996).

160. Wu,J., Brown,S.H., von,D.S. & Taylor,S.S. PKA type IIalpha holoenzyme reveals a combinatorial strategy for isoform diversity. *Science* **318**, 274-279 (2007).

161. Xiao,H. *et al.* Insights into the mechanism of microtubule stabilization by Taxol. *Proc. Natl. Acad. Sci. U. S. A* **103**, 10166-10173 (2006).

162. Zaccolo,M. & Pozzan,T. Discrete microdomains with high concentration of cAMP in stimulated rat neonatal cardiac myocytes. *Science* **295**, 1711-1715 (2002).

163. Zakhary,D.R., Fink,M.A., Ruehr,M.L. & Bond,M. Selectivity and regulation of A-kinase anchoring proteins in the heart. The role of autophosphorylation of the type II regulatory subunit of cAMP-dependent protein kinase. *J. Biol. Chem.* **275**, 41389-41395 (2000).

164. Zakhary,D.R., Moravec,C.S. & Bond,M. Regulation of PKA binding to AKAPs in the heart: alterations in human heart failure. *Circulation* **101**, 1459-1464 (2000).

165. Zhang,J.H., Chung,T.D. & Oldenburg,K.R. A Simple Statistical Parameter for Use in Evaluation and Validation of High Throughput Screening Assays. *J. Biomol. Screen.* **4**, 67-73 (1999).

166. Zimmermann,B., Hahnefeld,C. & Herberg,F.W. Applications of biomolecular interaction analysis in drug development. *TARGETS* **1**, 66-73 (2002).

Publications

Original article

- Hundsrucker C, Krause G, Beyermann M, Prinz A, Zimmermann B, Diekmann O, Lorenz D, Stefan E, Nedvetsky P, Dathe M, Christian F, McSorley T, Krause E, McConnachie G, Herberg FW, Scott JD, Rosenthal W & Klussmann E: High-affinity AKAP7delta-protein kinase A interaction yields novel protein kinase A-anchoring disruptor peptides. *Biochem J.* 2006 **396**(2):297-306

Review

- Szaszak M, Christian F, Rosenthal W & Klussmann E: Compartmentalized cAMP signalling in regulated exocytic processes in non-neuronal cells. *Cell Signal.* 2008 **20**(4):590-601

Patent applications

- Klussmann E, Rosenthal W, Christian F, Szaszak M, Zimmermann B & Genieser HG: AKAP-PKA-Interaktionshemmer als potentielle Therapeutika
- Klussmann E, Rosenthal W, Christian F, Rademann J & Meyer S: Non-peptidic inhibitors of AKAP-PKA interaction. PCT/DE2006/000897

Poster presentations

- Christian F, Zimmermann B, Hampel K, Drewianka S, Cacciatore G, Kashin D, Vargas C, Szaszak M, Immig H, Friedl S, Zenn M, Schmieder P, von Kries JP, Genieser HG, Herberg FW, Rosenthal W & Klussmann E: Targeting Compartmentalised PKA Signalling with Small Molecules. 16th Protein Kinase Meeting, Oslo, Norway, September 25-28, 2008
- Christian F, Szaszak M, Zimmermann B, Vargas C, Lorenz D, Immig H, Friedl S, Baillie GS, Zenn M, Houslay MD, Schmieder P, von Kries JP, Herberg FW, Rosenthal W & Klussmann E: Small Molecules Interfering with Compartmentalised cAMP Signalling. MDC/FMP PhD students retreat, Templin, Germany, September 18-20, 2008
- Szaszak M, Christian F, Lorenz D, Furkert J, Rosenthal W & Klussmann E: FMP-API-1: A Small Molecule Targeting AKAP-PKA Complexes with a Positive Inotropic Effect. 2nd International Conference on Anchored cAMP Signalling Mechanisms, Portland, Oregon, USA, October 14-16, 2007
- Christian F, Szaszak M, Lorenz D, Furkert J, Hundsrucker C, von Kries JP, Rosenthal W & Klussmann E: Targeting Compartmentalised cAMP Signalling with Small Molecules. Workshop on Chemical Genomics, Helmholtz Centre for Infection Research, Braunschweig, Germany, March 5-6, 2007
- Christian F, Szaszak M, Meyer S, Zapke J, Lorenz D, Hundsrucker C, von Kries JP, Rademann J, Rosenthal W & Klussmann E: 15th Protein Kinase Meeting, Oslo, Norway, September 21-24, 2006